Optimization of Digital TV coverage prediction and broadcasting antennas

Keyur K. Mistry

Department of Computing and Engineering

University of Huddersfield

This dissertation is submitted for the degree of

Doctor of Philosophy

30th June 2020

Declaration

I hereby declare that except where specific reference is made to the work of others, the contents of this dissertation are original and have not been submitted in whole or in part for consideration for any other degree or qualification in this, or any other University. This dissertation is the result of my own work and includes nothing which is the outcome of work done in collaboration, except where specifically indicated in the text.

Keyur K. Mistry

30th June 2020

Acknowledgments

I would like to express my gratitude to my supervisor Dr. Pavlos Lazaridis, Reader in Electronics and Communications, University of Huddersfield for his excellent support and mentorship throughout my research. I also feel privileged to be supervised by Dr. Zaharias Zaharis, Aristotle University of Thessaloniki and retired Prof. Ian Glover, University of Huddersfield. This research work would not have been possible without their valuable guidance, feedback, and support.

I feel pleasured to recognize that all the antennas presented in this research work were fabricated in the University of Huddersfield Electronics Lab. Therefore, I would like to extend my thanks to Martin Webster and David Bray, who helped me in fabricating all the antennas presented in this work.

I would also like to thank team of National Physical Laboratory (NPL), UK and Rohde and Schwarz for providing the resources required for antenna measurements. Furthermore, I would like to thank the Arqiva team of Emley Moor for providing me with the required data for the propagation studies and measurements.

I express my sincere thanks to the University of Huddersfield for providing me with the Vice-Chancellor's scholarship and bursary throughout my PhD studies. I am also thankful to them for providing me with all the resources required for my research work and support me financially to publish papers and attend conferences to get feedback and ideas for my research.

I also thank all members of the Systems, Telecommunications and Antenna Research (STAR) group, University of Huddersfield for their valuable feedback.

Lastly, I am thankful to my parents, fiancé, and brother, who have always supported me financially and mentally to successfully carry out this research work. I am also thankful to my late grandfather for supporting me throughout my studies. Their continuous motivation and encouragement have helped me to stay focussed during my studies.

Abstract

The work described in this thesis focuses on: 1. designing novel antenna techniques and 2. radio propagation and coverage prediction studies in UK, North Macedonia and Greece. Log-Periodic dipole antennas (LPDAs) are a class of antennas that are widely used for ultra-high frequency (UHF) television (TV) reception. Because of the evolution of mobile technologies and excellent building penetration properties in the UHF band, parts of this spectrum are being allocated to Long-Term Evolution (LTE) frequency bands. The new spectrum allocation gives rise to interference problems between these closely spaced frequency bands. Therefore, in order to provide good quality-of-service (QoS) to UHF TV users, new reception antennas are required with band rejection that could eliminate the interference of LTE-800 MHz band and GSM-900 MHz band. Thus, this thesis proposes a design methodology and prototype of a novel LPDA that can provide band rejection in the LTE-800 MHz and GSM-900 MHz bands without using any external filters. The proposed antenna provides good matching, high band rejection and ensures better QoS compared to other existing antennas in the market. It is a cost-effective antenna design as it also removes the cost of using external filters. Furthermore, the LPDA design was also implemented on printed circuit boards (PCBs) in an attempt to reduce the overall size of the antenna. Several miniaturization techniques for reducing the size of LPDAs were reviewed and two prototypes for printed log-periodic dipole antenna (PLPDA) with wide bandwidth are proposed in this thesis. The first prototype follows the conventional PLPDA, designed to operate from 0.7 GHz to 8 GHz. The second prototype is a novel PLPDA design with triangular longest dipole that has an operating frequency range from 0.4 GHz to 8 GHz. Furthermore, two prototypes for elliptical patch antennas are proposed for GPS and Iridium applications and Real-Time locating systems. This work also demonstrates an accurate simulation-assisted antenna gain determination technique in order to improve the accuracy of gain measurements. Lastly, radio propagation and coverage prediction studies were carried out using three measurement campaigns whose results were compared to several propagation models using simulations. The electric field strength, path profiles and coverage prediction were carried out for: 1. Turtel analogue TV transmitter, 2. Emley Moor digital TV transmitter and 3. Belmont digital TV transmitter.

List of Publications

Papers under review

[1] **K. K. Mistry,** P. Lazaridis, Z. Zaharis, I. Gravas, T. Loh, D. Cheadle, M. Akinsolu and B.Liu, "An optimized Wearable-Ready Elliptical Patch Antenna for GPS and Iridium applications", IEEE Transaction on Antennas and Propagation, Submitted in September, 2019.

[2] **K. K. Mistry,** P. Lazaridis, Z. Zaharis, I. Chochliouros, T. Loh and D. Cheadle, "A novel design of UHF TV reception antenna with LTE-800 and GSM-900 protection", IEEE Access, Submitted in December 2019.

Published journal papers

[1] **K. K. Mistry**, P. Lazaridis, Z. Zaharis, M. Akinsolu, T. D. Xenos and I. Glover, "Time and Frequency Domain Simulation, Measurement and Optimization of Log-Periodic Antennas", Wireless Personal Communications, vol. 107, no. 2, pp. 771-783, 2019. **Contributions:** *This article acts a ground work to develop a good understanding of simulating Log-periodic dipole antennas in the CST software. Moreover, this article compares several optimization algorithms present in the CST software to optimize the benchmark antenna. A significant part of this contribution is explained in Chapter 2. This article is referenced as [63] in the thesis.*

[2] D. Upton, R. Haigh, P. Mather, P. Lazaridis, **K. K. Mistry**, Z. Zaharis, C. Tachtatzis and R. Atkinson, "Gated pipelined folding ADC based low power sensor for large-scale radiometric partial discharge monitoring", *IEEE PES Transactions on Power Delivery*, August 2019.

Contributions: *This research article was a part of EPSRC project: Radiometric detection of Partial discharge in high voltage sub-station. Major contributions involved data collection and field measurement of the proposed technology.*

[3] I. Gravas, Z. Zaharis, T. Yioultsis, P. Lazaridis, **K. K. Mistry** and T. Xenos, "Optimal Synthesis of Feeding Network for Implementation of Dolph-Chebyshev Current Distribution on Microstrip Antenna Arrays", IEEE Transactions on Antennas and Propagation, pp. 1-1, 2019. Available: 10.1109/tap.2019.2925276. **Contributions:** *This research article was a result of research collaboration between*

University of Huddersfield and Aristotle University of Greece. Major contributions involve optimization of microstrip array using different optimization algorithms to achieve required performance.

[4] E. Tziris, P. Lazaridis, Z. Zaharis, J. Cosmas, **K. K. Mistry** and I. Glover, "Optimized Planar Elliptical Dipole Antenna for UWB EMC Applications", IEEE Transactions on Electromagnetic Compatibility, pp. 1-8, 2019. Available: 10.1109/temc.2019.2923781.
Contributions: *This is a part of collaborative research work where I majorly contributed in developing novel antenna design concept, fabrication of the proposed antenna and its measurements. The correlation between the measurements and simulations is presented in this paper.*

[5] V. Grout, M. Akinsolu, B. Liu, P. Lazaridis, **K. K. Mistry** and Z. Zaharis, "Software Solutions for Antenna Design Exploration: A Comparison of Packages, Tools, Techniques, and Algorithms for Various Design Challenges", IEEE Antennas and Propagation Magazine, vol. 61, no. 3, pp. 48-59, 2019. Available: 10.1109/map.2019.2907887.
Contributions: *This article was a result of collaborative research between University of Huddersfield and Wrexham Glyndwr University. The Wrexham Glyndwr University proposes a novel optimization algorithm that was tested on several benchmark antenna models. My contributions were to use their optimization algorithm to optimize the benchmark antenna to meet the specified requirements. Additionally, the results were compared with various other optimization algorithms that already exist in different electromagnetic simulation packages.*

[6] D. W. Upton, B. I. Saeed, P. J. Mather, M. Sibley, P. Lazaridis, **K. K. Mistry**, I. Glover, F. Torres, C. Tachtatzis, R. Atkinson and M. Judd, "Low power radiometric partial discharge sensor using composite transistor-reset integrator," in IEEE Transactions on Dielectrics and Electrical Insulation, vol. 25, no. 3, pp. 984-992, June 2018.
Contributions: *This research article was a part of EPSRC project: Radiometric detection of Partial discharge in high voltage sub-station. The transistor-reset integrator technology is a part of Wireless System Network that was developed for this project. Major contribution involved data collection and outdoor field measurements to validate the proposed technology.*

Published conference papers

[1] **K. K. Mistry**, P. Lazaridis, Z. Zaharis, M. Akinsolu, B. Liu and T. Loh, "Accurate antenna gain estimation using the Two-Antenna Method", *IET Antenna and Propagation Conference*, Birmingham, November 2019.

Contributions: *This article presents a novel simulation-assisted antenna gain measurement technique using the two-antenna method. Since this technique involves the use of the CST software to estimate the optimal distance between the antenna, it reduces the time and efforts required during the actual measurement. A significant amount of work from this article is presented in Chapter 6. This article is referenced as [162] in the thesis.*

[2] **K. K. Mistry**, P. Lazaridis, T. Loh, Z. D. Zaharis, I. Glover and B. Liu, "A novel design of a 10-dipole log-periodic antenna with LTE-800 and GSM-900 band rejection", *2019 IEEE MTT-S International Conference on Numerical Electromagnetic and Multiphysics Modeling and Optimization (NEMO)* Institute of Electrical and Electronics Engineers Inc., Cambridge, MA, USA.

Contributions*: This article presents a novel LPDA antenna that serves as a cost-effective solution to solve the interference problems due to the coexistence of UHF-TV and mobile-LTE and GSM band. The design approach and results from this paper have been reproduced and explained in detail in Chapter 3. This article is referenced as [34] in the thesis.*

[3] U. Khan, P. Lazaridis, H. Mohamed, D. Upton, **K. K. Mistry**, B. Saeed, P. Mather, R. Atkinson, C. Tachtatzis and I. Glover, "Received Signal Strength Intensity Based Localisation of Partial Discharge in High Voltage Systems," *2018 24th International Conference on Automation and Computing (ICAC)*, Newcastle upon Tyne, United Kingdom, 2018, pp. 1-5.

Contributions: *This research article was a part of EPSRC project: Radiometric detection of Partial discharge in high voltage sub-station. It presents localization algorithm that was used along with the wireless system network to detect the partial discharge. My major contributions involved in validating the localization algorithm by performing field measurements using the wireless sensor network.*

[4] D. W. Upton, R. P. Haigh, B. I. Saeed, U. Khan, H. Mohamed, **K. K. Mistry**, P. Mather, P. Lazaridis, F. Torres, C. Tachtatzis, R. Atkinson, M. Judd and I. Glover, "Low Power High-Speed Folding ADC Based Partial Discharge Sensor for Wireless Fault Detection in Substations," *2018 2nd URSI Atlantic Radio Science Meeting (AT-RASC)*, Meloneras, 2018, pp. 1-4.

Contributions: *This research article was a part of EPSRC project: Radiometric detection of Partial discharge in high voltage sub-station. Major contribution involved data collection and outdoor field measurements to validate the proposed technology.*

[5] B. Saeed, P. Lazaridis, H. Mohamed, D. Upton, **K. K. Mistry,** P. Mather, and I. Glover. "Localisation of Partial Discharge by Using Received Signal Strength". In *2nd URSI Atlantic Radio Science Conference Proceedings*

Contributions: *This research article was a part of EPSRC project: Radiometric detection of Partial discharge in high voltage sub-station. Major contribution involved data collection, outdoor field measurements to validate the proposed technology and also contribute in writing a section of the paper.*

[6] B. Saeed, D. Upton, M. D. F. Q. Vieira, F. Torres, H. Mohamed, K. Mistry and I. Glover. A Supervisory System for Partial Discharge Monitoring. *2nd URSI Atlantic Radio Science Conference (URSI AT-RASC)*, Meloneras, 2018.

Contributions: *This research article was a part of EPSRC project: Radiometric detection of Partial discharge in high voltage sub-station. Major contribution involved data collection, outdoor field measurements to validate the proposed technology and also contribute in writing a section of the paper.*

[7] E. N. Tziris, P. I. Lazaridis, K. K. Mistry, *et al*., "1.62GHz Circularly Polarized Pin-Fed Notched Circular Patch Antenna," *2018 2nd URSI Atlantic Radio Science Meeting (AT-RASC)*, Meloneras, 2018, pp. 1-3.

Contributions: This is a part of collaborative research work where I majorly contributed in developing novel antenna design concept, optimization, fabrication of the proposed antenna and its measurements. The correlation between the measurements and simulations is presented in this paper.

[8] **K. K. Mistry**, P. I. Lazaridis, E. N. Tziris, Z. D. Zaharis, B. Liu, T. D. Xenos, & I. A. Glover, "A Design of Elliptical Edge-Fed Circularly Polarized Patch Antenna for GPS and Iridium Applications", *2018 2nd URSI Atlantic Radio Science Meeting, AT-RASC 2018*,

2018.

Contributions: *This article presents a dual-band circularly polarized antenna that can be used for GPS and Iridium applications. The design technique and results from this paper were used to improve the antenna performance and reproduce the optimized results, that are discussed in Chapter 7. It is referenced as [143] in this thesis.*

[9] **K. K. Mistry**, P. I. Lazaridis, Z. D. Zaharis, T. D. Xenos, E. N. Tziris and I. A. Glover, "An optimal design of printed log-periodic antenna for L-band EMC applications," *2018 IEEE International Symposium on Electromagnetic Compatibility and 2018 IEEE Asia-Pacific Symposium on Electromagnetic Compatibility (EMC/APEMC)*, Singapore, 2018, pp. 1150-1155.

Contributions: *This article presents a printed LPDA antenna that can be used as an alternative to the conventional LPDA for L-band EMC applications. The antenna design technique reduces the actual size of the antenna compared to the conventional LPDAs. Major part of this paper is reproduced in Chapter-4 and the knowledge acquired while designing this antenna provided the base for proposing the novel miniaturization technique proposed in Chapter-5. This article is referenced as [121] in this paper.*

[10] E. N. Tziris, J. P. Cosmas, Z. D. Zaharis, T. D. Xenos, P. I. Lazaridis, **K. K. Mistry** and I. A. Glover, "Invasive weed optimized planar elliptical dipole antenna for ultra-wideband EMC applications," *2018 IEEE International Symposium on Electromagnetic Compatibility and 2018 IEEE Asia-Pacific Symposium on Electromagnetic Compatibility (EMC/APEMC)*, Singapore, 2018, pp. 233-236.

Contributions: *This is a part of collaborative research work where I majorly contributed in developing novel antenna design concept, fabrication of the proposed antenna and its measurements. The correlation between the measurements and simulations is presented in this paper.*

[11] H. Mohamed, P. I. Lazaridis, U. Khan, B. Saeed, **K. K. Mistry**, D. Upton, P. Mather and I. Glover, "Partial discharge detection in smart grid using software defined radio," *2017 25th Telecommunication Forum (TELFOR)*, Belgrade, 2017, pp. 1-4.

Contributions: *This research article was a part of EPSRC project: Radiometric detection of Partial discharge in high voltage sub-station. Major contribution involved programming the software defined radio, data collection and outdoor field measurements to validate the proposed technology.*

[12] **K. K. Mistry**, P. I. Lazaridis, Z. D. Zaharis, T. D. Xenos and I. A. Glover, "Optimization of log-periodic dipole antenna with LTE band-rejection," *Loughborough Antennas & Propagation Conference (LAPC 2017)*, Loughborough, 2017, pp. 1-5. **Contributions:** *This article presents a novel LPDA antenna that serves as an cost-effective solution to solve the interference problems due to the coexistence of UHF-TV and mobile-LTE and GSM band. The design approach and results from this paper have been reproduced and explained in detail in Chapter 3. This article is referenced as [12] in the thesis.*

[13] H. Mohamed, P. Lazaridis, D. Upton, U. Khan, **K. K. Mistry**, B. Saeed, P. Mather, M. F. Q. Vieira, K. W. Barlee, R. Atkinson, I. A. Glover, "Partial discharge localisation based on received signal strength," *2017 23rd International Conference on Automation and Computing (ICAC)*, Huddersfield, 2017, pp. 1-4. **Contributions:** *This research article was a part of EPSRC project: Radiometric detection of Partial discharge in high voltage sub-station. Major contribution involved programming the software defined radio, data collection and outdoor field measurements to validate the proposed technology.*

[14] D. W. Upton, B. I. Saeed, U. Khan, A. Jaberi, H. Mohamed, **K. K. Mistry**, P. Mather, P. Lazaridis, M. F. Q. Vieira, R. Atkinson, C. Tachtatzis, E. Iorkyase, M. Judd and I. A. Glover, "Wireless sensor network for radiometric detection and assessment of partial discharge in HV equipment," *2017 XXXIInd General Assembly and Scientific Symposium of the International Union of Radio Science (URSI GASS)*, Montreal, QC, 2017, pp. 1-4. **Contributions:** *This research article was a part of EPSRC project: Radiometric detection of Partial discharge in high voltage sub-station. Major contribution involved designing antenna, data collection and outdoor field measurements to validate the proposed technology.*

[15] **K. K. Mistry** *et al*., "Measurement, simulation and optimization of wideband log-periodic antennas," *2017 XXXIInd General Assembly and Scientific Symposium of the International Union of Radio Science (URSI GASS)*, Montreal, QC, 2017, pp. 1-4. **Contributions:** *This article acts a ground work to develop a good understanding of simulating Log-periodic dipole antennas in the CST software. Moreover, this article compares several optimization algorithms present in the CST software to optimize the*

benchmark antenna. A significant part of this contribution is explained in Chapter 2. This article is referenced as [62] in the thesis.

Contents

List of Figures

List of Tables

List of Abbreviations

UK – United Kingdom

DTT– Digital Terrestrial Television

DSO – Digital Switchover

DVB-T/T2 – Digital Video Broadcasting Terrestrial/ Second Generation Terrestrial

OFDM – Orthogonal Frequency-Division Multiplexing

UHF – Ultra High Frequency

LTE- Long Term Evolution

4G – Fourth Generation

5G – Fifth Generation

BT – British Telecom

WRC – World Radio Communications

SRTM – Shuttle Radar Topography Mission

VHF – Very High Frequency

DAB – Digital Audio Broadcasting

LPDA – Log periodic dipole antenna

DTV – Digital Television

PLDPA – Printed log periodic antenna

GPS – Global Positioning System

CST – Computer Simulation Technology

GSM – Global System for Mobile communications

EMC – Electromagnetic Compatibility

NPL – National Physical Laboratory

SADEA – Surrogate Model Assisted Differential Evolution for Antenna Synthesis

PSADEA – Parallel Surrogate Model Assisted Differential Evolution for Antenna Synthesis

UWB – Ultrawideband

MWS – Microwave Studio

FIT – Finite Element Method

FFT – Fast Fourier Transform

TLM – Transmission Line Matrix

TRF – Trusted Region Framework

CMA-ES – Covariance Matrix Adaptation Evolutionary Strategy

VSWR – Voltage Standing Wave Ratio

PSO – Particle Swarm Optimization

IWO – Invasive Weed Optimization

ADIWO – Adaptive Dispersion Invasive Weed Optimization

PSOvm – Particle Swarm Optimization with velocity mutation

FCC – Federal Communication Commission

DF – Direction Finding

NTL – Non-uniform Transmission Line

AUT – Antenna under test

RHCP – Right-hand circular polarization

LHCP – Left-hand circular polarization

AR – Axial ratio

RG – Realized gain

FTB – Front-to-back ratio

QoS – Quality of Service

UN – United Nations

ITU – International Telecommunications Union

EIRP – Equivalent Isotropic Radiated Power

ERP – Effective Radiated Power

FSPL – Free Space Propagation Loss

LOS – Line of Sight

NLOS – Non-line of Sight

FM – Frequency Modulation

ATV – Analogue Television

ITM – Irregular Terrain Model

IOT – Inductive Output Tube

Chapter 1 Introduction

1.1 Research background

In the United Kingdom (UK), Digital Terrestrial Television (DTT) was first introduced on the 15th of November 1998. The replacement of analogue terrestrial television by DTT in the UK is referred to as "Digital Switchover (DSO)", also known as "analogue switch off". The UK government started an attempt to switch from analogue to digital on the 17th of October 2007 and their intention was to achieve nationwide digital switchover by the 24th of October 2012 with the help of an independent body called "Digital UK". This raised a demand for the government to provide subsidised upgrades or replacements of receiving equipment that included set-top boxes and receiving antennas. Presently, DTT in the UK, comprises of more than hundred TV, radio and other interactive broadcasting services that are being received by standard TV units. Since 2013, Freeview is the only DTT service that broadcasts programs in the UK.

DTT uses radio waves that are transmitted using antennas installed on tall transmitting masts or towers and are received by the users using receiving antennas that are usually installed on household rooftops. The receiving antennas are usually installed outdoors. For the transmitting antennas to cover a wider area including the urban as well as rural regions, the placement of the transmitting mast is highly strategic. DTT in UK has adopted Digital Video Broadcasting Terrestrial (DVB-T/T2) technology to broadcast compressed audio, video and other data in a single transport stream with the help of the Orthogonal Frequency-Domain Multiplexing (OFDM) modulation technique.

However, the UHF TV spectrum is very precious because of its favourable building penetration properties and thus the mobile communication community demanded to assign a part of this spectrum to mobile technologies because of the evolution of 4G, and now the upcoming 5G.

Due to this reason, the UK government cleared the 800 MHz band for LTE-4G purpose. In addition to this, with the introduction of 5G technology, the UK government intends to clear the 700 MHz band for mobile communications. However, clearing these bands and upgrading the technology requires careful planning.

1.1.1 800-MHz clearance

Since early 2003, the UK was one of the first European countries that recognized the usefulness of the UHF TV band because of its excellent building penetration properties. They identified the necessity of 14 8-MHz channels to be made available for mobile communication applications. Acknowledging this necessity, Ofcom made an announcement to propose plans listing the potential benefits and structure for the clearance of the 800-MHz band (790 MHz to 862 MHz). Finally, in February 2013, Ofcom auctioned the 800 MHz spectrum as well as the 2.6 GHz band to Vodafone, EE, Telefonica, 3 UK and British Telecom (BT). The 800 MHz band can be visualized as shown in Figure 1.

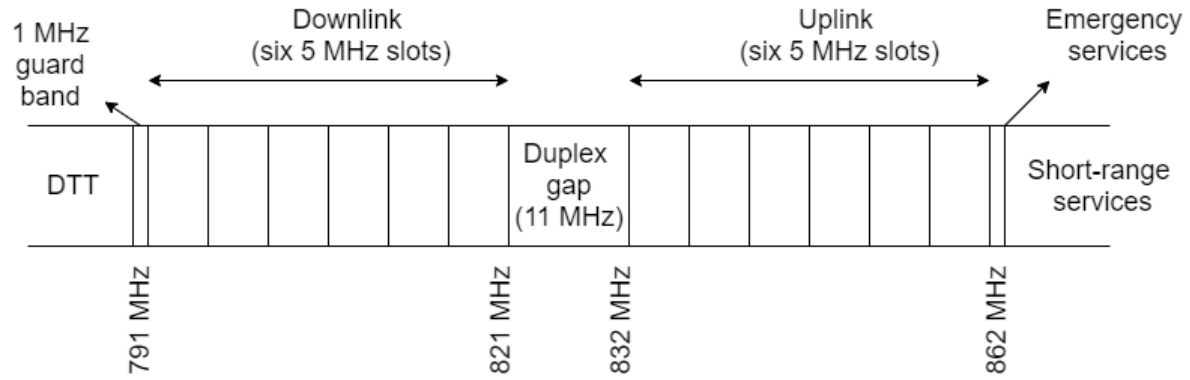

Figure 1. LTE-800 MHz band [1].

However, the 800 MHz band clearance was a challenging task and several obstacles were faced during the clearance. Some of them are listed as:

1. **Rooftop aerials**

The rooftop aerials had to be upgraded or external filters were required to reject LTE-800 band to avoid interference from this spectrum. Therefore, antenna installation for a big population during the clearance proved to be expensive.

2. **Clearing DTT from channels 61 and 62**

The decision to clear the 800-MHz band urged radio engineers to re-plan the frequency assignment of TV channels 61 and 62 to some other channels. The frequency planning and assignment is an expensive process and the reports by Digital Britain Report [2] suggest that the cost of clearance of this band was estimated to be around £115-125 million.

1.1.2 700-MHz clearance

Currently, 250 million customers in Europe are viewing television using DTT services. In the UK, around 20 million households use DTT services by Freeview. In November 2014, it was decided that the clearance of the 800-MHz band would be carried out with a further handover to 700-MHz clearance by the year 2020 to meet the increasing demand for mobile data. It is suggested that most of the users will just have to retune their TV sets, however, it is estimated that around 140,000 to 270,000 homes will be required to replace and realign their receiving antenna installed on their rooftops. Ofcom also suggested that few households might even have to replace their TV units. Several solutions in market as well as Ofcom suggest that external filters will be required to be added at the back of TV or the receiving antenna to avoid interference from the newly launched mobile services. This will require the consumers to buy antennas as well as filters. However, in this thesis, antenna prototypes are proposed that can solve this problem without using external filters, thereby reducing the costs for the consumers. The total costs due to the clearance of the 700 MHz band for the UK taxpayers is estimated to be around £600 million, whereas for overall Europe it is estimated to be around EUR 4 billion. The clearance of the 700 MHz band started in 2017 and Ofcom suggested a rollout plan that estimates to clear this band by the end of 2020 throughout the UK [3]. They suggested to carry out the clearance in different quartiles from Q1 to Q4. An overview of the rollout plan released by Ofcom for the clearance of the 700-MHz band is shown in Figure 2.

The spectrum showing the previous UHF band and the UHF band after the 700-MHz and the 800-MHz clearance is shown in Figure 3.

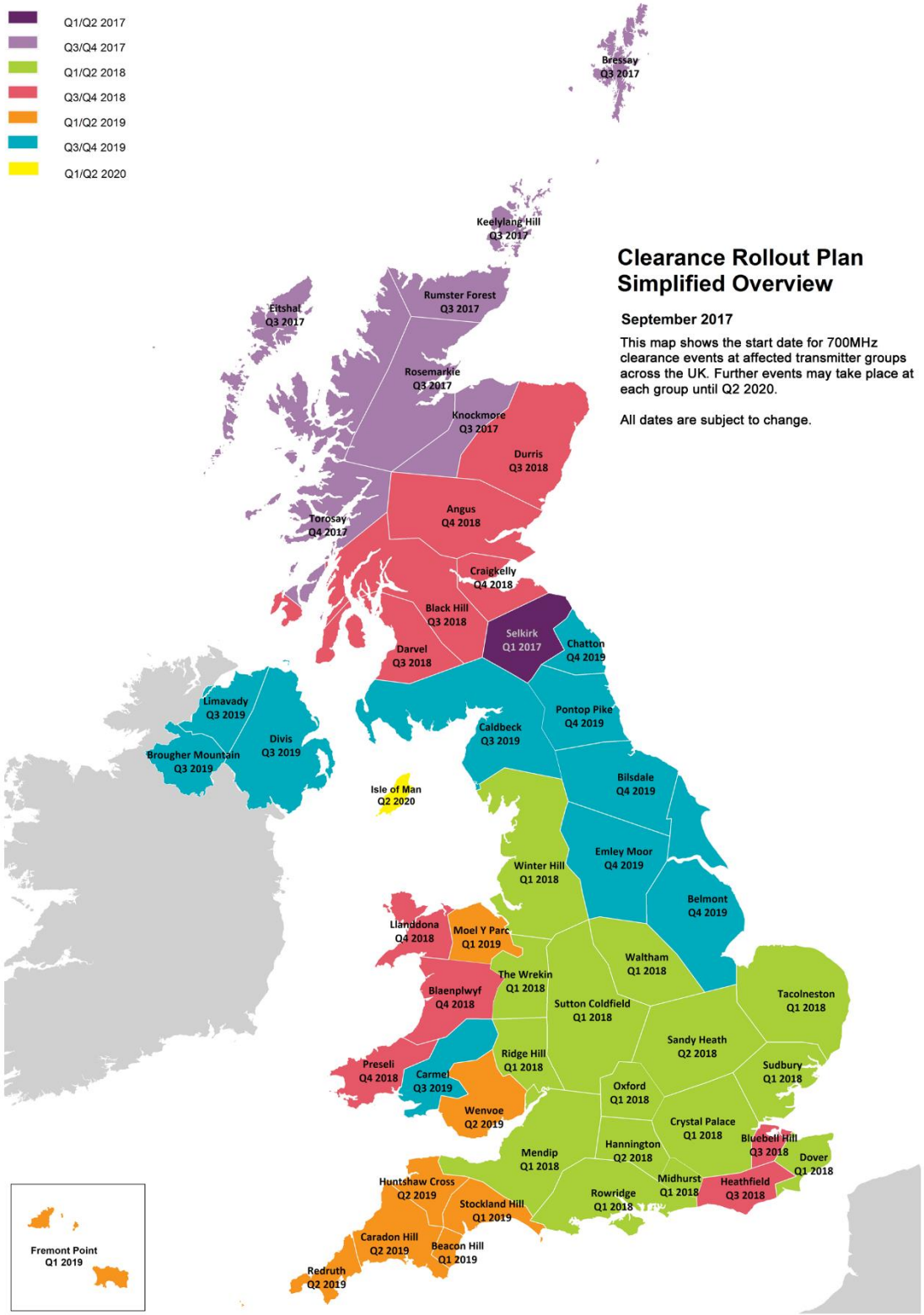

Figure 2. Rollout plan released by Ofcom for 700-MHz clearance [3].

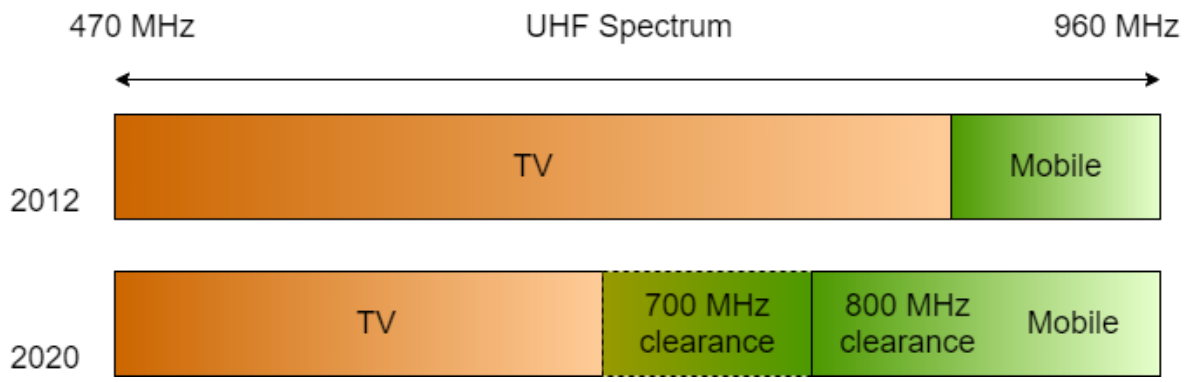

Figure 3. Spectrum band after 700-MHz clearance [4].

The decisions regarding radio spectrum are made at the World Radio Communication Conference (WRC) and the upcoming global review of the UHF spectrum is planned for 2023, also known as WRC 23. The decisions made on the 700 MHz clearance in WRC are shown as a timeline in Figure 4 [4].

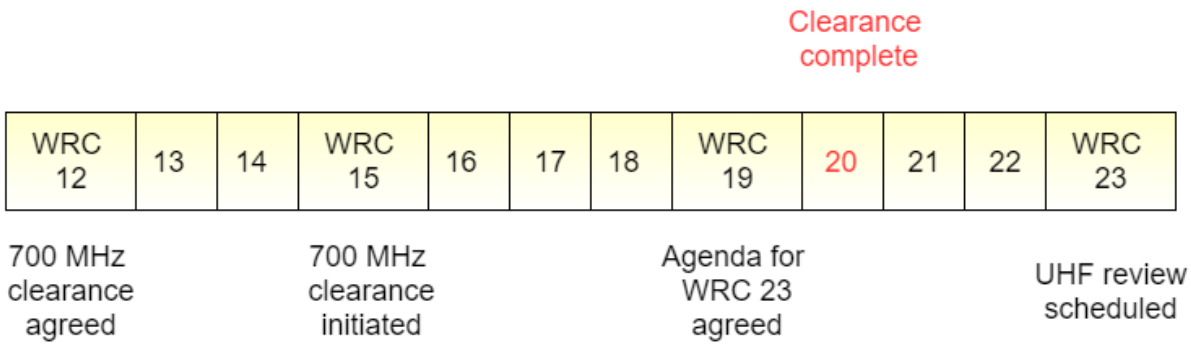

Figure 4. WRC timeline for UHF spectrum review [4].

The clearance of the UHF spectrum for the mobile technologies will require the upgrading the current broadcasting infrastructure. Thus, there is a need for an in-depth study radio wave propagation in all sorts of environment. Radio propagation and coverage prediction using propagation models helps radio engineers to design cost-efficient radio systems by strategically placing the base systems for communication. Radio planning software like ICS Telecom (commercial software), Radio Mobile (freeware) and propagation models designed in Matlab are used by Radio Engineers to study radio propagation and coverage prediction. In addition to this, NASA SRTM (Shuttle Radar Topography Mission) provides a database of 3D terrain

elevation data of all the countries that can be used to obtain accurate simulated results. Softwares like ICS Telecom, Radio Mobile and algorithms developed in Matlab provides access to classical as well as empirical models for the simulation at Very High frequency (VHF) and Ultra-High frequency (UHF) bands for Digital Video Broadcasting (DVB-T and DVB-T2) and Digital Radio (DAB) applications.

1.2 Research motivation

The 700 MHz and 800 MHz clearance of UHF spectrum and its allocation to mobile communications raises the requirement to redesign the currently available antenna designs in such a way that they provide rejection characteristics. Log-periodic dipole array (LPDA) antennas are mostly used for UHF TV reception. Therefore, there is a need to investigate the LPDAs and further optimize them so that they can be used after the 700 MHz and 800 MHz clearance. Furthermore, since the LPDAs are also utilised for gain measurement and Electromagnetic Compatibility (EMC) measurement applications, it is necessary to reduce the size of the LPDA by printing them on a substrate with specific dielectric permittivity. Investigation of printed LPDA (PLPDA) and side-reduction or miniaturization techniques is required to present novel antenna design with wide frequency response. Because of the clearance, the modifications are required not only at the receiving end but also at the transmitting end. This includes appropriate radio planning of the broadcasting system in such a way that the transmitting stations provides optimal coverage. To achieve optimal coverage from the stations, it is necessary to perform radio propagation and coverage prediction studies using several propagation models so that an appropriate coverage model can be estimated.

1.3 Research objectives

The objectives of this research are:

1. Develop design methodologies for LPDA design and optimisation in CST Studio Suite.

2. Design cost-efficient LPDAs to solve the interference problems caused due to the co-existence of UHF DTV band with LTE-800 MHz and GSM-900 MHz bands that provides high-rejection without using any external filters.
3. To design PLPDAs with wide bandwidth capable of operating from 0.4 GHz to 8 GHz.
4. To develop a simulation-assisted technique for accurate antenna gain measurements.
5. Design patch antennas for GPS, Iridium and real time location system applications.
6. To perform radio propagation and coverage prediction and measurement studies.

1.4 Thesis outline

Chapter 1 presents a brief introduction to antenna simulation and measurement as well as radio propagation and coverage prediction studies. It also highlights the primary objectives of this research.

In chapter 2, a background of design and optimisation methodology for log-periodic antennas is discussed. It also introduces the time domain and frequency domain simulations in CST Studio Suite electromagnetic simulation software. Furthermore, it provides a comparison of optimization algorithms available in CST, which were applied on a conventional 10-dipole LPDA with an operating frequency range between 450 MHz to 900 MHz.

Chapter 3 provides two cost-efficient LPDA designs capable of rejecting the LTE-800 MHz and GSM-900 MHz band without using any external filters. The first design consists of 10-dipoles and the second design consists of 14-dipoles. The front five dipoles were optimized to create a distinguished anomaly compared to the conventional LPDA design to provide the band-rejection characteristics in the higher frequency band. Both antenna designs contribute towards providing a solution to solve interference problems caused due to the co-existence of the UHF DTV band with the LTE-800 MHz band and the GSM-900 MHz band.

Chapter 4 demonstrates a methodology to design PLPDAs for Electromagnetic Compatibility (EMC) applications. This antenna operates from 0.8 GHz to 2.6 GHz and provides a gain of above 4.5 dBi.

Chapter 5 discusses several miniaturization techniques to reduce the size of conventional PLPDAs as well as increase their operating bandwidth. This chapter also present two wideband prototypes. The first design is a 25-dipole PLPDA that has an operating frequency range from 0.7 GHz to 8GHz. The second prototype is an optimised version of the first design to provide an operating frequency range from 0.4 GHz to 8 GHz. The optimised prototype consisted of a triangular shaped 25^{th} dipole instead of a straight dipole. The optimization of the last three dipole lengths, last four spacings between the dipoles and thickness of the last four dipoles were the parameters used to optimise the antenna.

In Chapter 6, a simulation-assisted gain determination technique is proposed using the two-antenna method. The measurement setup of the two-antenna method is replicated in the simulation software to determine the appropriate separation distance between identical antennas that can be used for the actual measurements so that an accurate gain estimation of the antenna can be obtained. A 10 dipole LPDA LTE-reject antenna is used to test the gain determination technique in collaboration with NPL.

Chapter 7 provides a methodology to design a dual-band elliptical patch antenna for GPS and Iridium applications. The antenna proposed in this chapter provides circular polarization and a gain of above 5 dBi in its operating frequency range. The measurements for this antenna were performed in an anechoic chamber at the National Physical Laboratory (NPL). The optimisation of the antenna is performed using the Parallel Surrogate Model Assisted Differential Evolution for Antenna Synthesis (PSADEA) algorithm.

Chapter 8 provides a design of another elliptical patch antenna that operates from 3.7 GHz to 4.2 GHz. This antenna is used for an ultra-wideband (UWB) system for localisation applications. The antenna was successful in improving the localisation range of the system from 75 meters to 250 meters. This antenna provides a boresight gain of above 5 dBi.

Chapter 9 discusses radio propagation and coverage prediction studies. Radio propagation terminology is initially explained. The data from three measurement campaigns for the electric field strength and coverage prediction is compared with simulations performed using different propagation models in three different softwares: ICS Telecom, Radio Mobile and Matlab.

Chapter 10 discusses the conclusions drawn as well as the future works that can be carried out starting from this research work.

Chapter 2 Introduction to Log-Periodic Dipole Antennas

Log-periodic dipole antennas (LPDAs) are a unique class of antennas that are widely used for wideband applications because of its ability provide flat gain over a wide frequency range. They are popularly used for TV reception, spectrum monitoring and Electromagnetic Compatibility measurements (EMC). This chapter provides LPDA design methodology and proposes a UHF TV-reception LPDA antenna that operates from 470 MHz to 860 MHz. The antenna is first simulated in time-domain as well as frequency domain to ensure that the antenna is modelled accurately using the design methodology. The antenna was fabricated, and a comparison of simulated and measured results are also presented in this work. A good agreement between the practically measured realized gain and the simulated realized gain is observed. Further to this, an optimization of this antenna was performed using various algorithms provided in CST Studio Suite in order to improve voltage standing wave ratio (VSWR), realized gain and front-to-back ratio of the antenna. A comparison of optimizing the antenna using various algorithms such as Trusted Region Framework (TRF), Nelder Mead Simplex algorithm, Classic Powell and Covariance Matrix Adaptation Evolutionary Strategy (CMA-ES) is also presented in this chapter. The TRF algorithm performed best and optimized as per the pre-defined goals specified for the antenna. **A significant part of this chapter has already been published in a conference [62] and a journal [63].**

2.1 Introduction

LPDAs are popularly used for TV reception and EMC measurements because of its wideband characteristics and ability to provide almost flat gain over its operating frequency range [5]. Increasing the number of dipoles in LPDA can provide a higher gain [6]. Compared to Yagi-Uda antenna, LPDA is highly directional and provide better front-to-back ratio, but relatively

lower gain [7]. However, the operating bandwidth of LPDA is larger compared to the Yagi-Uda antenna array. The design of an LPDA is very similar to the Yagi-Uda antenna, however the feeding pattern of both the antennas differentiate them from each other. In Yagi-Uda antenna only one dipole is connected to the feeding source leaving other dipoles passive, whereas in LPDA, all the dipoles are connected to the feeding source [8]. A design procedure for LPDA is proposed by Carrel in [9, 10].

The LPDA consists of several dipoles, that are arranged in an increasing order of dipole lengths, connected to a conducting boom. When the dipole length "L" is equal to half-wavelength "(λ/2)", the resonance condition for that dipole is achieved. Thus, each dipole attains the resonance condition for certain frequencies. The dipoles with larger or small lengths than λ/2 will act as reflectors or directors respectively for the dipole in resonating state. The wideband characteristics of an LPDA is obtained due to several dipoles with different lengths [8].

A basic geometry of an LPDA is shown in Figure 5. The dipoles of an LPDA are arranged in a parallel sequence in such a way that the end of the dipoles lies within the same angle 2α from the front part of the antenna. The angle of intersection can be defined in [11] as :

$$\alpha = \tan^{-1}\left[\frac{1-\tau}{4\sigma}\right] \tag{1}$$

where τ is a scaling factor defined as the ratio of the lengths or diameters of two consecutive dipoles, as given by

$$\tau = \frac{L_{n+1}}{L_n} = \frac{d_{n+1}}{d_n} \tag{2}$$

and σ is a spacing factor constant is expressed as

$$\sigma = \frac{s_n}{2L_n} \tag{3}$$

where, L_n and d_n are respectively the length and the diameter of the nth dipole, while s_n is the spacing between the n^{th} dipole and its consecutive $(n+1)^{th}$ dipole.

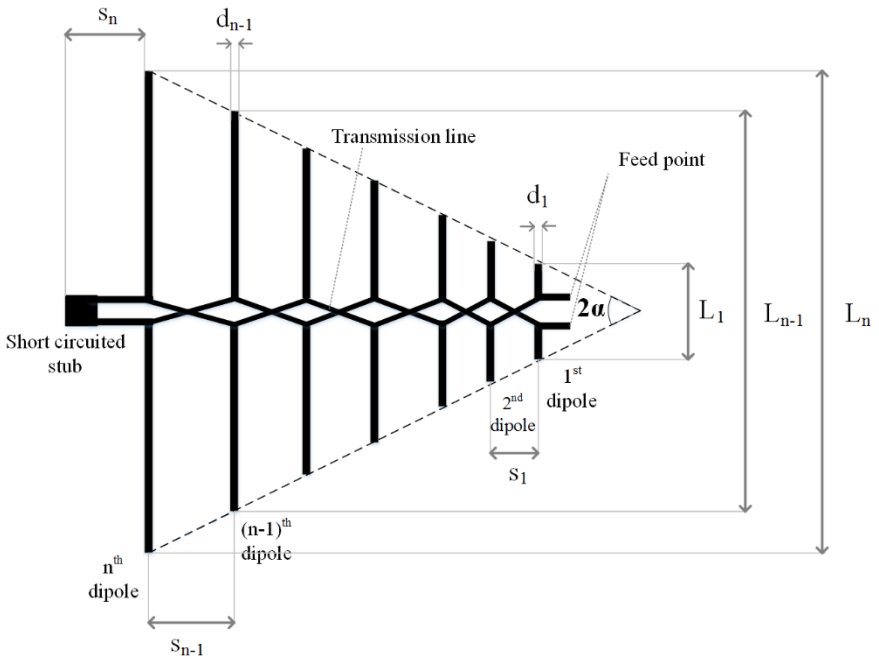

Figure 5. Log. Periodic dipole array geometry.

The dipoles are connected to the feeding line in such a way that the consecutive dipoles have opposite phase [12]. In order to reduce the fabrication costs, the LPDAs often have dipoles with constant diameter [13]. Carrel's graph is used to select the values of τ and σ according to the predefined average directivity required for the antenna [9, 14, 15].

2.2 Time domain and frequency domain simulation

Researchers often find selecting a type of solver for the simulation, a challenging task. There is no best suited solver for all types of applications, therefore the selection of solvers totally depends on type and size of antenna to be simulated. The time domain solver in the CST Microwave Studio (MWS) is based on the finite integration technique (FIT) describing Maxwell's equations on a time-grid space whereas the frequency domain solver is based on the finite element method (FEM). The calculations involving antennas with wide frequency range,

mostly find time domain method suitable, as the frequency response is calculated using Fast Fourier Transform (FFT) after a single simulation run. Another advantage of using time domain method is that the spectrum calculations can be performed using fine frequency resolution without any additional effort. Due to this reason, the time domain solver is mostly used for simulations that involve electrically large structures. The simulation time is longer if the number of mesh cells are larger. In CST, time domain solver uses either the hexahedral or the hexahedral TLM (Transmission-Line Matrix) meshing technique for simulation. The time domain simulation analysis is performed on a port-by-port basis.

On the other hand, in frequency domain method, discrete simulations are performed at discrete frequencies separated from each other by a specified frequency step to cover the entire operating bandwidth. Due to this reason, for such a simulation method, adaptive mesh refinement is required at every frequency to obtain accurate results. The frequency domain simulation stops as soon as the return loss converge. Nevertheless, a single simulation can provide results for all the ports in a single calculation. Thus, the frequency domain solver is used for narrowband simulations that involves electrically small structures. Frequency domain solver in CST, uses either the hexahedral or tetrahedral meshing technique [16].

2.3 LPDA measurements and simulations

A 10-dipole LPDA is presented in this work that can operate in former analogue TV band from 470 MHz to 860 MHz. The fabricated antenna was measured using Rohde & Schwarz FSH8 portable spectrum analyzer in an open field condition. The gain measurements for this antenna was performed with the help of biconical dipole antennas using the reference antenna method. The simulation of this antenna was performed in CST Studio Suite 2016 and the comparison of the simulated and measured results are presented in this chapter. The results presented in this includes the VSWR, realized gain and front-to-back ratio of the antenna.

The realized gain of the antenna is defined as the difference between gain and mismatch loss of the antenna. The expressions for realized gain and mismatch loss are given below [8]:

$$Mismatch\ Loss\,(dB) = -10\log_{10}\left[1-\left[\frac{VSWR-1}{VSWR+1}\right]^2\right] \tag{4}$$

$$Realized\ Gain\,(dBi) = Gain\,(dBi) - Mismatchloss\,(dB) \tag{5}$$

Followed by the comparison of simulated and measured results of the initial LPDA design, an optimization was performed in CST using several algorithms like TRF, Nelder Mead Simplex algorithm, Classic Powell and Covariance Matrix Adaptation Evolutionary Strategy (CMA-ES) in order to improve the antenna performance.

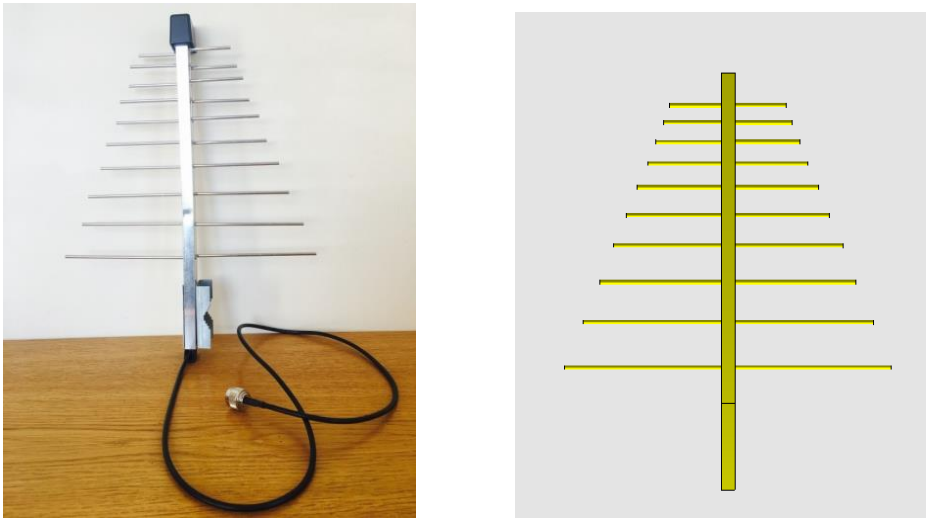

Figure 6. Fabricated LPDA (left) and simulated model of LPDA (right).

In Figure 6, the fabricated LPDA (left) and the CST model of the LPDA (right) is presented. The antenna comprises of a short-circuited stub at the rear-end. The antenna comprised of 564,435 mesh cells that were obtained by discretization of the model using hexahedral meshing technique. The feeding to the antenna was provided using a discrete port of 50Ω impedance connecting the front part of both the booms. The 50 Ω impedance port is used for discrete port in the simulation because the coax cables and power amplifiers are mostly designed with 50Ω impedance and usually the feeding to the antenna is provided using the coax cables. The time-domain and frequency-domain simulations were performed for this antenna. Figures 7, 8 and

10 show respectively the comparative results of VSWR, realized gain and front-to-back ratio. The time domain and frequency domain results are in good agreement, as expected. Figure 7 shows that the VSWR of the antenna is below 2 for most of its frequency range. The lower VSWR values below 2 shows that antenna is well matched and will have lower radiation losses. However, the VSWR values are relatively slightly high from 650 MHz to 750 MHz and thus further improvement is required in this range. This graph also shows a good agreement between the time-domain and frequency domain simulation of the antenna.

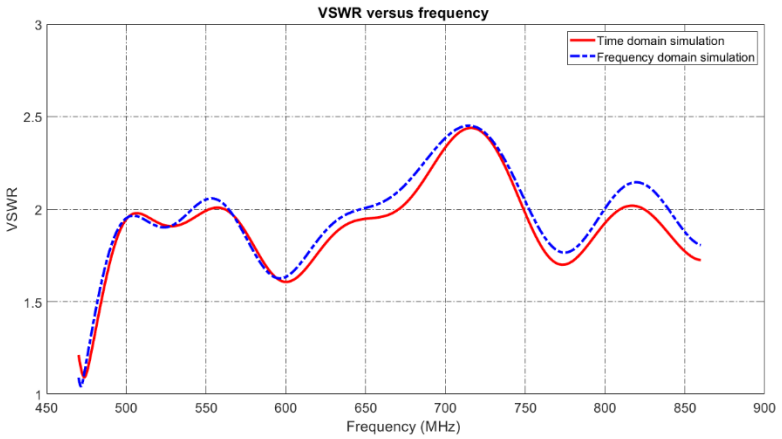

Figure 7. Comparison between VSWR values derived from simulations in time and frequency domain.

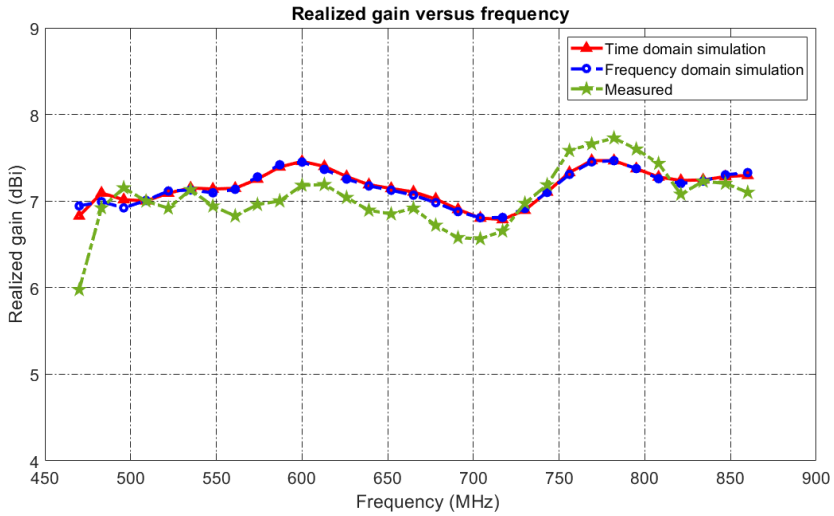

Figure 8. Comparison between realized gain values derived from simulations in the time and the frequency domain and open-field measurements (green line).

Figure 8 shows that the measured realized gain is very close to both the simulated realized gain. The antenna provides a gain of around 7 dBi in its operating frequency range. The realized gain presented in this figure is reasonably flat with the values mostly ranging between 6.5 to 7.5 dBi. The antenna with such values of realized gain are suitable to be used for UHF TV reception applications. The difference between the measured and simulated realized gain (time domain) is show in Figure 9. The maximum difference is obtained from 570 MHz to 700 MHz and thus an improvement in this frequency region is required. A minimal difference is observed for the realized gain from 470 MHz to 570 MHz and 700 MHz to 890 MHz. Thus, it is evident to conclude that the simulation results and measurement results are in good agreement.

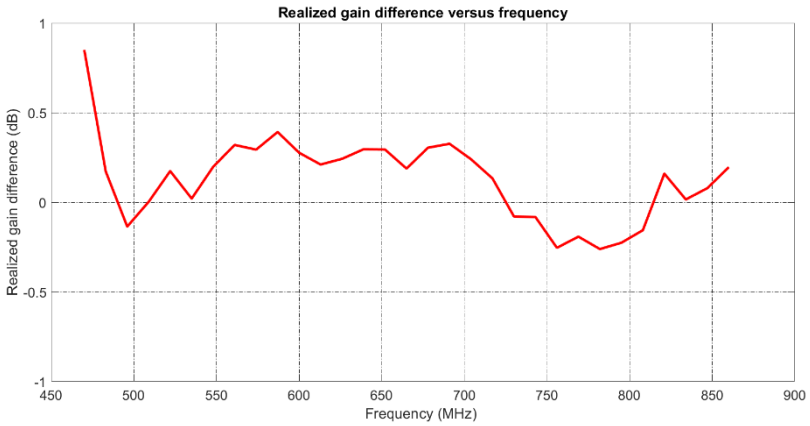

Figure 9. Difference of simulated realized gain (time domain) and measured realized gain versus frequency.

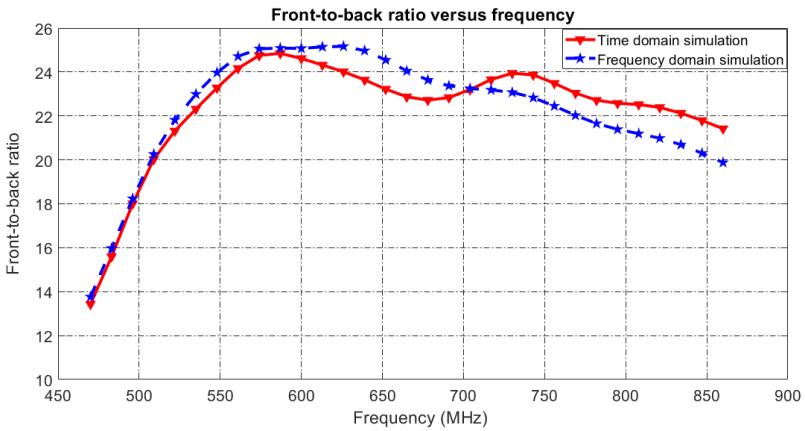

Figure 10. Comparison between front-to-back ratio values (dB) derived from simulations in time and frequency domain.

Figure 10 presents the comparison of the simulated and measured front-to-back ratio of the antenna. It validates the highly directional behaviour of this LPDA. The simulated and the measured front-to-back ratio also show good agreement between the measurement and simulation.

Followed by the preliminary check of the antenna model, the time domain and frequency domain provide enough confidence to validate the modelling accuracy of the antenna. The measured and simulated results suggest that the CST model approximates with good accuracy the actual antenna. Optimization of this antenna is then performed using various optimization algorithms included in CST MWS.

2.4 LPDA optimization

CST comprises of global optimizers as well as local optimizers. However, the search capability is larger in global optimizers compared to local optimizers. Trusted Region Framework (TRF), Nelder Mead Simplex algorithm and Classic Powell algorithm are examples of local optimizers. On the other hand, CMA-ES is an example of a global optimizer.

TRF algorithm creates a linear model on the basis of the initial data recorded from a trust region around a starting point. This new model then acts as a new starting point until the point of convergence of an accurate model is obtained. TRF algorithm is suggested as one of the most robust algorithm offered by CST. TRF algorithm provides global convergence and predicts improves fitness function values obtained by adjusting the limits. [17]. In 1965, Nelder Mead Simplex algorithm was introduced by Nelder and Mead. This is an improved version of the Simplex search algorithm that was proposed in 1962 by Spendley, Hext and Himsworth [18]. In this algorithm, multiple points are distributed across the parameter search space in order to determine the optimum value. This algorithm is mostly used as a solution for complex problems that involves relatively few parameters. Classic Powell algorithm is considered to be a simple and robust optimizer, which can be used for a problem involving few parameters. The time of termination of the optimization process is decided by the accuracy requirement set before the start of the process. Compared to other algorithms, it is relatively a slower algorithm. However, it provides accurate results in some cases. CMA-ES is a self-adaptive evolution strategy and a

global optimizer, which was developed by Hansen and Ostermeier [19]. CMA-ES initializes strategy parameters like the number of variables, population size and their bounds in a well-defined fashion and thus does not require parameter tuning by the user [19, 20]. This algorithm is based on the evolution of a population of individuals. A comparison of CMA-ES with particle swarm optimization (PSO) is presented in [21]. CMA-ES solves a problem by generating a population of individuals using a Gaussian distribution [20, 22].

In order to optimize the LPDA to goals set in Table 1, optimization algorithms including TRF algorithm, Nelder Mead simplex algorithm, Classic Powell and CMA-ES are used. The half-dipole lengths (Ln /2), radius of the dipoles (rad), gap between the boom (gap), length of the boom (l_boom), width of the boom (b_boom), height of the boom (h_boom), length of the connector (l_connector) and spacing between the dipoles (sn) are the geometry parameters to be considered while performing optimization.

Table 1. Goals and weights for the antenna optimization.

Parameter	Operator	Goal value	Weight
VSWR	<	1.5	10
Gain (dBi)	>	8	0.5
Front-to-back ratio (dB)	>	20	0.2

The fitness function is defined using the linear combination of the optimization goals according to the weights assigned to each goal as specified in Table 1. The optimization algorithms aim at minimizing the value of this fitness function. The global minimum of the fitness function is achieved after selecting appropriate values of the geometric parameters considered for optimization. Figures 11, 12 and 13 presents the optimized results of VSWR, realized gain and front-to-back ratio of the optimized antenna. The optimized results are compared with the simulated results of the initial antenna model.

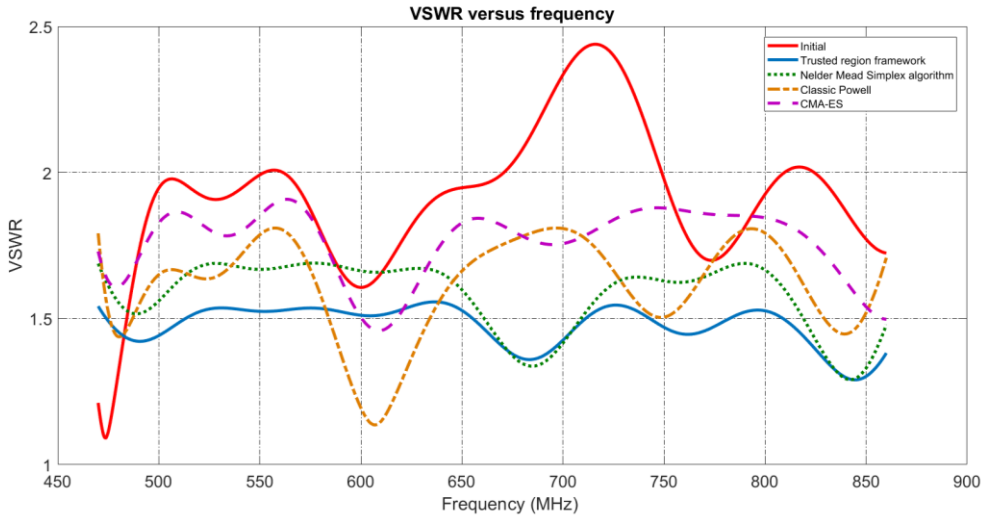

Figure 11. Comparison between optimized and initial VSWR values.

Figure 11 suggests that TRF algorithm was the best performer, followed by the Nelder Mead Simplex algorithm, to minimize the VSWR of the initial antenna. The TRF algorithm achieved VSWR of around 1.5 in the entire operating frequency range. On the other hand, other algorithms obtained VSWR values that oscillated between 1.5 to 2. The plot suggest that CMA-ES exhibited the highest VSWR compared to other algorithms and thus presented poorest performance.

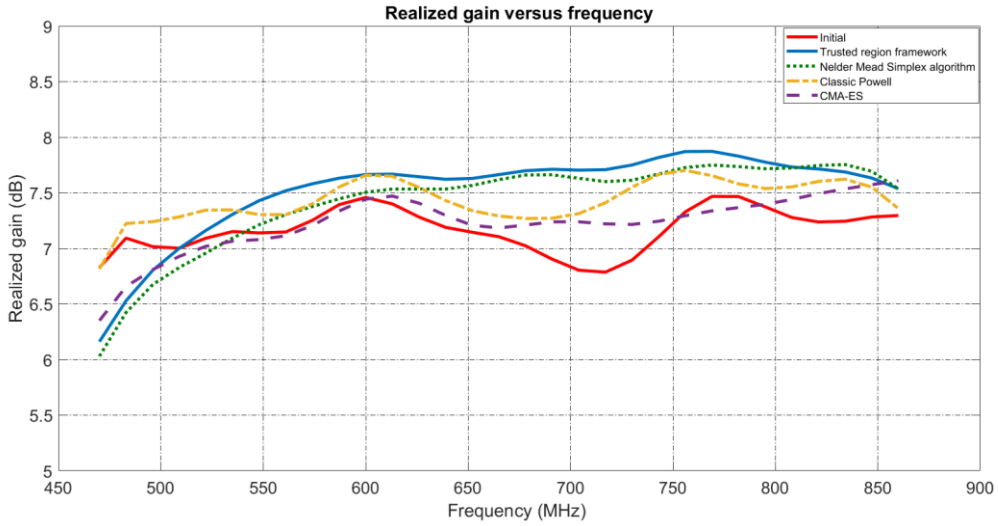

Figure 12. Comparison between the optimized and the initial realized gain.

Even in Figure 12 , the TRF algorithm performed best by achieving a flat gain of approximately 7.8 dBi. Other algorithms also improved the realized gain of the initial antenna by achieving the gain between 7 dBi and 7.8 dBi above 550 MHz. A significant increase of 1 dB is observed in realized gain of the initial antenna using TRF algorithm from 670 MHz to 750 MHz. Similar to the case of VSWR, CMA-ES presented poorest performance by providing lowest realized gain compared to other algorithms.

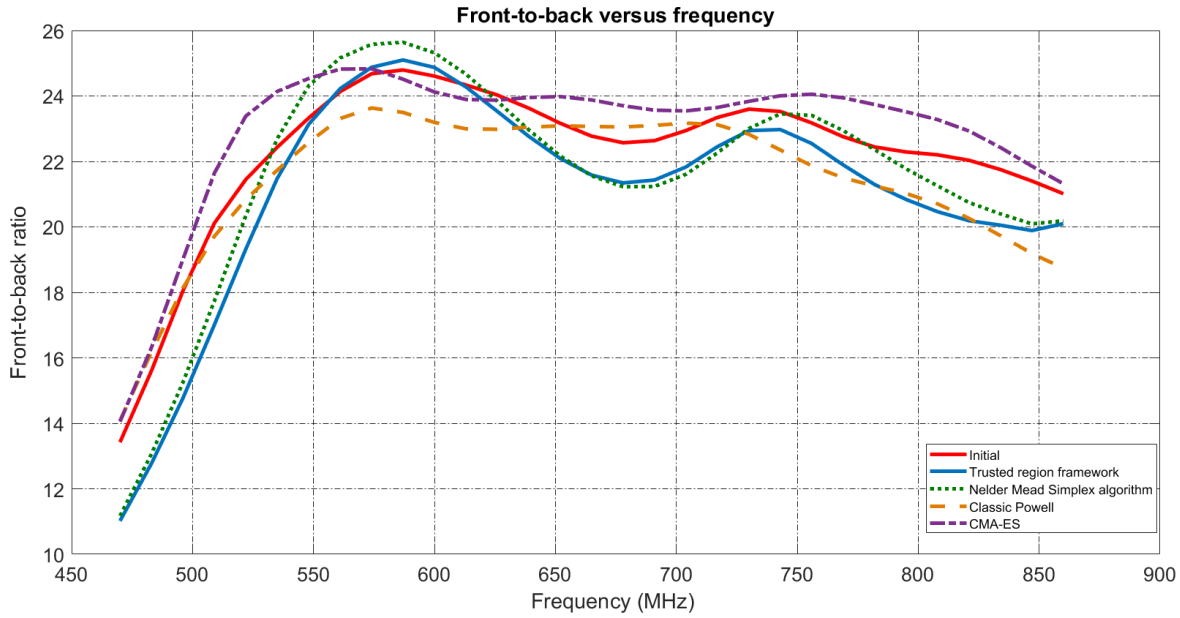

Figure 13. Comparison between optimized and initial front-to-back ratio.

Figure 13 suggests that CMA-ES was the best performer and maximized the front-to-back ratio above 20 dB. The Nelder Mead Simplex algorithm and TRF algorithm also presented promising results in optimizing the front-to-back ratio of the antenna. The optimal dimensions obtained using various algorithms and the initial dimensions of the antenna are compared and listed in Table 2. The optimization algorithms have been configured to change the antenna dimensions only by ±10% from their initial values. The numbers inside the brackets (in Table 2) show the changes relative to the initial antenna dimensions.

Table 2. LPDA geometry before and after optimization (dimensions in cm).

Parameters	Initial	TRF	Nelder Mead	Classic Powell	CMA-ES
b_boom	1.30	1.42	1.41	1.30	1.30
h_boom	1.30	1.43	1.40	1.43	1.24
l_boom	30.60	32.58	32.25	29.30	30.10
gap	1.10	0.99	1.02	1.03	1.06
l_connector	8.00	8.56	8.26	8.30	8.11
L1	9.80	10.76	10.78	10.74	9.90
L2	11.00	12.1	12.06	12.04	11.46
L3	12.40	11.84	12.22	12.40	12.12
L4	14.00	13.72	13.94	13.96	13.22
L5	16.00	15.82	15.80	16.00	15.46
L6	18.00	17.76	17.84	17.96	17.78
L7	20.60	19.82	19.88	20.58	20.5
L8	23.20	22.46	22.68	23.16	23.20
L9	26.40	25.76	26.16	26.34	26.70
L10	29.80	31.30	32.54	29.92	31.24
rad	0.20	0.22	0.21	0.22	0.19
s0	3.00	2.72	2.71	2.70	2.84
s1	1.60	1.45	1.55	1.44	1.53
s2	1.80	1.77	1.91	1.68	1.82
s3	2.00	2.05	2.05	1.91	2.05
s4	2.20	2.41	2.37	2.41	2.23
s5	2.60	2.49	2.34	2.58	2.69
s6	2.80	2.82	2.72	2.52	2.82
s7	3.40	3.10	3.06	3.07	3.51
s8	3.70	3.68	3.81	3.99	3.69
s9	4.20	4.00	3.78	4.48	4.20

2.5 Conclusion

This chapter presents an accurate CST modelling and simulation of a 10-dipole LPDA in time domain and frequency domain. A comparison of the measured and simulated results of this LPDA validates the accurate modelling of this antenna. In order to improve the performance of this antenna, an optimization was performed using several algorithms included in CST. A comparative study on the results obtained using these algorithms was also carried out in this work. TRF algorithm demonstrated the fastest convergence and provided the best optimized results with lowest fitness function value compared to other algorithms. Log-periodic antennas

are generally used for UHF TV reception. A frequency range from 470 MHz to 900 MHz was allocated for UHF TV applications. However, due to the clearance of 800 MHz band for LTE mobile communications, the present UHF TV reception antennas need to be re-designed in order to provide a high-rejection in the LTE-800 MHz band. Thus, the next chapter presents a novel antenna design technique that is used to design antennas with LTE-800 MHz band rejection capabilities.

Chapter 3 LPDA design with LTE-800 and GSM-900 band rejection

3.1 Introduction

The decision to move from analog to digital broadcasting television systems in 2008 has led to a more efficient utilization of the frequency spectrum that in turn, benefited mobile communication frequency allocations. Followed by this transition, and in order to ensure the efficient use of spectrum, the European Parliament [23] urged European Member States to reallocate some TV broadcasting services in the UHF band to mobile communications. Reference [24] advocates the benefits of allocating a so-called digital dividend band of 790 MHz-862 MHz to LTE-4G mobile wireless broadband services by the European Commission, based on a research analysis of the cost/benefit ratio. As described in [25], the harmonized plan to deploy Long-Term Evolution (LTE), also known as fourth generation (4G) mobile broadband network, to the UHF TV broadcasting band of 800 MHz was adopted in Europe (ITU region 1) to effectively utilize the spectrum for mobile services because of the excellent radio wave building penetration capabilities at these frequencies. The adopted LTE-band plan suggested a paired spectrum or frequency division duplex (FDD) of 30 MHz for uplink and 30 MHz for downlink transmission in the spectrum of 790 MHz-862 MHz (channels 61-69). The spectrum for uplink and downlink transmission is made up of 6 blocks of 5 MHz bandwidth in the frequency band of 791 MHz-821 MHz and 832 MHz-862 MHz respectively with a duplex gap of 11 MHz. The broadcasting of Digital Terrestrial Television (DTT) is carried until 790 MHz, leaving a gap of only 1 MHz between the DTT and the LTE 800 MHz band, which makes them both subject to interference effects. Reference [26] provides a detailed study of the interference effects caused due to the coexistence of TV broadcasting services with LTE mobile systems in the 800 MHz band, resulting in degrading the quality of service (QoS) of the TV

broadcasting services. Thereafter, a worldwide resolution [27] on the allocation of the 700 MHz band between 694 MHz and 790 MHz (channels 52-69) was passed in WRC-12 (World Radiocommunication Conference) [28] and the provisions to use this band in Region 1 were made in WRC-15 [29]. A detailed research on the interference problems due to the coexistence of TV broadcasting services with LTE mobile systems in the 700 MHz band has been illustrated in [30].

This chapter presents two LPDA antenna design, one with 10-dipoles and another with 14-dipoles. The number of dipoles to be used for the design depends on the gain requirement and frequency range of operation. For UHF TV reception purpose, antennas are required to operate from 470 MHz to 790 MHz and usually requires more than 6 dBi realized gain to receive TV signals. Due to this reason, 10-dipole antenna was designed first. Thereafter, a 14-dipole LPDA was also designed in order to achieve higher gain. **The results for the 10-dipole LPDA proposed in this chapter is published in [34] and additional results were reproduced from this paper.**

3.2 10-dipole LPDA design

This study presents a novel design of a 10-dipole log-periodic dipole antenna capable of rejecting 4G-LTE mobile service 800 MHz band as well as GSM 900 MHz band. The proposed antenna provides a cost-efficient solution to solve interference problems caused due to the coexistence of TV broadcasting services and LTE mobile services, without using any external band stop filters. The antenna design presented in this chapter operates in the frequency range of 450 MHz – 790 MHz (UHF TV reception passband), thereby rejecting the LTE 800 MHz band as well as the GSM 900 MHz band. The proposed design provides good matching for the antenna in the passband. The antenna has a relatively high gain around 8 dBi in the passband which drops to -5 dBi in the stopband. Furthermore, the antenna is highly directive throughout the passband.

3.2.1 Traditional Carrel's 10-dipole LPDA

Log-periodic dipole arrays (LPDAs) are considered as one of the most suitable antennas for TV reception because of their exceptional broadband characteristics [5]. Compared to Yagi-Uda antennas, which are also used for TV reception, LPDAs provide flatter gain over the wide operating bandwidth, and thereby show the potential to become a better solution for this application [7, 8]. Additionally, LPDAs provides better front-to-back ratio but relatively lower gain compared to Yagi-Uda antennas. The difference in the performance between these two antennas is partly due to the feeding pattern [10]. A very useful design procedure for traditional LPDAs was proposed by Carrel [9] and a basic geometry of LPDA based on these guidelines is shown in Figure 14.

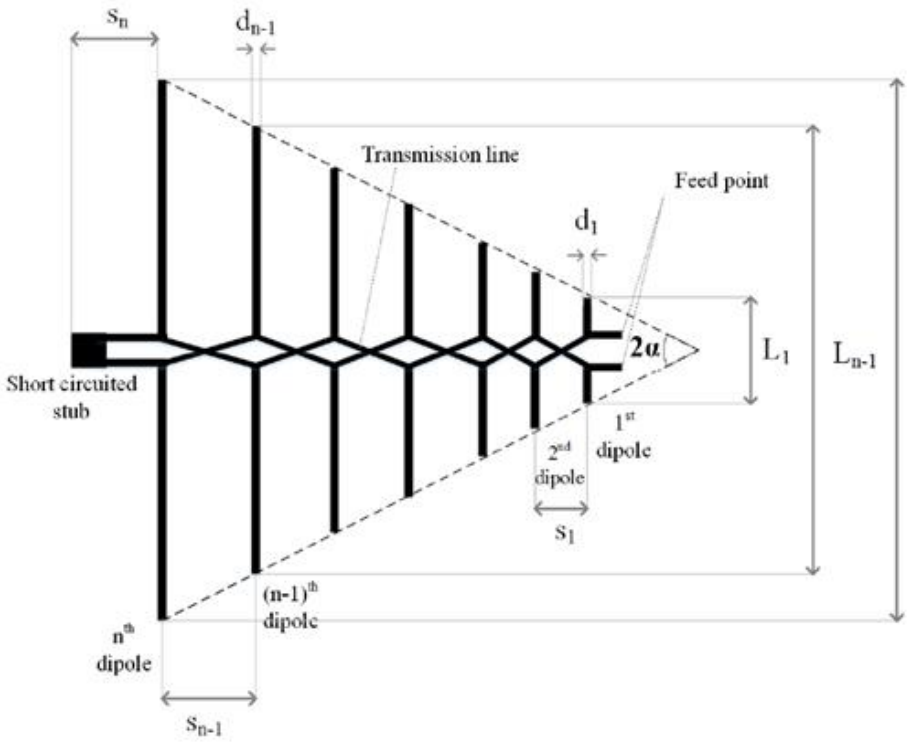

Figure 14. Basic geometry of a traditional LPDA proposed by Carrel [9].

A traditional LPDA consists of two conducting longitudinal supports, also known as "booms", which are responsible for feeding the half-dipole elements of the antenna. The two booms are

separated by each other using a fastener at the rear end of the antenna, which also acts as a short-circuiting stub. The separation between the two booms may vary depending on the type of matching to be obtained. In most of the cases, the antenna is matched to 50-ohms or 75-ohms impedance. Each conducting boom feeds the alternate half-dipoles of the antenna, in a crisscross fashion. In other words, if the first half-dipole is connected to the boom 1 (upper-boom), then the other half-dipole should be connected to boom 2 (lower-boom). These two half-dipoles together form a dipole. This configuration provides a 180-degree change of phase of the feeding between two consecutive dipoles. The change of phase ensures that the radiation pattern of the antenna points in the forward direction, thereby providing directional characteristics [31]. Unlike the Yagi-Uda antennas, the arrangement of dipoles is made in such a manner that all the dipoles are in contact with the conducting boom, thereby making all the dipoles active. Each dipole of the LPDA resonates at a particular frequency. The number of dipoles used in the antenna has a significant impact on its gain. The gain significantly increases by incrementing the number of dipoles used [6, 15, 32].]. In most cases, the feeding to the boom is provided using a coaxial cable through the front end of the antenna in order to avoid pattern distortion. A fastener is attached at the rear part of the antenna, acting as a short circuit stub as well as a point of support for the antenna, as shown in Figure16.

Design guidelines proposed by Carrel [9] consist of specific design equations that need to be followed in order to calculate the dimensions of the antenna. All the dipole elements of the LPDA are confined to the half-angular sector, also known as apex angle, which is mathematically defined as:

$$\alpha = \tan^{-1}\left[\frac{1-\tau}{4\sigma}\right] \tag{6}$$

The scaling factor τ is the ratio of the lengths or diameters of two consecutive dipoles, mathematically written as:

$$\tau = \frac{L_{n+1}}{L_n} = \frac{d_{n+1}}{d_n} \tag{7}$$

where, L_n and d_n are respectively the length and the diameter of the nth dipole.

The spatial arrangement of the dipole elements is defined by the spacing factor, mathematically represented as:

$$\sigma = \frac{s_n}{2L_n} \tag{8}$$

where s_n is the spacing between the nth dipole and its consecutive (n+1)th dipole and L_n is the length of nth dipole.

The scaling factor and spacing factor of the LPDA play a significant role in determining its physical properties.

3.2.2 Proposed 10-dipole LPDA geometry

This chapter presents a design of a 10-dipole log-periodic antenna capable of rejecting the LTE mobile services band, thereby mitigating the interference problems caused due to its coexistence with TV broadcasting services. Initially, the dimensions of the antenna were calculated using the basic design procedure proposed by Carrel [9]. Recently and in order to mitigate problems of interference caused due to the coexistence of the LTE 800 MHz band with the traditional UHF-TV band used by most TV tuners, various TV reception antennas have been designed, which can operate in the new TV band of 470 MHz -790 MHz while rejecting the 800 MHz band with the inclusion of external band stop filters. An optimal design of LPDA has been proposed in [33], which was obtained after optimizing Carrel's model using Particle Swarm Optimization with Velocity Mutation algorithm (PSOvm). The model provides rejection in the 800 MHz band, however, the relatively low VSWR of the antenna in the LTE-band still leaves the possibility of receiving interference from other angles. This unconventional design of the LPDA was optimized by using a much longer than usual first dipole. On the contrary, an optimized 10-dipole log-periodic dipole antenna has been proposed in [12], which provides good band stop characteristics above 790 MHz, without using external filters, in addition, to avoiding intereference from LTE-band from all the angles. This initial

design suggested that in order to achieve LTE rejection characteristics in the higher frequency band of the bandwidth, the dimensions of the shorter dipoles could be adjusted.

Motivated by the initially optimized design proposed in [12], this chapter presents an optimized version of this LPDA [34], by optimizing the first three dipoles of the LPDA and the spacing between them only, instead of considering all the dipoles of the antenna. The antenna proposed in this chapter achieves better matching, better LTE rejection and a higher realized gain compared to the antenna design in [12]. Additionally, it also provides better return loss, better directivity and higher and flatter realized gain than Carrel's model. The optimization of the antenna dimensions was performed with the Trusted Region Framework (TRF) algorithm available in CST using the optimization goals specified in Table 3. The parameters that were used to optimize the initial design are shown in Table 4, along with the range of the dimension values that were specified to vary during the optimization. However, several other optimization algorihms can be used to optimize the antenna performance and geometry, such as Invasive Weed Optimization (IWO) in [35-39], Particle Swarm optimization (PSO) in [40-42], Adative Dispersion IWO (ADIWO) in [43] and Particle Swarm Optimization with Velocity Mutation (PSOvm) in [44].

Table 3. Optimization goals and specifications.

Parameters	**Goals**	**Frequency (MHz)**	**Weight**
S11	< -14 dB	470-790 (Passband)	10.0
Realized gain	> 10 dBi	470-790 (Passband)	1.0
Front-to-back ratio	> 14 dB	470-790 (Passband)	0.2
S11	> -1 dB	810-960 (Stopband)	5.0
Realized gain	> -10 dBi	810-960 (Stopband)	1.0

The adjustment to the length of the first three dipoles has been made because of the fact that the shorter dipoles are responsible for the antenna performance at higher frequencies. The parameters that were considered for optimization included the first three dipole lengths (L1, L2 and L3) and the spacing between these dipoles (s0, s1, s2 and s3). These parameters were restricted to change by ± 30 %, while configuring the settings for TRF algorithm before the optimization. Table 4 shows the minimum and maximum values of the parameters that were considered for the optimization.

Table 4. Range of parameters considered for optimization.

Parameters	**Minimum**	**Maximum**
L1	48.3 mm	89.7 mm
L2	39.1 mm	72.67 mm
L3	44.2 mm	82.0 mm
s0	19.6 mm	36.4 mm
s1	10.7 mm	19.9 mm
s2	13.0 mm	24.2 mm
s3	15.4 mm	28.6 mm

The arrangement of shorter dipoles has been made in such a manner that the length of the 2nd dipole is smaller than the 1st dipole but bigger than the 3rd dipole. However, the 3rd dipole is shorter than the 2nd and 4th dipoles. The dipole lengths after the 4th dipole keep increasing in the classic design fashion until the last dipole. The designed antenna has the following dimensions: 356 mm x 302.6 mm x 35 mm (length x width x height). Both conducting booms are attached together using a cuboidal fastener acting as a short circuit stub and providing a point of attachment to any other support. The cuboidal fastener extends 45 mm long, 15 mm wide and 35 mm high. The front view and side view of the CST designed model of the antenna is shown in Figure 15 and Figure 16 respectively. The final dimensions of the antenna after the optimization are shown in Table 5.

Table 5. Dimensions of the optimized LPDA

Carrel's antenna model		**Proposed design**	
Parameters	***Values***	***Parameter***	***Values***
L1	49 mm	L1	72.7 mm
L2	55 mm	L2	64.2 mm
L3	62 mm	L3	56.0 mm
L4	69 mm	L4	60.7 mm
L5	80 mm	L5	78.6 mm
L6	89 mm	L6	90.1 mm
L7	102 mm	L7	101.8 mm
L8	114 mm	L8	117.7 mm
L9	130 mm	L9	133.5 mm
L10	149 mm	L10	151.3 mm
L-boom	380 mm	L-boom	356 mm
H-boom	15 mm	H-boom	15 mm

W-boom	15 mm	W-boom	15 mm
Dipole radius	2 mm	Dipole radius	2 mm
Stub_width	15 mm	Stub_width	15 mm
s0	25 mm	s0	24.1 mm
s1	16 mm	s1	11.4 mm
s2	17 mm	s2	14.9 mm
s3	20 mm	s3	17.9 mm
s4	23 mm	s4	25.3 mm
s5	26 mm	s5	27.3 mm
s6	28 mm	s6	27 mm
s7	33 mm	s7	36.3 mm
s8	37 mm	s8	40.4 mm
s9	40 mm	s9	40.6 mm
gap	10 mm	gap	5 mm
Stub_length	79 mm	Stub_length	45 mm
Stub_height	38 mm	Stub_height	35 mm

The CAD model is designed in CST using several parameters, where, L_n is length of the n^{th} dipole, s_n is distance between the n^{th} and $(n+1)^{th}$ dipole, L-boom is length of the boom, W-boom is width of the boom, H-boom is heigth of the boom, gap is the distance between the two parallel booms. The dimensions of the cuboidal fastener, that connects the end of the boom, acting as a short-circuiting stub, are represented by Stub_length, Stub_width and Stub_height in Table 5. The antenna designed using Carrel's method was matched to 75 ohm impedance. However, the gap between the booms in the optimized antenna design has been reduced to 5mm from 10mm to provide 50 ohm impedance.

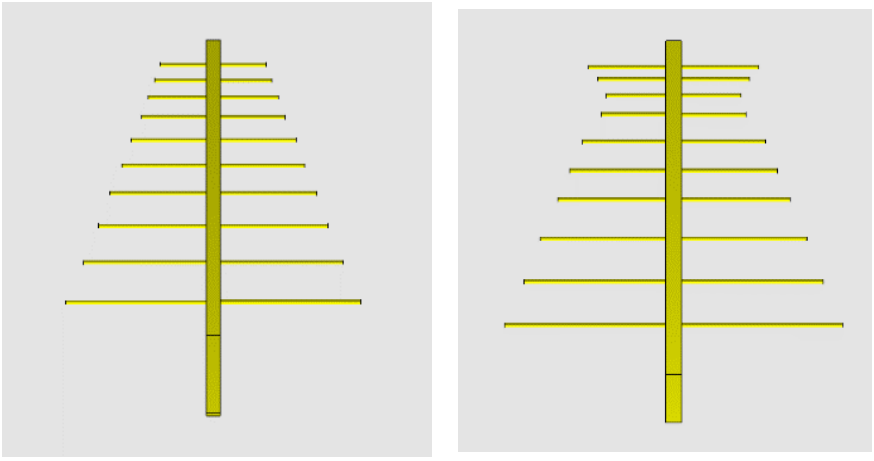

Figure 15. Front view of Carrel's model (left) and the proposed 10-dipole LPDA (right) in the CST.

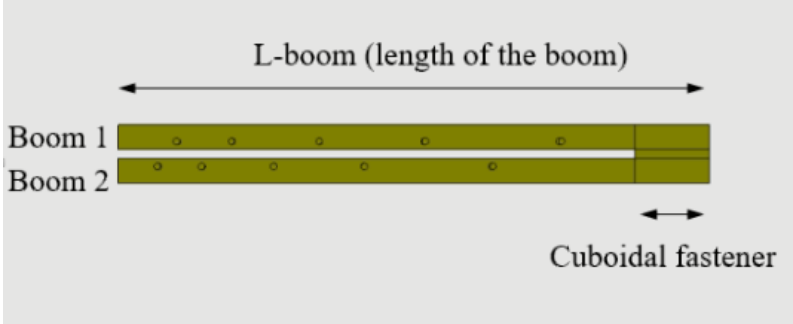

Figure 16. Side view of the proposed 10-dipole LPDA (right) in the CST.

The proposed LDPA design was then fabricated using aluminum, by making sure that it followed the exact dimensions of the design obtained from the optimized CST model, as shown in Figure 17.

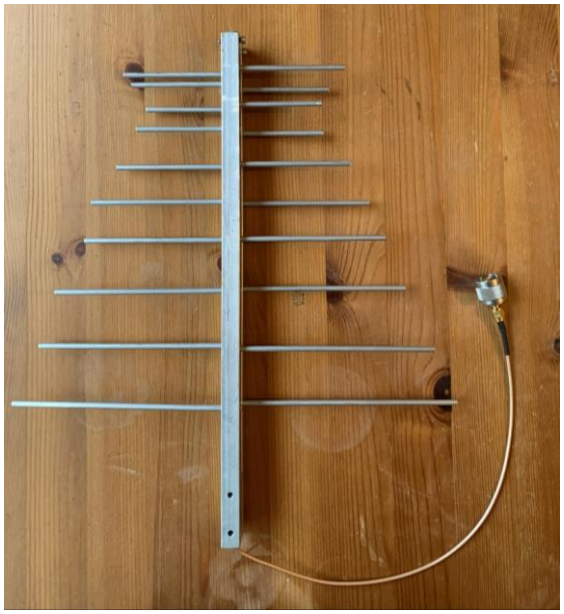

Figure 17. Fabricated optimized LPDA design.

3.2.3 LPDA simulations and measurements

Finite-difference time-domain (FDTD) variants are commonly used in the solution of Maxwell's equations [45, 46]. Here, a Finite Integration Technique (FIT) simulation of this design is performed in CST electromagnetic simulation software with an accuracy of -50 dB

using a hexahedral meshing consisting of 4,668,482 mesh cells. Open boundary conditions were set for the proposed design having a 10^{-4} estimated reflection level. The feeding to the conducting boom was provided by an excitation port with a 50 Ω impedance attached at the front end of the antenna, connecting the two center points of the booms. Farfield monitors were setup with a resolution of 10 MHz starting from 450 MHz to 1000 MHz. All the measurements presented in this chapter were performed in anechoic chambers at the National Physical Laboratory (NPL), Teddington, UK.

The simulated surface current density of the optimized LPDA design at four different frequencies: (a) 470 MHz, (b) 650 MHz, (c) 790 MHz and (d) 1000 MHz are shown in Figure 18. These four frequency points were selected in order to analyse the behaviour of the LPDA at three frequency points in its operating bandwidth (470 MHz – 790 MHz) and at a frequency point in the rejection band (800 MHz – 1000 MHz).

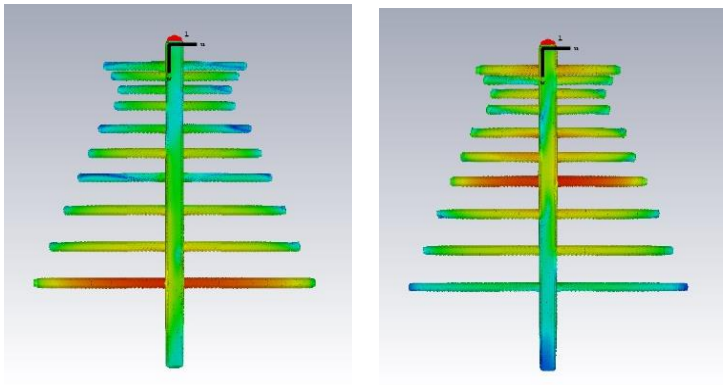

(a) (b)

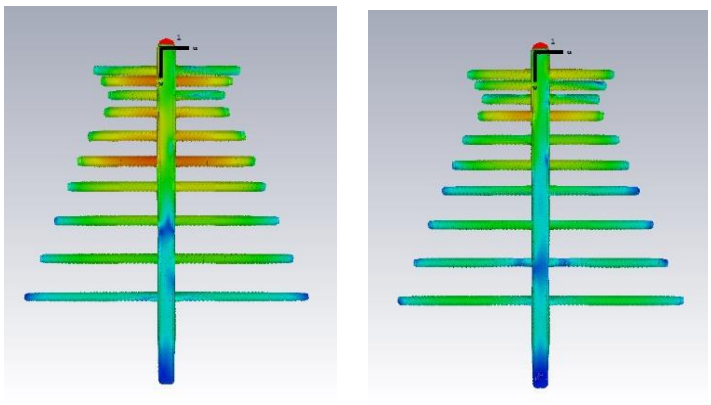

(c) (d)

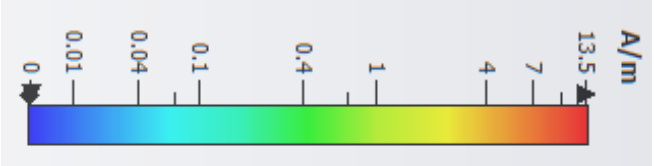

Figure 18. Simulated surface current density of the optimized LPDA at (a) 470 MHz, (b) 640 MHz, (c) 790 MHz and (d) 1000 MHz.

Figure 18 (a)-(d) provide a good evidence of the fact that different dipoles of LPDA provides resonance at different frequencies. In Figure 18 (a), the maximum current density of the LPDA is at the longest dipole as it is responsible for the resonance at the lowest frequency of the bandwidth. Similarly, maximum current density of the LPDA is at the 7th dipole in the case of 650 MHz as it is approximately at the center of the bandwidth. However, in Figure 18 (c), the current density is higher at the 2nd and 6th dipole of the LPDA. This is due to the intentional anomaly created in the LPDA design that traps the energy between these two dipoles, thereby providing the high rejection after this frequency. Figure 18 (d) shows that a minimal current density is observed in the LPDA at 1000 MHz which shows that the antenna does not resonates at this frequency.

Figure 19 presents the comparison of the simulated return loss of the antenna proposed in this chapter with the measured and simulated results of the antenna designed by Carrel's method. The curves suggest that the proposed optimized design provides better matching for the antenna with lower S11 values in the TV broadcasting band (passband) whereas much higher S11 values are observed in the LTE 800MHz and also in the GSM 900MHz mobile service bands (stopband), as compared to the antenna designed by Carrel's method. Consequently, the return loss of the new antenna design demonstrates better rejection in the stopband compared to Carrel's antenna design.

Figure 20 demonstrates the comparison of simulated and measured realized gain achieved by the antenna designed using Carrel's method and the optimized antenna design proposed in this chapter. It is evident from this figure to conclude that the new antenna design achieves a flatter and higher realized gain compared to the Carrel's antenna design. It also shows that the realized gain value is below 0 dBi in the stopband, thereby achieving rejection characteristics from all the angles of arrival of radiation.

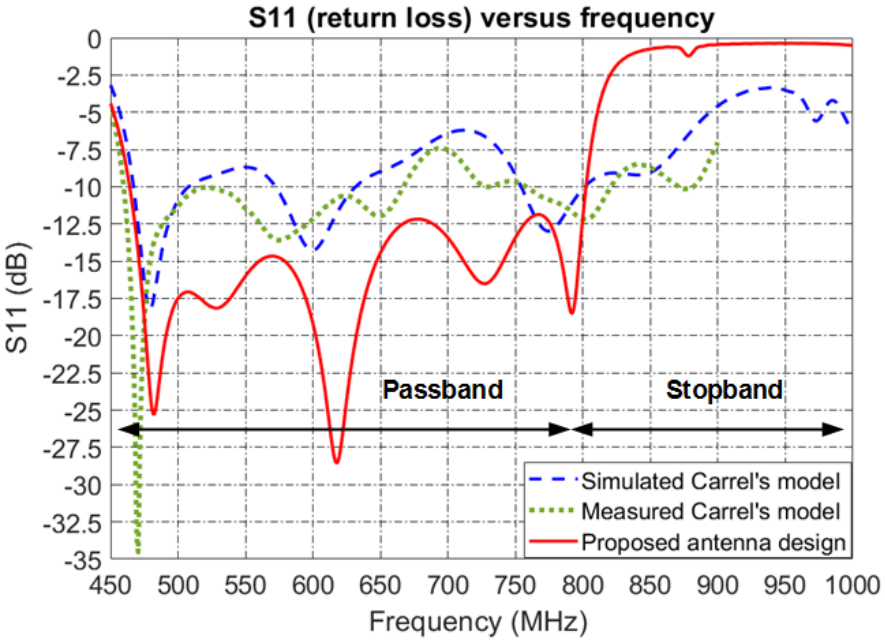

Figure 19. Comparison of return loss of the proposed antenna design with Carrel's design.

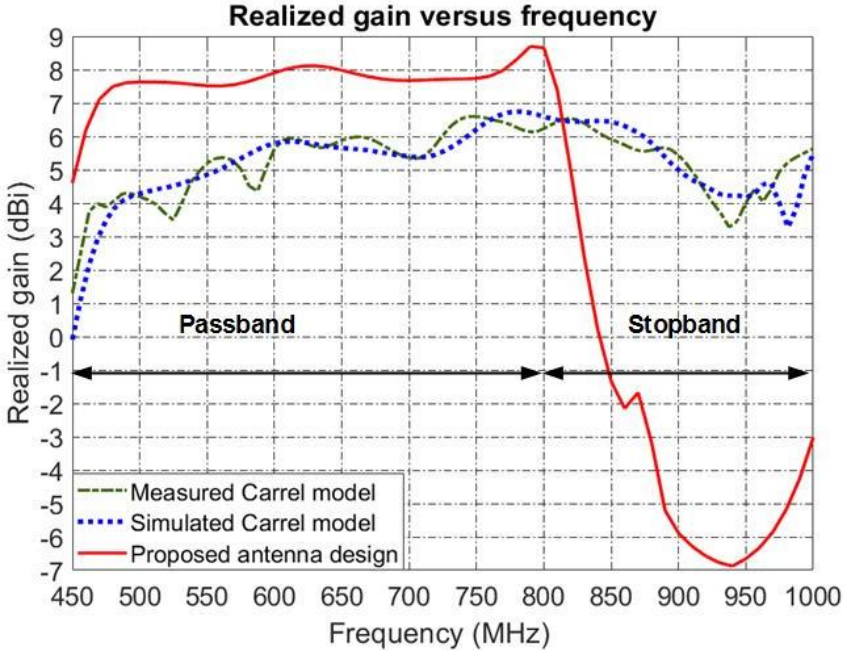

Figure 20. Comparison of realized gain of the proposed antenna design with Carrel's model.

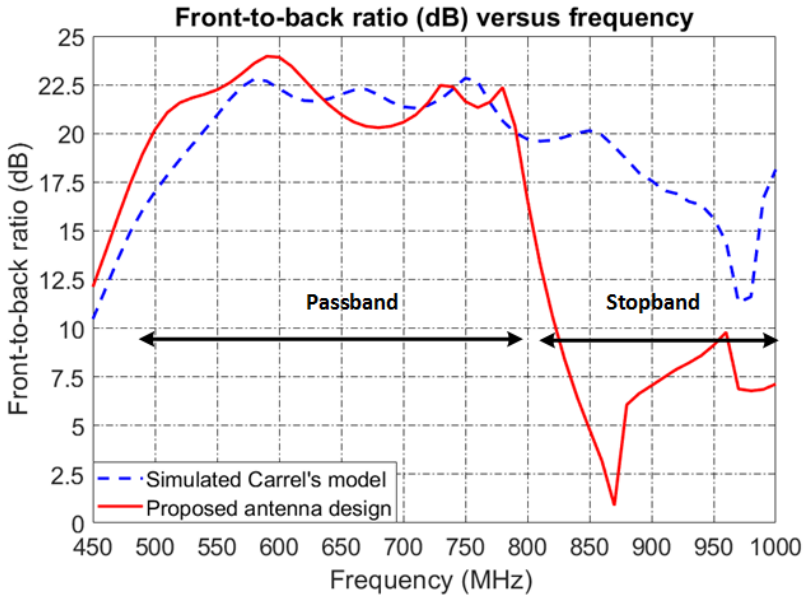

Figure 21. Comparison of front-to-back ratio of the proposed antenna design with Carrel's design.

Figure 21 presents a comparison plot of the simulated and measured front-to-back ratio of Carrel's antenna design and the new antenna design proposed in this chapter. The plot shows that a somewhat better front-to-back ratio is achieved by the new antenna design in the passband.

Figure 22 shows the measurement setup to determine the radiation pattern in the E-plane of the proposed fabricated antenna in an NPL anechoic chamber. In order to calculate the radiation pattern of the fabricated antenna, another reference antenna is required. In this case, the Schwarzbeck USLP-9143B log-periodic antenna was used as the reference antenna. The fabricated antenna and the reference antenna are placed at a separation distance of 2m and both of them are placed 1.2m above the ground. In order to calculate the radiation pattern of the antenna in E-plane, the orientation of both the antennas are such that they are parallel to the ground.

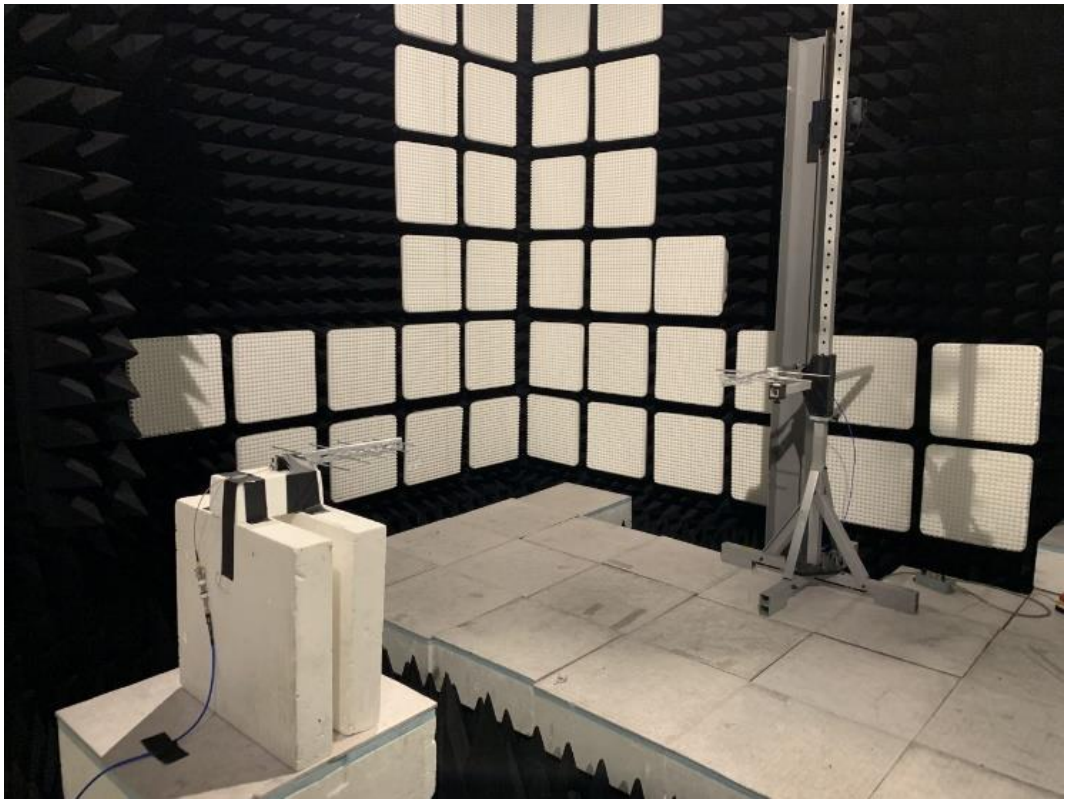

Figure 22. E-plane radiation pattern measurement setup of the proposed fabricated antenna in NPL anechoic chamber.

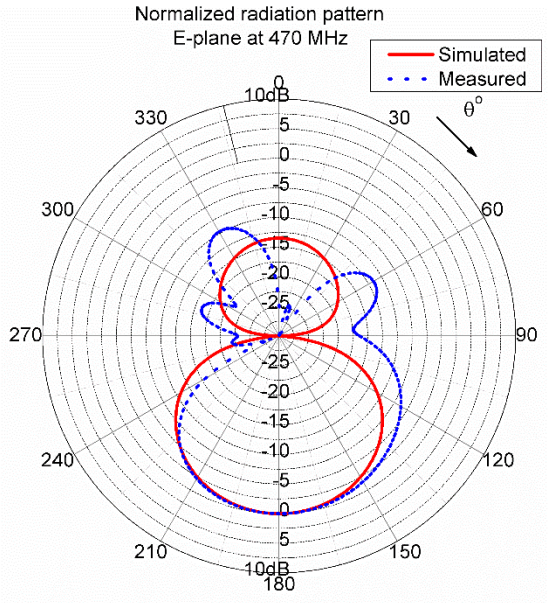

(a)

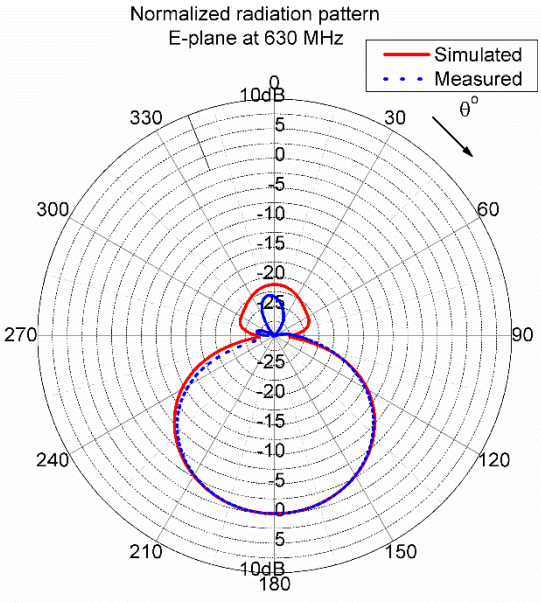

(b)

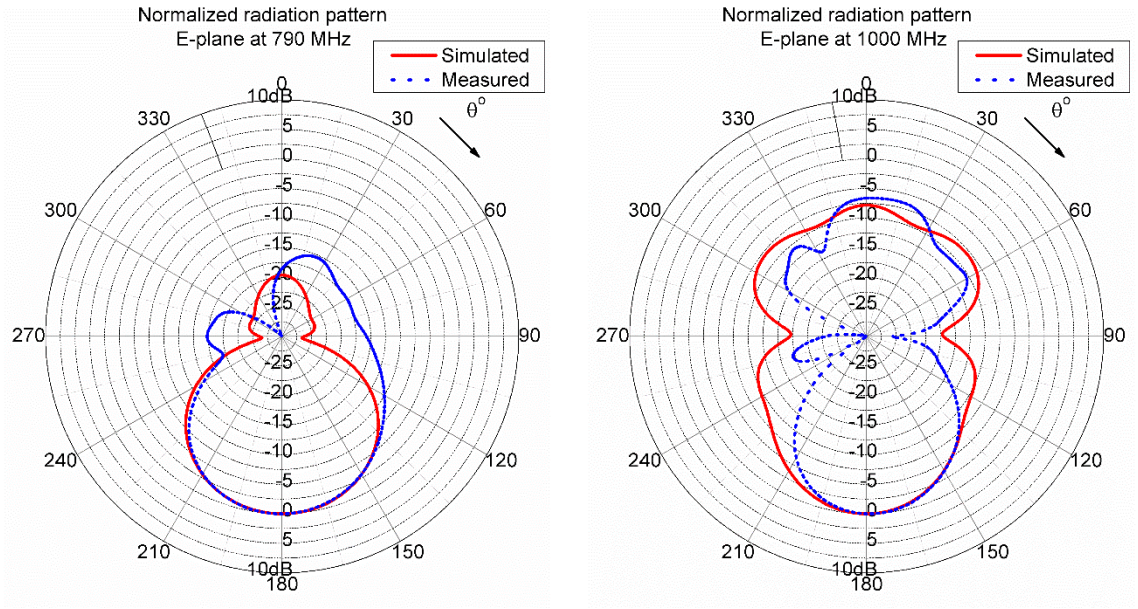

(c) (d)

Figure 23. Measured and simulated radiation pattern in E-plane at (a) 470 MHz, (b) 650 MHz, (c) 790 MHz and (d) 1000 MHz.

Figure 23 shows the comparison of the simulated and measured radiation patterns in E-plane of the optimized LPDA at (a) 470 MHz, (b) 630 MHz, (c) 790 MHz and (d) 1000 MHz. This plot suggests that a good agreement between the simulated and measured results are obtained. It also suggests that the antenna exhibits highly directional behaviour at 470 MHz, 630 MHz and 790 MHz, however, the performance of the antenna degrades at 1000 MHz. Furthermore, the radiation pattern of the fabricated antenna in H-plane was determined by following exactly the same measurement setup as for the E-plane, with the only difference in the orientation of the antennas. For determining the radiation pattern of the LPDA in H-plane, both, the fabricated antenna and the reference antenna were placed perpendicular to the ground. Figure 24 shows the measurement setup for determining the H-plane radiation pattern in an NPL anechoic chamber. Followed by the measurement, Figure 25 shows the comparison of the simulated and measured radiation pattern of the optimized LPDA in H-plane at (a) 470 MHz, (b) 630 MHz,

(c) 790 MHz and (d) 1000 MHz. The radiation pattern plot in Figure 25 validates the good agreement obtained between the measured and simulated results of the proposed LPDA design.

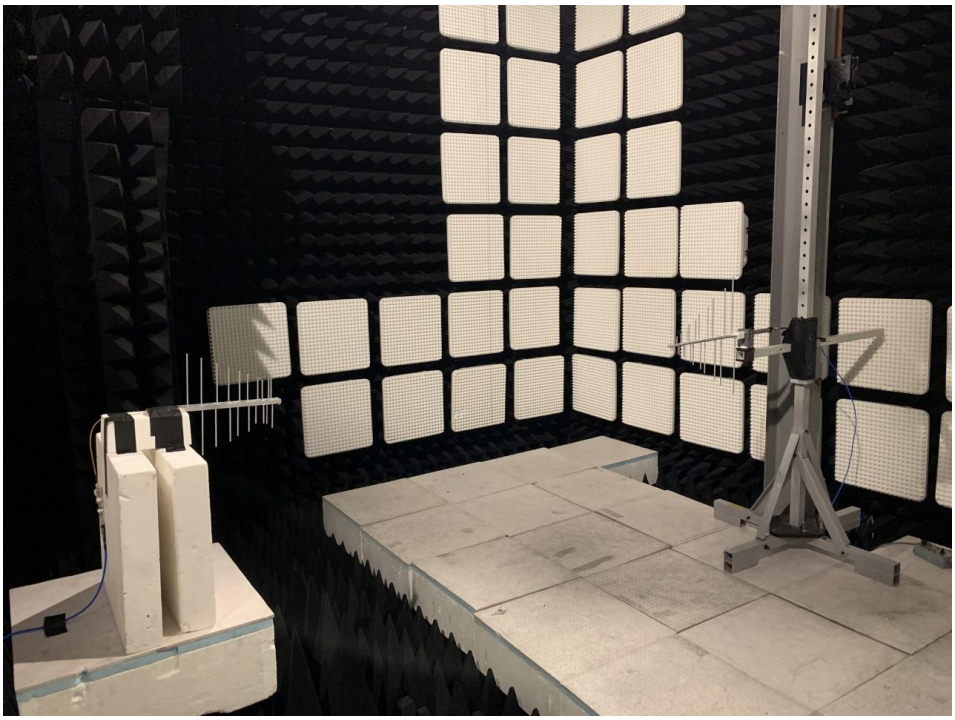

Figure 24. H-plane radiation pattern measurement setup of the proposed fabricated antenna in an NPL anechoic chamber.

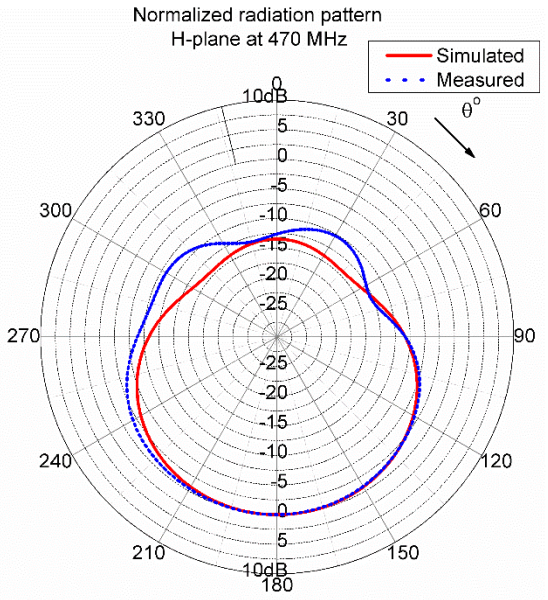

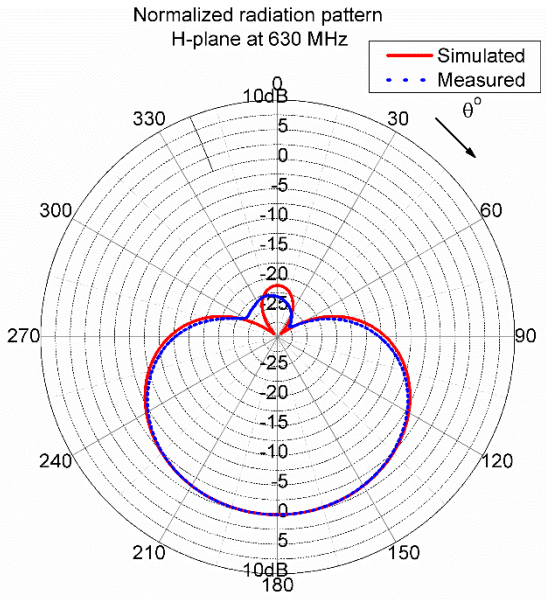

(a) (b)

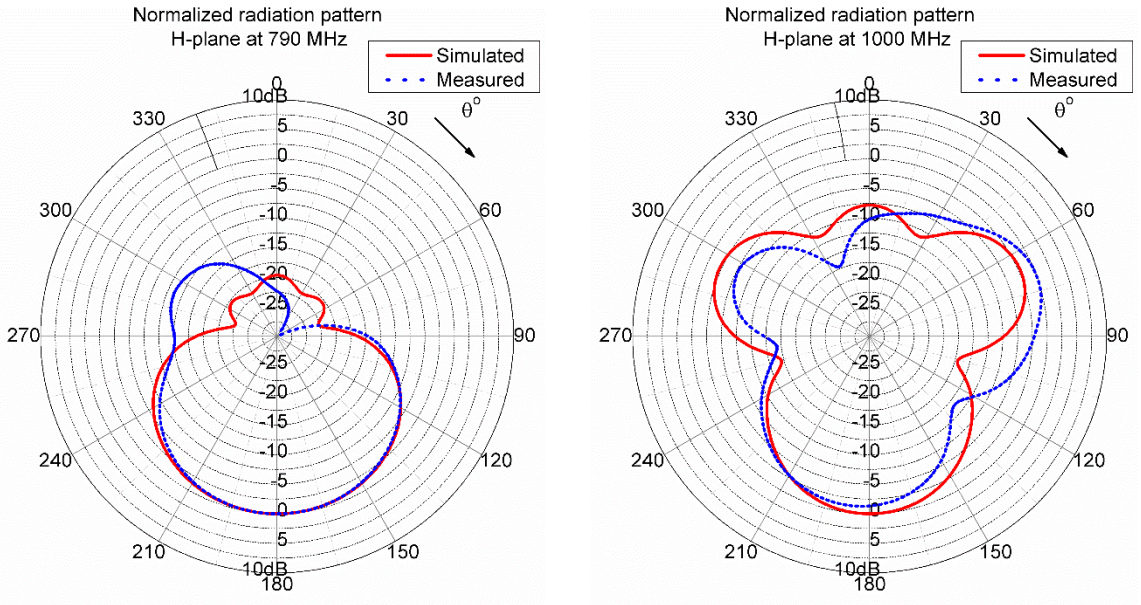

Figure 25. Measured and simulated radiation patterns in H-plane at (a) 470 MHz, (b) 650 MHz, (c) 790 MHz and (d) 1000 MHz.

3.3 Proposed 14-dipole LPDA geometry

Inspired by the antenna designed in previous section, another design of LPDA with 14 dipoles is presented in this section that can reject the LTE mobile services as well as provide higher gain compared to the previous design. This design also provides a solution to solve the interference problems caused due to coexistence of mobile service band with the UHF TV broadcasting band. The work in [6] and [32], suggests that increasing the number of dipoles and increasing the overall length of the antenna, significantly contributes in increasing the antenna gain. Motivated by the antenna design in [12], an LPDA with 14 dipoles is proposed in this section. The arrangement of the first five dipoles of this antenna is responsible to provide the rejection of LTE band. They are arranged in such a way that the length of the 2nd dipole is smaller than the 1st and 3rd dipoles. Furthermore, the length of the 4th dipole is longer than the 3rd and 5th dipoles. After the 5th dipole, all the other dipoles are arranged in the classic design fashion with increasing lengths until the last dipole.

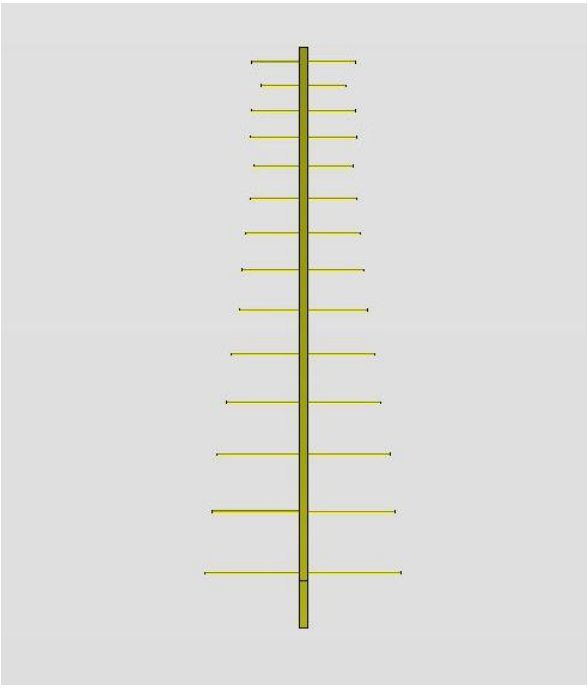

Figure 26. Proposed model of a 14-dipole LPDA with LTE-800 and GSM-900 band rejection.

The distinguished anomaly of first five dipoles is because the smaller dipoles are responsible for the antenna performance at higher frequencies. The overall dimensions of the proposed 14-

dipole LPDA are 985 mm x 320 mm x 41 mm. Since, this antenna has larger number of dipoles and thus longer boom length, the antenna provides higher gain compared to the 10-dipole LPDA.

A cuboidal fastener extending 80 mm long, 14 mm wide and 41 mm high is used at the rear part of the antenna for it to act as a short-circuiting stub as well as a point of support. TRF algorithm was used to optimize this antenna and the dimensions of the optimized design is shown in Table 6 and the CST model of the antenna is presented in Figure 6.

Table 6. Dimensions of 14-dipole LPDA.

Parameters	**Values (mm)**	**Parameters**	**Values (mm)**
Breadth of boom	14	Dipole diameter	4
Length of boom	985	gap	13
Height of boom	14	s0	25
L1	156	s1	40
L2	124	s2	43
L3	156	s3	45
L4	160	s4	49
L5	148	s5	55
L6	160	s6	59
L7	174	s7	62
L8	186	s8	68
L9	196	s9	75
L10	220	s10	82
L11	238	s11	88
L12	270	s12	97
L13	286	s13	104
L14	306		

3.3.1 LPDA measurements and simulations

The proposed 14-dipole LPDA operates in the frequency range from 470 MHz to 790 MHz. The model was discretized using hexahedral meshing technique and consists of 646,380 mesh cells. The simulations were performed with an accuracy of -50 dB. Open boundary conditions were set for the proposed design having a 0.0001 estimated reflection level.

The antenna was feeded using a discrete port with a 50 Ω impedance discrete that connects the center part of both the booms at the front end. Farfield monitors were setup with a resolution of 10 MHz starting from 450 MHz to 1000 MHz.

The fabricated antenna was measured using a Rohde & Schwarz FSH8 portable spectrum analyzer. Figure 27 shows the comparison of the simulated and practically measured return loss of the proposed antenna. The simulated and measured return loss are in good agreement with lower S11 values in its operating TV frequency range (passband). However, the S11 values are higher in the stopband consisting of LTE 800 MHz band and GSM 900 MHz band.

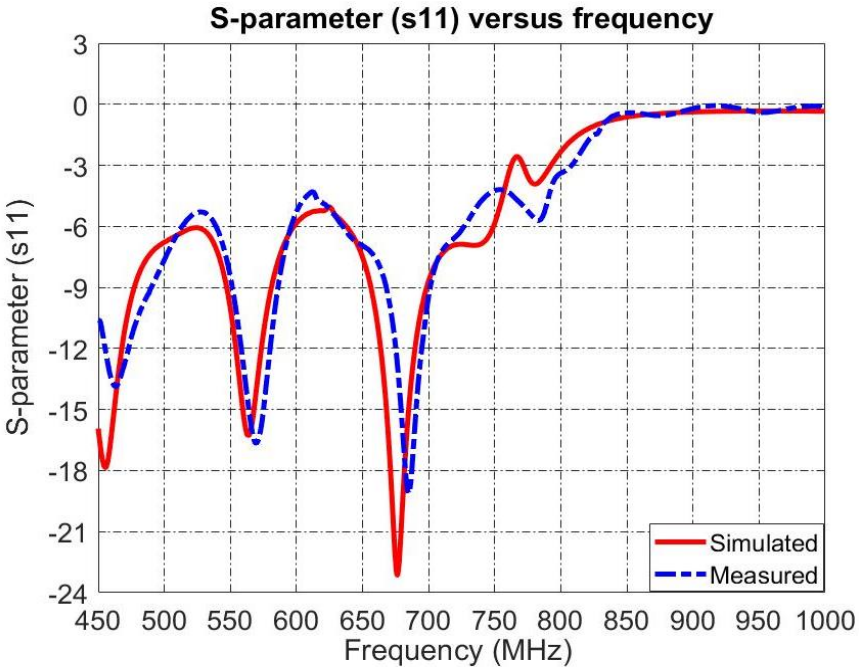

Figure 27. Comparison between the simulated and the measured return loss of the antenna.

Figure 28 shows the simulated realized gain of the proposed antenna. This graph also suggests that the antenna achieves high gain between 9 dBi and 11 dBi in the passband and achieves high rejection in the stopband by achieving a drop in gain to -6 dBi. The realized gain of the antenna demonstrates a higher gain compared to the 10-dipole LPDA [12].

Figure 29 presents the front-to-back ratio of the proposed antenna exhibiting a highly directive characteristics of the antenna with front-to-back ratio between 16 dB and 29 dB in the passband. As expected, the front-to-back ratio drops abruptly below 3 dB in the stopband.

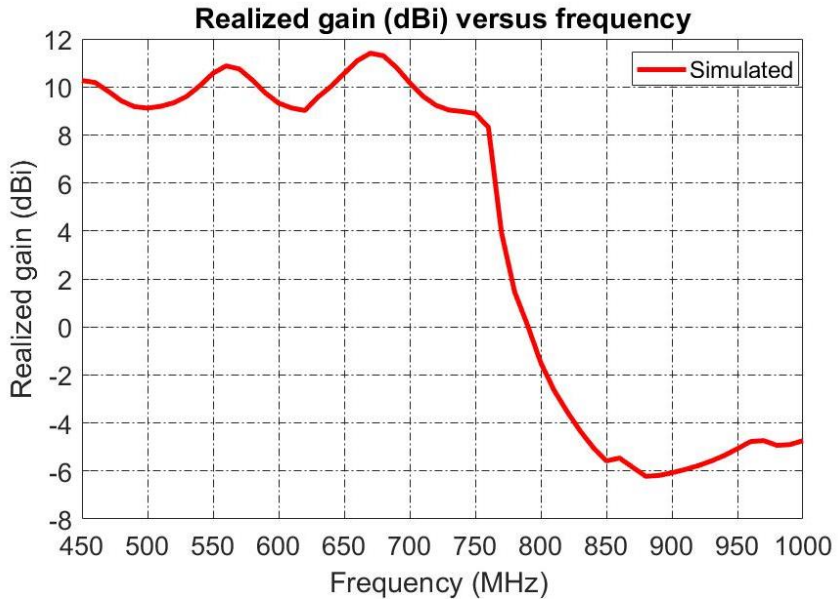

Figure 28. Simulated realized gain of the proposed 14-dipole LPDA.

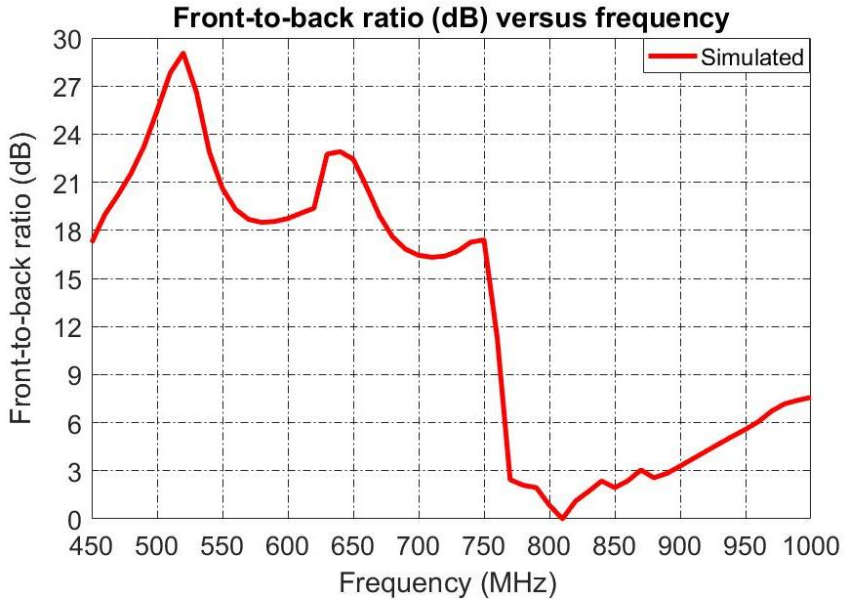

Figure 29. Simulated front-to-back ratio of the antenna.

3.4 Conclusion

The proposed 10-dipole and 14-dipole LPDA designs can be used as a cost-effective solution for UHF TV reception which is capable of rejecting the LTE 800 MHz band as well as the GSM 900MHz band without the addition of costly filters. This could help resolve the interference problem caused due to the coexistence of TV broadcasting services and mobile communications services, thereby enhancing the quality of service (QoS) of UHF TV signals. The proposed antenna design possesses good matching, relatively high and flat gain and highly directional characteristics in the passband combined with a high rejection in the stopband.

Furthermore, because of its wideband characteristics, the LPDAs are significantly used for Electromagnetic Compatibility measurement applications where they are used as reference antennas. However, the LPDAs used for such measurements are bigger in size and therefore, there is a need to have an LPDA with reduced size and still performing well in the desired frequency range. One of the techniques to obtain size-reduction of LPDAs is to use printed LPDA, where an LPDA is printed on top and bottom part of the substrate. The size-reduction obtained in this case depends on the dielectric permittivity of the substrate. Chapter 4 investigates a design procedure for a printed LPDA that can be used for EMC applications with operating frequency range from 0.8 GHz -2.5 GHz

Chapter 4 Printed Log-periodic dipole antennas

This chapter proposes a design methodology for a 12-dipole printed log-periodic dipole antenna (PLPDA). This antenna operates from 0.8 GHz to 2.5 GHz and is designed to be used for Electromagnetic Compatibility (EMC) measurement applications. The TRF algorithm is used to obtain the optimized antenna with low return loss values in order to achieve good matching for the antenna. The optimized design also achieves realized gain between 4.5 dBi and 6.3 dBi in addition to satisfactory front-to-back ratio. The proposed design was also fabricated on an FR4 substrate and the comparison of the simulated and measured return loss of the antenna is also presented in this paper. **A significant part of this chapter has already been published in a conference paper [121].**

4.1 Introduction

A well-designed EMC antenna play an important role in performing accurate EMC measurements [47]. The antennas used for EMC measurements are required to have wideband characteristics, high gain and highly directive characteristics [48-50]. LPDAs have frequency-independent radio electrical characteristics and can also provide flat gain, wideband and highly directional characteristics. Due to this reason, LPDAs are often considered best-suited for such applications [8]. As suggested in [15], they are widely used for high frequency (HF), very high frequency (VHF) and ultra high frequency (UHF) TV reception applications. However, for larger bandwidths, the size of LPDAs are often large and thus printed technologies can be used to design printed log-periodic dipole arrays (PLPDAs) that can provide compact as well as cost efficient solutions.

A design procedure for LPDA is proposed by Carrel in [9]. LPDA consists of a conducting boom to which several dipoles of different lengths are connected. These dipoles are arranged in an increasing order from the front to the rear part of the antenna. Each half-wavelength ($\lambda/2$) dipole resonates at its center frequency. At its resonance condition, the dipoles with greater

lengths than the resonant dipole will act as reflectors, while, the dipoles with smaller lengths than the resonant dipole will act as directors. In this way, the LPDA with varying dipole lengths provide wider operating frequency range for the antenna [10]. The two consecutive dipoles are in out of phase as the dipoles are connected to the feeding line in a crisscross manner [13]. In order to design an LPDA with a desired gain, the selection of spacing factor (σ) and scaling factor (τ) values, can be made using Carrel's graph [15].

A PLPDA is usually designed by printing the conducting parts including the boom and dipoles of the antenna on both the side of the substrate. Phase reversal between the two consecutive dipoles can be obtained by printing the consecutive half-dipoles to the opposite side of the PCB substrate [51]. The input impedance of the PLPDA highly depends on the type of feeding technique used to feed the antenna. Similar to conducting boom in LPDAs, the dipoles are connected to a feeding line in the case of PCB substrate. Usually, these feeding lines are printed on both the side of the PCB substrate that connects the consecutive half-dipoles. Campbell *et al.* in [52] presents a two-layered PLPDA that consists of a stripline conductor as a feed. An alternative approach is used in [51], where the coaxial cable is used to feed the antenna by connecting both the booms together by drilling a hole into the substrate and connecting the front part of the booms using a conducting wire. In this way, the antenna will act as its own balun and thereby provides wideband characteristics. PLPDA can comprise of dipoles of different shapes like rectangular, circular, elliptical, triangular or trapezoidal. The antenna performance significantly depends on the thickness of the substrate material (t_s) , width of feeding line ($w_{feedline}$) , width of dipoles (w_d) , length of dipoles (l_n) and spacing between the dipoles ($s_{n-1,n}$). Like LPDAs, increasing the number of dipoles will increase the gain of the PLPDA.

Several optimization algorithms can be used to improve the PLPDA performance. An optimization to reduce the size of the PLPDA is presented in [53, 54]. Another study that presents a useful comparison of the VSWR of log-periodic Koch dipole antenna and Euclidean PLPDA in [54]. The work suggested in [7], demonstrates a unique feeding technique for a 15-dipole PLPDA that provides lower S11 below -10 dB in the frequency range from 4 GHz to 16 GHz. A design of a compact planar dipole array antenna with gain enhancement technique is demonstrated in [55]. A novel 10-dipole PLPDA using half mode substrate integrated

waveguide (HMSIW) for UWB application that operates from 3.1 GHz to 10.6 GHz is shown in [56]. The optimization time required to obtain best design significantly depends on the type of algorithm selected. Different algorithms like particle swarm optimization (PSO) [42, 57, 58], invasive weed optimization [5, 43], Taguchi optimization [39, 59-61] etc. can be used to obtain the optimized results. A comparative study of the algorithms provided by Computer Simulation Technology Microwave suite (CST-MW) like Trusted Region Framework (TRF), Nelder Mead Simplex algorithm, Classic Powell and Covariance Matrix Adaptation Evolutionary strategy (CMA-ES) has been demonstrated in [62, 63]. Furthermore, the optimization time can be further reduced by selecting appropriate optimization parameters. For instance, in [12], while optimizing a 10-dipole UHF TV reception LPDA to provide band rejection at the LTE-800 band frequencies, only the lengths and spacings of the first four dipoles were considered for optimization.

A design of a 12-dipole PLPDA is presented in this chapter that operates from 0.8 GHz to 2.5 GHz. The antenna achieves good matching with low return loss values below -10 dB and satisfactory gain between 5 dBi and 6 dBi in its operating frequency range. This antenna is designed to be used for EMC measurements.

4.2 PLPDA design procedure

While designing the PLPDA, the most significant parameter that affects the antenna performance are the dipole lengths and the spacings between them. Therefore, it is necessary to first determine the scaling factor (τ) and the spacing factor (σ), so that the dipole lengths and spacings between them can be calculated.

In order to determine the value of τ and σ for a PLPDA that has 5 dBi gain, Carrel's graph [8] is used,

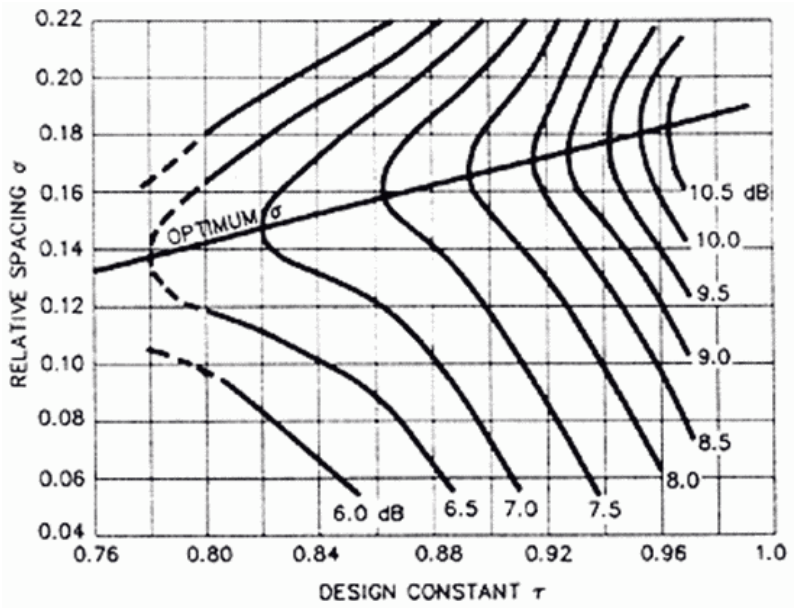

Figure 30. Carrel's graph to determine the gain from scaling factor versus spacing factor curve.

The optimum values for τ and σ can be determined using the intersection points obtained on the line σ = 0.243τ-0.051 depending on the desired gain (G). Furthermore, the number of dipoles "N" required for the antenna, can be evaluated by solving the following expression:

$$N = 1 + \left[\frac{\log B_s}{\log \frac{1}{\tau}} \right] \tag{9}$$

where, B_s is the structure bandwidth which can be calculated as:

$$B_s = \left[\frac{f_{upper}}{f_{lower}} \right] . B_{ar} \tag{10}$$

$$B_{ar} = 1.1 + 7.7(1-\tau)^2 \left[\frac{4\sigma}{1-\tau} \right] \tag{11}$$

where, B_{ar} is the active region bandwidth of the PLPDA.

Since, the antenna performance at the lowest frequency (f_{lower}) depends on the length of the longest element, this value is substituted in (12):

$$L_1 = \frac{1}{2}\left[\frac{c}{f_{lower}}\right] \tag{12}$$

where, c is the speed of light.

The lengths of consecutive dipoles can be determined by:

$$L_{n+1} = \tau . L_n \tag{13}$$

The spacing between the longest dipole and its consecutive dipole can be calculated by:

$$S_1 - S_2 = \left[\frac{L_1 - L_2}{2}\right].\left[\frac{4\sigma}{1-\tau}\right] \tag{14}$$

$$S_{n+1} = \tau . S_n \tag{15}$$

It should be noted that the equations (9) to (15) are used to design an LPDA in free space conditions. However, in case of PLPAs, the effect of dielectric constant of the substrate also need to be considered. A geometry of a PLPDA with n-dipoles is shown in Figure 31, where the effect of dielectric constant of the substrate is also taken into the account. Figure 31 shows a basic geometry of PLPDA with n-dipoles which is designed using equations (9) to (15), taking into consideration the effect of the dielectric constant of the substrate.

In this chapter, a 12-dipole PLPDA that operates between 0.8 GHz to 2.5 GHz is presented. The overall dimensions of the antenna are 150 mm x 160 mm x 1 mm (length x breadth x height). The dipoles of the proposed PLPDA are arranged in such a way that the width of the five short dipoles at the front end of the antenna are equal ($w_{12}= w_{11}= w_{10}= w_9= w_8$), whereas the remaining dipoles have varying width until the longest dipole. The length of the dipoles keeps increasing gradually from the shortest dipole at the front end of the antenna until the longest dipole at the rear end of the antenna. The proposed antenna is printed on FR4 substrate (with dielectric constant $\varepsilon_r= 4.3$) and 1 mm thickness. The width of the feeding line is 1 mm, which is printed on both the sides of the substrate in order to feed the dipoles, thereby providing 180-degree phase reversal.

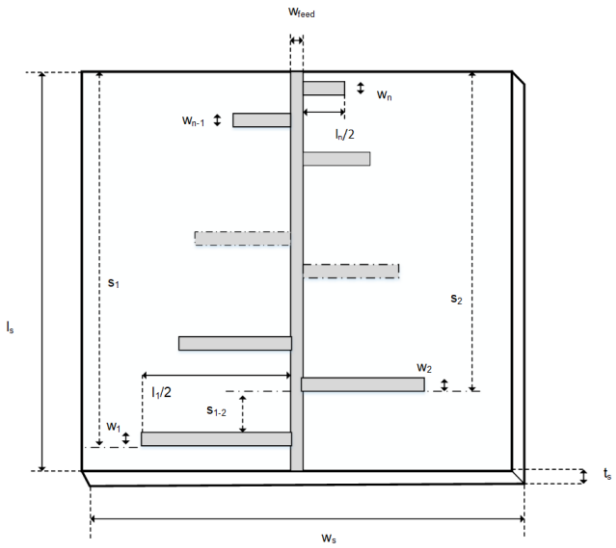

Figure 31. Basic geometry of PLPDA.

The feeding to this antenna can be provided using an SMA connector that is connected to the feeding line at the front end of the antenna. The antenna performance also depends on dielectric constant of the substrate its thickness. A computer-aided design (CAD) model of the proposed PLPDA is shown in Figure 32. The optimized dimensions of the proposed antenna is also shown in Table 7. These dimensions were obtained by optimizing the initial antenna design using TRF algorithm, that was calculated using equations (9) to (15) with the effect of dielectric constant taken into account. The parameters that were considered for the optimization included the length of the dipoles (l_n), width of the dipoles (w_n), spacing between the dipoles (S_{n-1}-S_n), width of the feed line (w_{feed}). Table 9 presents a list of optimization goals with respective weights assigned to each goal.

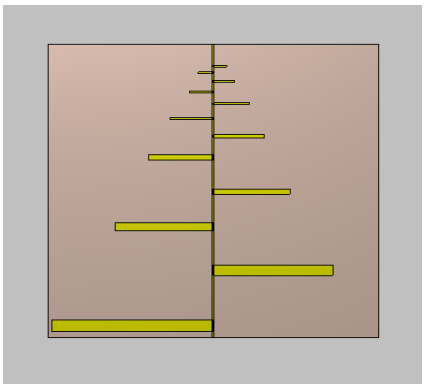

Figure 32. CAD model of PLPDA in CST.

Table 7. Dimensions of the proposed PLPDA antenna design.

Dipoles (n)	**Length of dipoles (l_n) in mm**	**Width of dipoles (w_n) in mm**	**Spacing (S_{n-1} - S_n) in mm**
1	156.3	5.8	3.3
2	115.8	5.3	28.5
3	94.9	3.8	23.0
4	74.1	2.8	18.3
5	62.2	2.7	17.5
6	49.3	1.5	11.3
7	41.9	1.0	9.2
8	34.8	0.9	7.5
9	22.8	0.9	5.7
10	20.5	0.9	5.5
11	14.6	0.9	4.3
12	12.8	0.9	3.5

In Table 7, (S_0-S_1) is the distance between the longest dipole and the edge of the substrate. The overall dimensions of the substrate is 150 mm x 160 mm x 1 mm. The width of the feed (w_{feed}) is 1 mm.

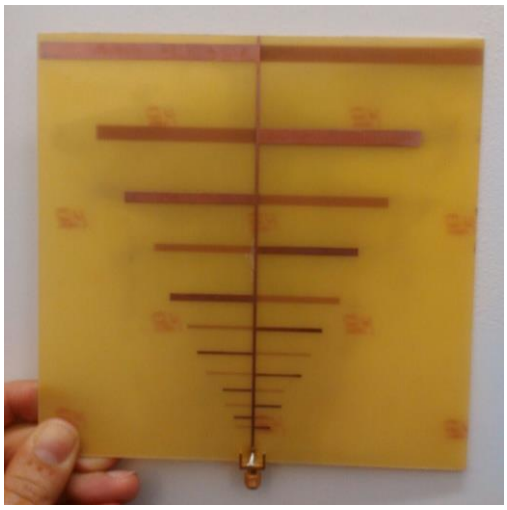

Figure 33. Optimized PLPDA on FR4 substrate.

Figure 33 shows the PLDPA on FR4 substrate with optimized dimensions. The feeding to the antenna is provided using a SMA connector, which connects the feeding line on the either side of the substrate.

4.3 PLPDA simulation and optimization

This chapter presents a design of a 12-dipole PLPDA antenna, whose dimensions were calculated using the equations (9) to (15) and, which was further optimized using TRF algorithm in order to obtain better antenna performance. The model of the calculated PLPDA design was developed and simulated in CST, followed by the optimization. The simulation is performed in time domain with accuracy of -40 dB. The model used hexahedral meshing with 943,500 mesh cells. The simulation was performed in open boundary conditions with estimated reflection level of 0.0001 and minimum distance to the structure set as one-fourth of wavelength at 800 MHz. The feeding to the antenna is provided using an excitation waveguide port attached at the front end of the antenna. The optimization of the calculated initial antenna design was performed using TRF algorithm, that generated a fitness function using the optimization goals and the respective weights for the parameters listed in Table 8. The role of TRF algorithm is to determine the best fitness function value. The settings of the TRF algorithm was setup in such a way that only to vary 20% of the initial value of the design parameter were allowed to alter. The parameters that were considered for the optimization were: length of the dipoles (l_n), width of the dipoles (w_n), spacing between the dipoles (S_{n-1}-S_n), width of the feed line (w_{feed}).

Table 8. Optimization goals.

Parameter	Target	Range (MHz)	Weight
S11	< -12 dB	800-1400	3.0
S11	< -12 dB	1450-1650	10.0
S11	< -12 dB	1700-2500	3.0
Realized Gain	> 3.5 dBi	800-2500	2.5

The optimization of the calculated design of PLPDA started with a fitness function value of 15.8, which improved to 1.5 at the end of optimization.

Figure 34 shows the comparison of S-parameter (S11 in dB) of the simulated and measured proposed optimized PLPDA antenna design in the frequency range of 0.8 GHz to 2.5 GHz. The curve of optimized PLPDA antenna suggests good impedance matching of the antenna, with S11 < -12 dB in the desired frequency range. Figure 35 shows realized gain of the proposed

optimized PLPDA antenna design in the frequency range of 0.8 GHz to 2.5 GHz. The antenna designs offer realized gain between approximately 5 dBi to 6 dBi. The curve suggests that the proposed antenna design provides sufficient gain and the optimization algorithm successfully met expectations.

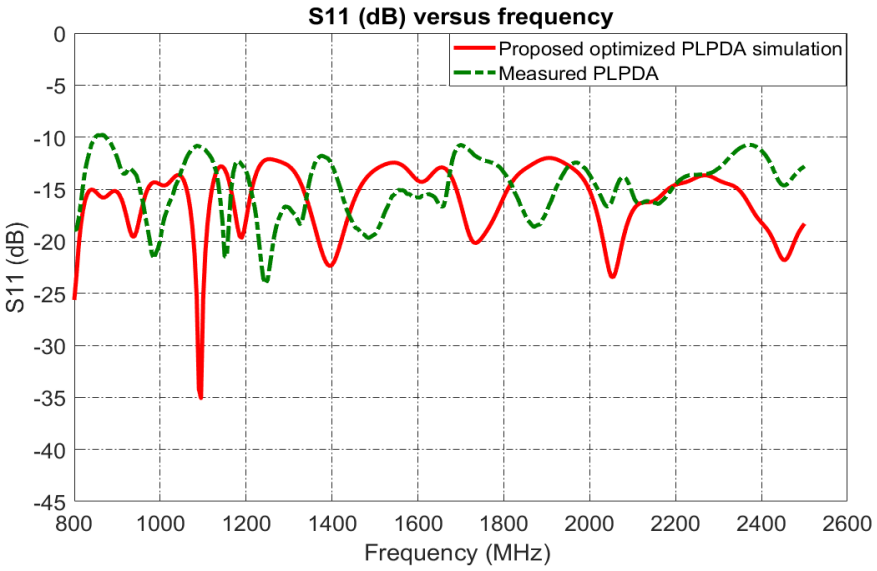

Figure 34. Comparison of S11 of the simulated and measured optimized PLPDA.

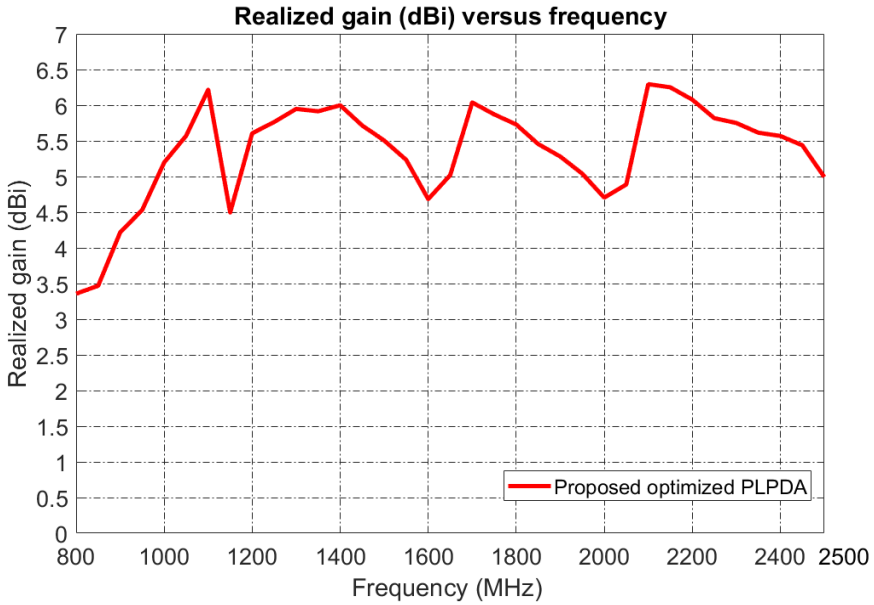

Figure 35. Simulated realized gain of the optimized antenna.

4.4 Conclusion

In this chapter, a 12-dipole PLPDA for L-band EMC application is designed. The optimized model is obtained by optimizing the initial antenna design using TRF algorithm, calculated using LPDA design equations by taking into account the dielectric constant instead of free space conditions. The proposed antenna operates in the frequency range from 0.8 GHz to 2.5 GHz. It also demonstrates low return loss values below -10 dB and provide highly directional characteristics. However, several EMC measurements often involves wider frequency range of operation. Also, at UHF frequencies, the size of PLPDAs are still big and therefore investigation of size-reduction technique is required where the frequency response at the lower frequencies can be improved without significantly increasing the overall size of the antenna. Therefore, several miniaturization techniques are discussed in Chapter 5. Furthermore, Chapter 5 also presents an PLPDA design built by following the design procedure discussed in Chapter 4. This antenna has an operating frequency range from 0.8 GHz to 8 GHz. Furthermore, this antenna design is improved by using a novel size-reduction technique that involves introduction of the triangular longest dipole to the previous PLPDA design and then optimizing it to achieve improved frequency response from 0.4 GHz to 0.8 GHz. This results in an PLPDA design with an operating frequency range from 0.4 GHz to 8 GHz as presented in Chapter 5.

Chapter 5 Miniaturization techniques for PLPDA antenna

With the rapid technological advancements over the last decade, there have been increased demands for new generation wireless devices and communication systems. An ultra-wideband (UWB) frequency range from 3.1 GHz to 10.6 GHz is legislated by the Federal Communication Commission (FCC) for the use of wireless communication systems [64, 65]. Most of the UWB systems require antennas with large bandwidth. Several researches propose utilising monopole antennas for this application [66]. Although some monopole antennas can have wide bandwidth, they do not provide fixed radiation patterns for the entire frequency range and thus an alternative antenna for this application is required. Vivaldi antennas and tapered slot antennas are also considered as good candidates for UWB application because of their stable radiation pattern over the operating frequency range and their ability to radiate or receive power in end-fire direction [67-69]. However, the size of these antennas can be large depending on the lowest operating frequency. Therefore, for such applications, wideband LPDAs are highly preferred because they are directive and provide flat gain, wide bandwidth and can be fabricated at a low cost. Moreover, they radiate in end-fire direction and also provides closely spaced multiple resonances in the operating frequency range.

Additionally, wideband directive antennas are also in huge demand by industrial as well as military organizations for direction finding (DF) applications over a wide range of frequency. Such applications require directive wideband antennas to determine the angle of the originating signal source in the azimuth plane as well as to have the ability to receive the signal over a wide frequency range [70, 71]. Moreover, DF techniques are also used for several civilian applications to track and locate targets. A fixed surveillance system requires a DF antenna in

the form of an array consisting of multiple antenna elements that are arranged in a circular formation. The antenna elements can be among several antenna types like dipole antennas, monopole antennas, bi-conical antennas, log-periodic antennas and Vivaldi antennas. A portable wideband DF antenna is proposed in [70] and [72]. DF antennas have also found its application in the drone market, where these antenna systems are deployed on vehicles as studied in [10] and [73]. LPDA are extensively used for DF applications because of their highly directive radiation pattern resulting in adequate front-to-back ratio in a wide range of frequencies [73]. However, the size of LPDAs is big and thus there is a case for size reduction of this antenna, to make it feasible to be deployed e.g. on drones.

Antennas are also used in anechoic and reverberation chambers for Electromagnetic Compatibility (EMC) measurements, where they are used as a source of electromagnetic waves. Such type of measurement requires the source antenna to be of small size with wideband characteristics [10]. LPDAs are also considered as one of the best candidates for this application.

The concept of frequency independent antennas with wideband operating frequency range was first proposed by Rumsey in [74]. The study conducted by Rumsey, provided the foundation for the origination of LPDA in the later years as suggested in [75]. The design procedure for a conventional LPDA was suggested by Isbell and Carrel [9, 11, 73, 76]. Different variants of LPDA and its characteristics are described in Chapter 1 and 2. Because, LPDAs can operate in a wide frequency range and have the ability to provide flat gain and highly directive radiation patterns, they are promising candidate for applications like UWB communication systems, DF, EMC and radars.

However, it is desirable that for the above applications the size of the antenna should be reasonably small. This puts a limitation on the use of LPDAs as for the lower frequencies the size of some dipole elements is large and thus there is a demand for smaller alternative antennas for such applications. In pursuit of reducing the size of LPDAs, several studies were carried out by designing microstrip PLPDAs [52, 77, 78]. The advantages of designing printed LPDAs (PLPDAs) involve miniaturization and low-fabrication cost. This chapter investigates several miniaturization techniques.

5.1 Miniaturization techniques for size-reduction of PLPDA

Several studies have been carried out and several techniques have been proposed to reduce the size of PLPDAs. This section of the chapter investigates various miniaturization techniques proposed by researchers to reduce the size of PLPDAs.

5.1.1 Top-loading techniques

Top-loading techniques involve addition of different shapes like T-shaped, double T-shaped, hat-shaped, arc-shaped, C-shaped or any other shaped element at the termination of the dipoles of the conventional PLPDA. However, while adding the top-loading element at the termination of the dipole, the physical length of the dipole should be the same as that previous one.

T-top loaded elements and hat-top loaded elements have been proposed and implemented in [79] to design a 48-dipole PLPDA which operates in the frequency range from 0.55 GHz to 9 GHz providing a realized gain of above 7 dBi in the operating frequency range. A convention 48-dipole PLPDA was initially designed with a scaling factor (τ) of 0.935 and a spacing factor (σ) of 0.174 in order to achieve a directivity of 9.5 dBi. However, in an attempt to reduce the length of the overall antenna, the spacing factor was reduced from 0.174 to 0.06 in order to achieve 20% size reduction of the boom length of the antenna, thereby reducing the resulting PLPDA length to 194 mm. Additionally, in order to reduce the overall width of the antenna, T-top loaded elements and hat-top loaded elements were introduced at the termination of the last 6 longer dipoles. This technique has reduced the overall width of the antenna by 27%. The overall dimension of 268 mm x 194 mm (length x width) of the antenna was achieved after implementing this technique. The study presented in this paper also demonstrates that for the same physical length, the resonance at the lowest operating frequency of the straight monopole can be lowered by using T-top loading elements. The resonance obtained in the lower frequency band obtained by introducing T-top loaded elements can be further lowered by introducing the vertical lengths to make it a hat-top loaded element. A simple analysis to support this technique was demonstrated in [79] by designing a straight monopole that

resonates at 1 GHz frequency. After the introduction of a T-top loaded element and a hat-top loaded element to the straight monopole, the resonance shifted from 1 GHz to 0.8 GHz and 0.7 GHz respectively. Therefore, a 35% of size reduction was obtained by introducing hat-top loaded element instead of using a straight monopole to obtain the resonance at 0.7 GHz. However, the limitation of such loading techniques is that it becomes difficult to attain the maximum impedance bandwidth because of the relatively higher Q-factor. Due to this reason, there is a need for bandwidth enhancement techniques to be introduced in the miniaturized version of the PLPDA. Again, in [79], bandwidth enhancement for the miniaturized PLPDA is obtained by introducing a feedline meander, a trapezoidal resistive stub for the modified dipoles and an arrow-shaped balun near the feeding of the antenna.

Another study presents a PLPDA that operates in the frequency range of 8 GHz to 18 GHz [80]. In this study, chamfered C-shaped top loaded elements are introduced to the dipole that acts as an inductive load. This technique suggests that the size of a conventional PLPDA is reduced by 60%. The reduced size of 13-dipole PLPDA with C-shaped loading is achieved with an overall dimension of 33 mm x 9 mm that can provide a realized gain between 6.1 dBi to 7.1 dBi in the operating frequency range [80].

A unique variant of T-shaped top loading in the form of circular -arc T- shaped loading is presented in [81]. This study presents an LPDA capable of operating in the frequency range of 0.82 GHz to 2.09 GHz with an average realized gain of 5 dBi. The approach proposed in [81] claims a reduction in the dipole lengths by 55%. The reflection coefficient of the antenna depends highly on the radius of the circular arc dipole and therefore, optimization of the circular arc radius needs to be done in order to choose the correct radius for the required design. Therefore, a similar approach can be used for PLPDA design.

An interesting study to reduce the width of PLPDA is presented in [82], where a PLPDA is designed to operate in the frequency range of 2.3 GHz to 8 GHz with an average gain of 5-6 dBi. Initially, a 9-dipole conventional PLPDA is designed to operate between 2.3 GHz to 8 GHz. The overall dimension of this conventional PLPDA design was 90 mm x 120 mm. The size of this conventional PLPDA was reduced by modifying the straight dipoles into T-shaped dipoles in such a way that the total length of the dipole does not change. This method provides

50% lateral size reduction of the conventional PLPDA, thereby achieving the dimensions of 45 mm x 125 mm. The size of this modified PLPDA was further reduced by introducing double T-shaped dipoles in such a way that the total length remains the same as the straight dipole. By this technique, 54% size reduction was observed in the modified dipole lengths compared to that of the original dipole elements. The overall dimension of this modified PLPDA design with double T-shaped top loading was found to be 38 mm x 125 mm.

5.1.2 Fractal-iterative technique

An alternate approach to miniaturize the PLPDA, similar to that of top-loading technique, involves the dipole to consist of fractal shapes in such a way that the total length for the current path is extended. Several fractal shapes can be used as suggested in [83]. A detailed comparison of PLPDAs with different fractal shapes and different iterations is shown in [84] for UWB applications. Additionally, a novel design of PLPDA with Giuseppe Peano fractals at the edge of truncated rhombic branches with spiral slots is also proposed in this reference, that can operate in the UWB band of 3.1 GHz to 10.6 GHz with a band rejection in the 5.8 GHz and 8.3 GHz band. The proposed PLPDA also provides a gain of more than 5 dBi in the operating frequency range and also leads to miniaturization of the conventional PLPDA by 11.1%. A comparison of several fractal techniques and their miniaturization percentage is shown in Table 9.

Table 9. Comparison of PLPDAs with different fractal shapes [84].

Reference #	Feeding technique	Fractional Bandwidth	Fractal shape	Miniaturization
[85]	Microstrip	47 %	Koch fractal	12 %
[86]	Microstrip	67 %	Meander line	21 %
[83]	Microstrip	67 %	Non-uniform line	32 %
[84]	HMSIW	109 %	Triangular Koch fractal	11.9 %
[84]	HMSIW	109 %	Square Koch fractal	10.3 %
[84]	HMSIW	109 %	Tree fractal-first iteration	27.1 %
[84]	HMSIW	109 %	Tree fractal-second iteration	35.1 %
[84]	HMSIW	109 %	Giuseppe Peano fractal in rhombus LPDA	11.1 %

*HMSIW= Half-mode surface integrated waveguide

Another attempt to miniaturize the conventional PLPDA was demonstrated in [87] using second-order Koch fractals. This reference shows how higher-order Koch fractals can be generated using four iterations. However, the proposed PLPDA antenna in this reference, used second-order Koch fractals to miniaturize a 9-dipole conventional PLPDA. The proposed PLPDA has reduced dimensions of 90 mm x 60 mm compared to that of the conventional PLPDA whose dimensions were 120 mm x 90 mm. The PLPDA design has the ability to operate from 2 GHz to 8 GHz and demonstrate an average gain of 5.8 dBi.

An interesting approach was suggested in [88], where instead of introducing reactive loading, the concept of non-uniform transmission line (NTL) was introduced in order to miniaturize the conventional PLPDA. This was done by the modulation of impedance profile of the straight dipole elements to a truncated Fourier series using optimized Fourier coefficients. This technique achieved 32 % of size reduction of the straight dipoles. The proposed PLPDA with truncated Fourier-series dipole has an operating frequency range of 2 GHz to 4 GHz and provides a peak gain of 7 dBi.

5.1.3 Truncated boom technique

Most of the miniaturization techniques are applied to the longest dipole of the PLPDA in order to reduce the lateral size of the PLPDA. For instance, Koch Fractalization method in [54, 84], top-loading in [79, 81, 82, 89], metamaterials in [89, 90] are mostly applied to the dipoles so that the lateral size of the PLPDA is reduced. However, a unique and useful approach is proposed in [91] that can be used to reduce the axial size of the PLPDA by reducing the boom length. The authors in [91], propose to use dual-band dipoles instead of single straight dipole. In this way, the number of dipoles required by the PLPDA to cover a wide operating band reduces, which in turn also reduces the boom length. The dual-band dipole is designed in such a way that it has a half-wave principle dipole which is then loaded with an auxiliary dipole that acts as a resistive load. This dual-band dipole then follows the conventional PLPDA pattern. The PLPDA proposed in [91], consists of 25 dual-band dipoles, and the antenna operates in 0.5 GHz to 10 GHz. The proposed design results in 40% size reduction in the total axial length of

the PLPDA compared to that of the conventional PLPDA. Also, the number of dipoles required to achieve same performance would require around 66 dipoles, and this number was reduced to 25 in the proposed PLPDA design. The total axial length in the case of 66-dipole conventional PLPDA was 364 mm and it was reduced to 218 mm in the case of the proposed 25 dual-band dipole PLPDA. Additionally, it was also observed that if a conventional PLPDA of the same length as that of the proposed PLPDA was designed, with reduced spacing factor, the total bandwidth was 58% lesser compared to the proposed PLPDA. The overall dimensions of the proposed PLPDA are 260 mm x 218 mm (lateral length x axial length). The proposed PLPDA uses a Rogers RO4003 as a substrate with dielectric constant of 3.55 and substrate thickness of 0.508 mm. The antenna is claimed to achieve a 5 dBi gain in the entire bandwidth. The only limitation to this technique is that the gain of the antenna is reduced. However, several gain enhancement techniques can be used to increase the gain of the proposed PLPDA antenna.

5.1.4 Reflector ground plane technique for gain enhancement

Several miniaturization techniques result in reduced size of the antenna, however, in several cases the gain of the antenna drops after miniaturization. An interesting approach is presented in [92], where a PLPDA is proposed that has an operating frequency range of 3.3 GHz to 20.7 GHz with an average gain of 6 dBi. The PLPDA design consists of 17 dipoles that follow the conventional PLPDA design. In addition to this, a ground plane is added after the longest dipole on both the side of the substrate. This ground plane acts as a reflector and thus provides increased gain for the antenna. The antenna was fabricated on an FR-4 substrate with dielectric constant of 4.4 and substrate thickness of 1.6 mm. In addition to this, the authors also demonstrate an interesting approach to provide band rejection in the operating bandwidth using U-shaped notches. A U-shaped slot is placed on the boom of the antenna and its position is optimized until the required band rejection is obtained. The design proposed in this paper makes use of a U-shaped slot that has dimensions of 6.87 mm x 2.6 mm in order to achieve a rejection in the 5.8 GHz WLAN band.

A similar approach to increase the gain of an PLPDA is proposed in [93], where a substrate integrated waveguide (SIW) is used after the longest dipole. The SIW acts as a reflector that leads to an increase in gain. Furthermore, the gain of the PLPDA was further increased by

adding parasitic patches after the end of the shortest dipole, which act as directors. This approach involves the idea of combining the benefits of log-periodic antennas and quasi-yagi antennas. The proposed antenna is designed to operate from 40 GHz to 50 GHz and in addition to this, it is also claimed to achieve a gain between 9-12.6 dBi. The technique of combining quasi-yagi and log-periodic designs provides a gain enhancement of around 2.5 dB to 3.4 dB compared to the conventional PLPDA [93].

5.1.5 Dielectric loading technique

A novel and useful technique to miniaturize the conventional PLPDA using two-stepped dielectric materials by adopting the dielectric-loading technique is presented in [94]. The PLPDA proposed in this reference can operate in the frequency range of 200 MHz to 803 MHz and provides a gain greater than 4 dBi. The design proposed in this study suggests utilising 22-sinusoidal dipoles instead of straight dipoles. The reason to use sinusoidal dipoles is that they provide extended current paths and can also provide a resonance at lower frequencies as compared to straight dipoles. A Polyflon substrate of dielectric constant of 2.55 and loss tangent of 0.0011 is used to fabricate the antenna. The thickness of this substrate is 3 mm. The uniqueness of this design is that it includes a 2 mm thick layer of air that is partially loaded within this substrate. The additional size reduction of the antenna is obtained by using a two-stepped dielectric material of dielectric constant of 10 and loss tangent of 0.0035 that is used to cover the antenna from both sides. Furthermore, four parasitic elements are added at the end of the first two sinusoidal dipoles in order to implement the capacitive loading technique to reduce the size of the antenna. The overall size of this antenna is 420 mm x 576.6 mm x 29.6 mm. Since, this antenna has high power handling capacity, it can find applications in airborne platforms.

5.1.6 Folded-planar helix (FPH) dipole

There have been successful attempts to miniaturize the PLPDA by replacing the straight dipoles with different sized and/or shaped dipoles to reduce the lateral size of the antenna. However,

most of these techniques lead to a deterioration of gain. A similar, yet useful, approach is proposed in [95], where the straight dipoles are replaced with folded planar helix (FPH) dipoles. Implementing this technique leads to a reduction of the dipole size by 39%. In addition to that, it leads to a deterioration of gain by only 0.2 dB, which is much smaller compared to other miniaturization techniques. The proposed PLPDA had an operating frequency range of 400 MHz to 800 MHz. An initial design was achieved by replacing the longest straight dipole with a FPH, which lead to size reduction by 18.2%. However, when two FPHs were used, the size was further reduced and a total reduction of 39% was obtained compared to the conventional PLPDA. This technique also gives an improvement in the front-to-back ratio of the antenna and achieves a gain of 5.5 dBi. Both the proposed antennas are designed on an FR4 substrate with a dielectric constant of 4.4 and substrate thickness of 3.2 mm. The overall dimensions of the proposed PLPDA with 1 FPH are 445 mm x 364 mm which is the reduced version of the conventional PLDPA whose dimensions were 445 mm x 445mm. The reduced version was obtained by replacing 2 dipoles with 2 FPHs which resulted in the reduced overall dimensions to 445 mm x 300 mm. Further reduction was obtained by using a meander dipole between the 2 FPH elements leading to the overall dimensions reduced to 445 mm x 273 mm.

5.2 PLPDA design for 0.7 GHz - 8 GHz

This section presents a wideband 25-dipole PLPDA that has an operating range from 0.7 GHz to 8 GHz. The antenna dimensions are derived using traditional PLPDA equations described in Chapter 4. The antenna design was required to provide a gain of above 5 dBi in its entire operating range and thus in order to satisfy the bandwidth and gain specifications, 25 dipoles were selected. Similar to traditional LPDAs, this PLPDA also consists of dipoles that are arranged in an increasing fashion from the front to the back part of the antenna. The only difference is, a dielectric substrate (FR4) with relative permittivity of 4.3 is present between the top and the bottom boom. Therefore, it can be suggested that the top boom and the dipoles attached to it are embedded on the top part of substrate, while the bottom boom and the dipoles attached to it are attached to the bottom part of the substrate. The thickness of the substrate is

1mm. The feeding is provided to the antenna using a coaxial cable that is connected to the top boom using solder paste. The conducting part of the cable is soldered to the start of the bottom boom through a drilled hole. The overall dimensions of the proposed antenna are: 250 mm x 170 mm x 1mm. The simulated and the fabricated model of the antenna is shown in the Figure 36.

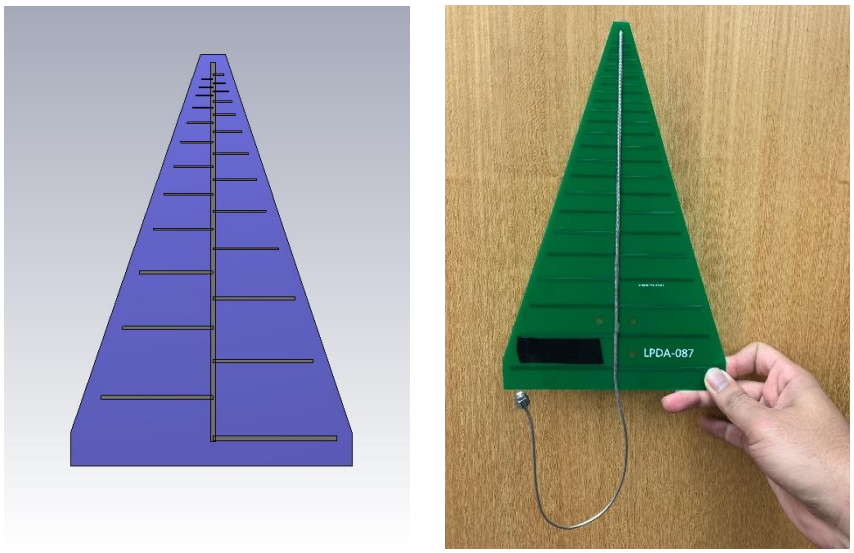

Figure 36. CST model (left) and fabricated model (right) of the proposed antenna.

The CST model consisted of 10,625,384 mesh cells with the smallest cell size of 0.35 mm. The simulation of this model was performed in time domain with -50 dB accuracy. The dimensions of this antenna are listed in Table 10.

Table 10. Dimensions of the proposed PLPDA.

Proposed PLPA design					
Parameters	***Values***	***Parameters***	***Values***	***Parameters***	***Values***
L1	5 mm	L14	22 mm	d1	0.5
L2	5.5 mm	L15	25 mm	d2	0.5
L3	6 mm	L16	28 mm	d3	0.5
L4	7 mm	L17	30.5 mm	d4	0.5
L5	8 mm	L18	34.5 mm	d5	0.5
L6	9 mm	L19	38 mm	d6	0.6
L7	10 mm	L20	43 mm	d7	0.7
L8	11 mm	L21	48 mm	d8	0.8

L9	12 mm	L22	53 mm	d9	0.9
L10	14 mm	L23	59 mm	d10	1 mm
L11	16 mm	L24	66 mm	d11	1 mm
L12	18 mm	L25	73 mm	d12	1 mm
L13	20 mm	s13	7 mm	d13	1 mm
s0	7 mm	s14	7 mm	d14	1 mm
s1	2 mm	s15	8 mm	d15	1 mm
s2	2 mm	s16	9 mm	d16	1 mm
s3	2 mm	s17	10 mm	d17	1 mm
s4	2 mm	s18	11 mm	d18	1 mm
s5	2 mm	s19	13 mm	d19	1 mm
s6	3 mm	s20	14 mm	d20	1.5 mm
s7	3 mm	s21	16 mm	d21	2 mm
s8	3.5 mm	s22	18 mm	d22	2 mm
s9	4 mm	s23	20 mm	d23	2 mm
s10	4.5 mm	s24	22 mm	d24	2.5 mm
s11	5 mm	L-boom	230 mm	d25	3 mm
s12	6 mm	H-boom	35 µm	W-boom	3 mm

where,

L_n = length of n^{th} dipole
s_n = spacing between n^{th} and $(n+1)^{th}$ dipole
d_n = width of n^{th} dipole
L-boom = length of the boom
W-boom = width of the boom
H-boom = thickness of the boom (equivalent to copper clad thickness in this case)

Figure 37 presents a comparison of the simulated and the measured return loss of the proposed antenna design. The graph suggests that antenna has low return loss below -10 dB in its entire operating frequency range from 0.7 GHz to 8 GHz. Thus, the antenna achieves good matching. Moreover, the graph also suggests that the simulated results are generally in good agreement with the measurements.

Figure 38 shows a comparison of the simulated and the measured realised gain of the antenna. The antenna achieves a flat gain of approximately 5.5 dBi in its operating frequency range. The measured and simulated results are in good agreement.

The gain of the antenna was measured using the two-antenna method. A picture showing the gain measurement setup is shown in Figure 39.

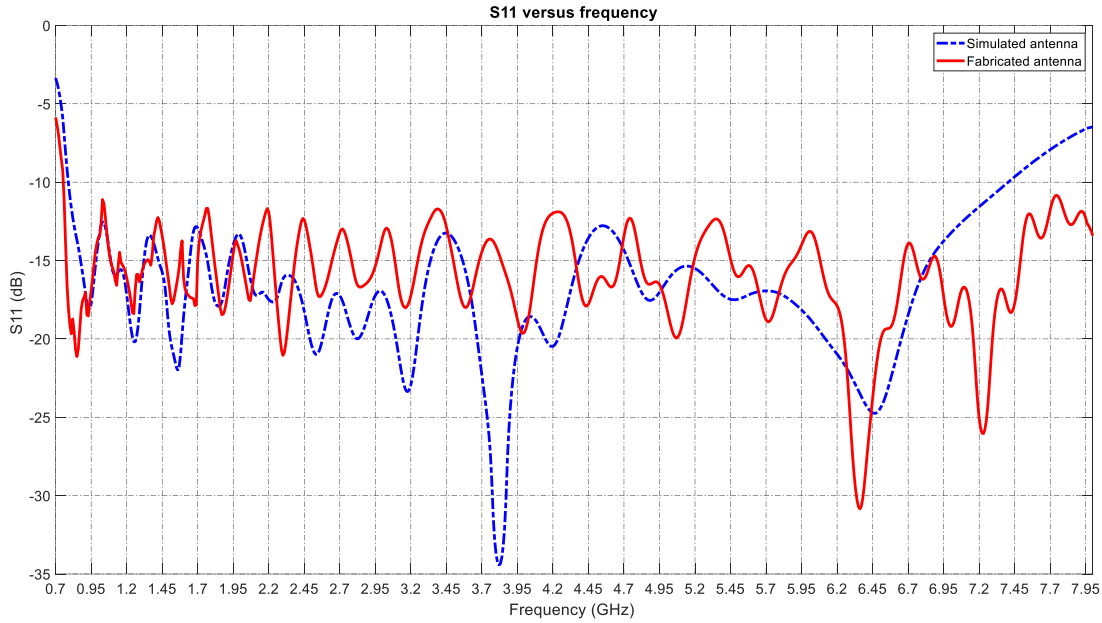

Figure 37. Comparison of the simulated and fabricated S11 of the proposed antenna design.

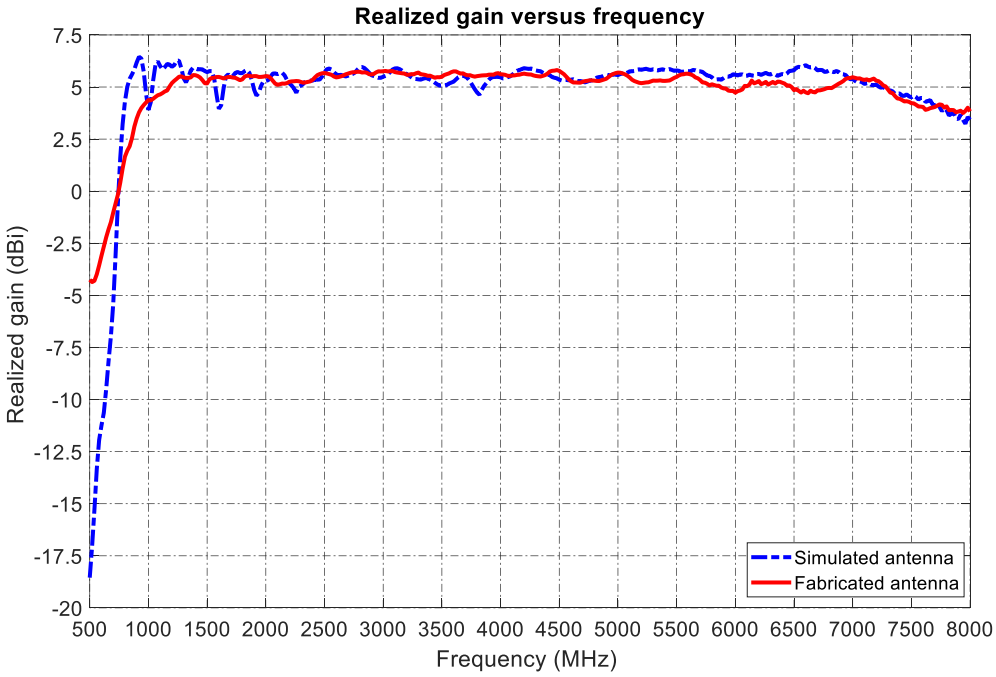

Figure 38. Comparison of the simulated and the fabricated realized gain of the proposed antenna design.

Figure 39. Gain measurement setup for the proposed PLPDA.

5.3 Novel PLPDA design for 0.4 GHz to 8 GHz

In order to increase the bandwidth of the antenna proposed in section 5.2 towards the lower frequencies, a novel antenna is proposed in this section that operates in the frequency range from 0.4 GHz to 8 GHz. From the understanding of the traditional PLPDAs, it is clear that the performance of the antenna at lower frequencies depends on the last few dipoles. Therefore, the longest straight dipole was replaced by a triangular dipole in order to increase the gain and bandwidth of the antenna. With the introduction of the new dipole, an optimisation of the last four dipole lengths, last three spacings and last four dipole widths was performed. The optimisation goals were to obtain S11 below -12 dB and a higher gain above 5.5 dB between 0.4 GHz to 1.2 GHz. The remaining frequencies were not considered as the optimisation would not significantly affect the frequencies higher than 1.2 GHz as only the last four dipole dimensions were considered for the optimization. The optimization goals can be clearly visualized in Table 11.

Table 11. Optimization goals.

Parameters	Goals	Frequency (MHz)	Weight
S11	< -12 dB	0.4 GHz – 1.2 GHz.	5.0
Realized gain	> 5 dBi	0.4 GHz – 1.2 GHz	5.0

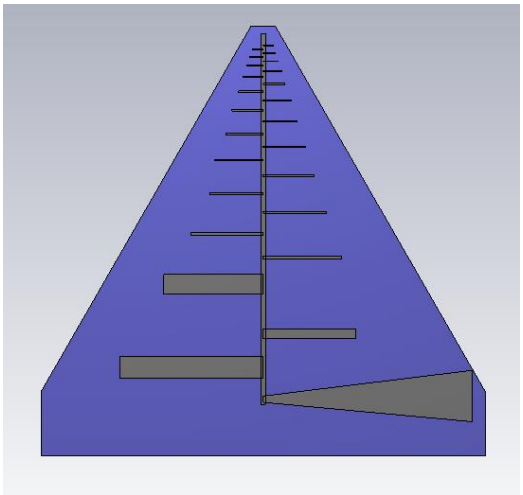

Figure 40. CST model of the proposed antenna design.

Figure 40 shows the CST model of the optimized antenna. The model consisted of 92,452,080 mesh cells with smallest cell unit of 0.35 mm. The simulations were performed in the time-domain with a -50 dB accuracy. The overall dimensions of the optimized PLPDA are 270 mm x 279 mm x 1 mm. The dimensions of the optimized antenna are shown in Table 12.

Table 12. Dimensions of the optimized PLPDA.

Proposed PLPA design					
Parameters	***Values***	***Parameters***	***Values***	***Parameters***	***Values***
L1	5 mm	L14	22 mm	d1	0.5
L2	5.5 mm	L15	25 mm	d2	0.5
L3	6 mm	L16	28 mm	d3	0.5
L4	7 mm	L17	30.5 mm	d4	0.5
L5	8 mm	L18	34.5 mm	d5	0.5
L6	9 mm	L19	38 mm	d6	0.6
L7	10 mm	L20	43 mm	d7	0.7
L8	11 mm	L21	48 mm	d8	0.8
L9	12 mm	L22	53 mm	d9	0.9
L10	14 mm	L23	59 mm	d10	1 mm

L11	16 mm	L24	66 mm	d11	1 mm
L12	18 mm	L25	73 mm	d12	1 mm
L13	20 mm	s13	7 mm	d13	1 mm
s0	7 mm	s14	7 mm	d14	1 mm
s1	2 mm	s15	8 mm	d15	1 mm
s2	2 mm	s16	9 mm	d16	1 mm
s3	2 mm	s17	10 mm	d17	1 mm
s4	2 mm	s18	11 mm	d18	1 mm
s5	2 mm	s19	13 mm	d19	1 mm
s6	3 mm	s20	14 mm	d20	1.5 mm
s7	3 mm	s21	16 mm	d21	2 mm
s8	3.5 mm	s22	18 mm	d22	2 mm
s9	4 mm	s23	20 mm	d23	2 mm
s10	4.5 mm	s24	22 mm	d24	2.5 mm
s11	5 mm	L-boom	230 mm	d25	3 mm
s12	6 mm	H-boom	35 µm	W-boom	3 mm

Figure 41 presents simulated return loss of the proposed PLPDA. It suggests that the antenna has a good matching with low S11 values below -10 dB in most of the operating frequency range. Further improvement of return loss is required at lower frequencies.

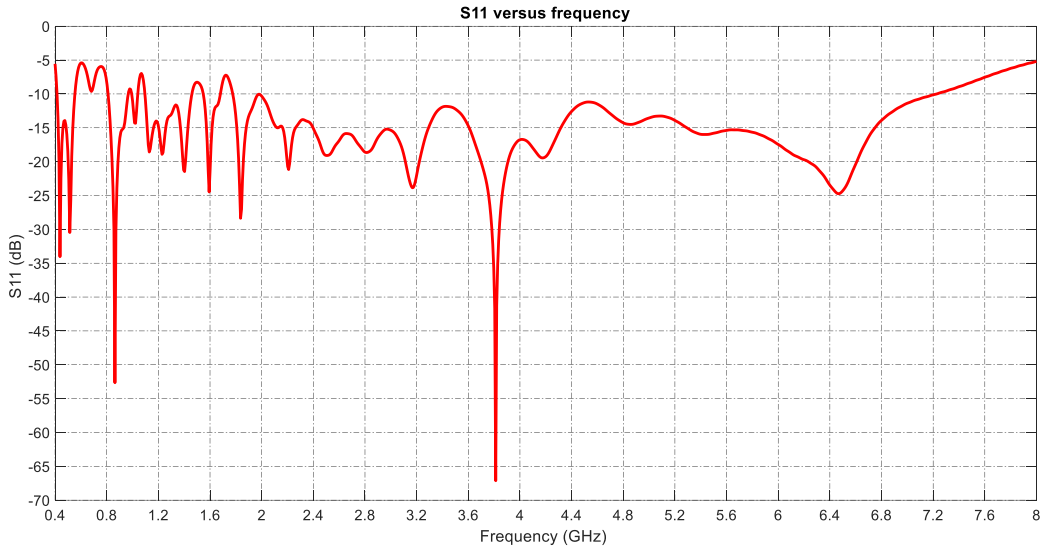

Figure 41. Simulated S11 of the proposed antenna.

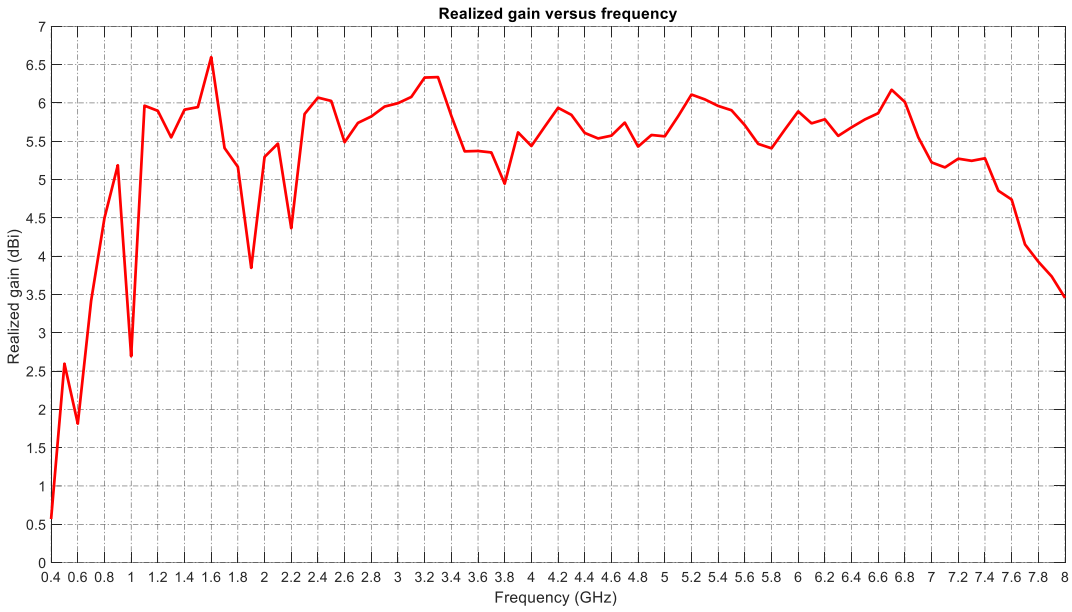

Figure 42. Simulated realized gain of the proposed antenna.

Figure 42 shows the simulated realized gain of the proposed antenna. The graph suggests that antenna provides a gain of above 5.5 dBi in most of its frequency range, however, lower values of gain are observed from 0.4 GHz to 1 GHz. The performance of the proposed antenna can be further improved by investigating and introducing other gain enhancement techniques and re-optimizing the antenna.

5.4 Conclusion

This chapter reviews several miniaturization techniques to reduce the size of PLPDAs. Two prototypes of PLPDA are proposed that operate in a wide bandwidth. The first prototype proposed was a 25-dipole PLPDA that operates from 0.7 GHz to 8 GHz and provides a gain of above 5.5 dBi. The second prototype is an optimized design of the first prototype that includes a triangular longest dipole instead of the straight dipole. Replacing the shape of the longest dipole and optimizing the lengths, diameters and spacings of the last three dipoles provided a higher bandwidth compared to the first prototype. The optimized design operates from 0.4 GHz to 8 GHz and provides a gain of above 5 dBi. The TRF algorithm was used to optimize both prototypes. The LPDAs and PLPDAs are significantly used for gain measurements. However,

the antennas designed for VHF and UHF operations are big in size. For gain measurements, the antenna under test and the reference antenna are placed in such a way that they face each other and are separated by a specific distance. Ideally, this distance should be approximately the farfield distance of the antenna. However, the farfield distance for the antenna at VHF and UHF frequencies is significantly big. Therefore, in actual measurement setup, the farfield distance is not used and repetitive measurements are conducted at different distances so that the gain of the antenna can be accurately determined. Chapter 6 provides a novel modification to this gain determination technique where instead of repeating the measurements, the whole measurement setup is created in CST, and the S21 simulations are performed in order to determine the optimal distance of separation between the test antenna and the reference antenna that can be used for actual measurement. This technique not only reduces the time taken for measurements but also reduces the labour required for the measurement setup.

Chapter 6 Accurate antenna gain determination using the two-antenna method

This chapter demonstrates a simulation-assisted measurement technique to determine the gain of an antenna accurately in an open test site or anechoic chamber. The proposed technique is based on the two-antenna gain measurement method using Friis equation in far-field free-space conditions, with the actual measurement test setup modelled in CST Studio Suite for simulation. An LTE-reject UHF TV log-periodic dipole antenna is used to validate the gain measurement technique in this paper. The simulation of the two-antenna gain measurement method is used in order to estimate an appropriate minimum separation distance between the two antennas that needs to be used for actual measurements to ensure far-field free-space conditions. Determining this minimum separation distance using several simulations instead of actual measurements saves time and effort because it eliminates the need to perform measurements at various separation distances. The measured realized gain obtained using this technique provides a good agreement with the simulation and thus validates the accuracy of this technique. **A significant part of this chapter has already been published in a conference [162]**.

6.1 Introduction

Measuring the gain of an antenna accurately is a very challenging task and is most commonly performed in an environment with non-reflecting characteristics like in an anechoic chamber or an open test site [96]. Measurements that are performed in anechoic chambers provide excellent free space antenna gain estimates, however, such measurements are expensive and also require the size of the chamber to be sufficiently large compared to the wavelength of the antenna under test (AUT). In addition to this, it also requires taking into consideration the type

of absorbers that are used on the floor and on the walls, depending upon the frequency range of the measurements. This contributes in making the measurements in the anechoic chamber an expensive and time-consuming process [97]. Therefore, for such cases, a cheaper yet effective alternative to anechoic chamber measurements is to perform the measurements in an open test site. Performing the measurements at an open test site location requires to ensure that the selected site has low-noise. The reflections due to the ground may lead to inaccurate results and thus installing diffraction fences on the ground surface helps in reducing the ground reflections [97]. The IEC CISPR 16 on Electromagnetic Compatibility (EMC) describes the height scan measurement technique which involves determining the height where constructive interference occurs in order to reconstruct the direct wave using the measured values of constructive and destructive interference [98]. However, this technique is difficult to implement for directive antennas like log-periodic antennas because the vertical beam is narrow in this case. Another unique technique to eliminate the effects of ground reflections was proposed in [99], where time-domain pulses with duration and rise time of the order of 50 ps were generated in order to characterize the performance of antenna in the desired frequency range. The Antenna Time-Domain Measurement (ATDM) technique promises to reduce the duration of measurement compared to the frequency-domain measurements and the hardware implementation of this technique is described in [99]. Another alternative to reduce the effect of ground reflections is to perform an inverse Fourier transform on the data obtained through frequency-domain measurements as described in [100] and [101]. However, these techniques are not applicable in case the AUT is a narrow-band antenna. The reason behind this is that narrow band antennas produce time-domain responses that are much longer than the propagation delay of reflections. As a solution to this, a study in [102] suggested that narrow-band antennas could be measured in reverberation chambers with the help of statistical model of propagation. One of the accurate and cost-effective ways of measuring the gain of an antenna is by using two-antenna method combined with a distance scan method. This method has been implemented to determine the gain of UHF log-periodic directional antennas in [103] that were designed to be used for a transhorizon propagation measurement campaign [104]. The idea of the distance scan method was introduced after a helicopter measurement campaign was performed in order to characterise VHF broadcasting antennas in [105] However, finding the appropriate distance for the separation between two identical antennas in order ensure far-field

conditions as well as to minimise ground reflections is a challenging and time-consuming task. Therefore, in this paper, an accurate antenna gain estimation technique is proposed as a modification of the two-antenna method, where the appropriate distance between the two antennas is determined using the simulation of the test setup performed in CST Studio Suite. Furthermore, the accuracy of the antenna gain measurements can be improved by considering the exact phase centre of the antenna [106, 107], which may depend on frequency. The gain determination of an LPDA by considering the phase centre is demonstrated in [108]. Additionally, the numerical investigation of the field regions of wire based antenna systems and the study of boundaries of near and far field regions in the simulations is described in [109, 110] respectively.

6.2 Two-antenna method

The two-antenna method is a measurement technique that uses the Friis transmission equation to determine the gain of an antenna [111] in the far-field. This technique requires two samples of test antennas that are geometrically and electrically identical. The two identical antennas are separated by a distance in such a way that they face each other and are at the same height from the ground. One of the antennas will act as a radiating antenna and the other antenna will act as a receiving antenna. It should be made sure that the antennas are well matched in terms of impedance and polarization. A Rohde & Schwarz FSH8 portable spectrum analyzer was used to determine the power transferred from Antenna-1 to Antenna-2. The Friis Transmission equation is used to determine the gain of the antenna using the measured transferred power as shown in:

$$\frac{P_r}{P_t} = \left(\frac{\lambda}{4\pi R}\right)^2 G_t G_r \tag{16}$$

where, $G_t = G_r = G$

G_t= gain of the transmitting antenna

G_r= gain of the receiving antenna

This equation can be re-written in terms of dB as:

$$G_{dB} = \frac{1}{2}\Bigg[\underbrace{20\log_{10}\left(\frac{4\pi R}{\lambda}\right)}_{\text{FSPL}} + \underbrace{10\log_{10}\left(\frac{P_r}{P_t}\right)}_{\text{s21}}\Bigg] \tag{17}$$

where,

G_{dB}= Gain of AUT in dB
R= distance between two antennas
P_t= transmitted power
P_r= received power
λ= wavelength
FSPL= Free-Space Propagation Loss

The S21 recorded by the spectrum analyzer and the accurate distance between the antennas will provide the gain of the antenna using equation (17). However, the only drawback of this technique is the estimation of the minimum distance between the antennas in the far-field that will provide less ground reflections and thus more accurate results. Inappropriate estimation of this distance may lead to inaccurately measured gain. Therefore, usually several measurements are recorded varying distance by moving one of the antennas away from the other. The measurements performed in [8], involved recording several measurements by varying the distance between the two antennas from 2 meters to 20 meters. This is a time-consuming process. The technique proposed in this paper provides a modification to this two-antenna method, where this distance can be estimated correctly using simulations of the test setup in CST Studio Suite, thereby reducing the overall time of measurements.

6.3 Antenna under test

To validate the measurement using the two-antenna method, a 10-dipole log-periodic antenna (LPDA) was used as a test case. This log-periodic antenna is a directional antenna that is used for ultra-high frequency (UHF) TV reception and has an operating frequency range from 470

MHz-790 MHz. This LDPA is a modified version of a traditional 10-dipole LPDA that has the capability to reject the LTE-800 MHz band and GSM-900 MHz band. The rejection capability was obtained by optimizing the traditional 10-dipole LPDA, and the design procedure is demonstrated in [12]. This optimized design is used in this paper to demonstrate the two-antenna method for determining the realized gain of the antenna. The CST model of the antenna is shown in Figure 43. Another variant of LPDA has also been proposed in [33] using Particle Swarm Optimization with velocity mutation algorithm (PSOvm).

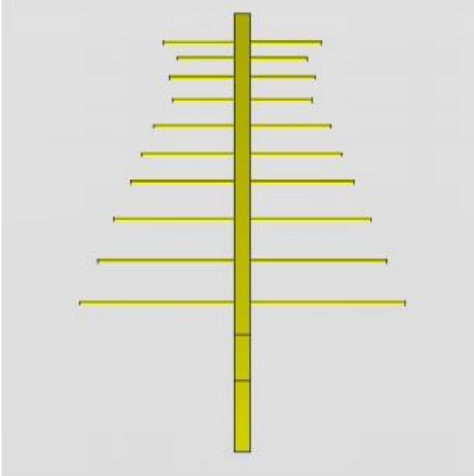

Figure 43. CST model of 10-dipole LPDA used as the AUT.

However, this antenna was further optimized using the Trusted Region Framework (TRF) algorithm [63] in CST Studio Suite and described in [34].

6.4 Proposed simulation-assisted antenna gain measurement

In order to validate the two-antenna method and find the appropriate far-field distance R (in meters) between the two antennas for the two-antenna method, an identical setup was created in the simulation software. This was done by creating an identical model of the AUT and placing it at a distance R. The top view of the test setup in the simulation software is shown in Figure 44.

The model of this setup consists of hexahedral meshing with a minimum of 2,244,156 mesh cells and a maximum of 4,838,556 mesh cells for 1m and 5m separation distance between the two antennas respectively. The simulation was performed in the time domain in order to obtain the power transferred from one antenna to the other. Several simulations were performed by varying the distance R between the two antennas from 1m to 5m in order to obtain a good estimation of the minimum distance that would provide accurate free-space far-field results.

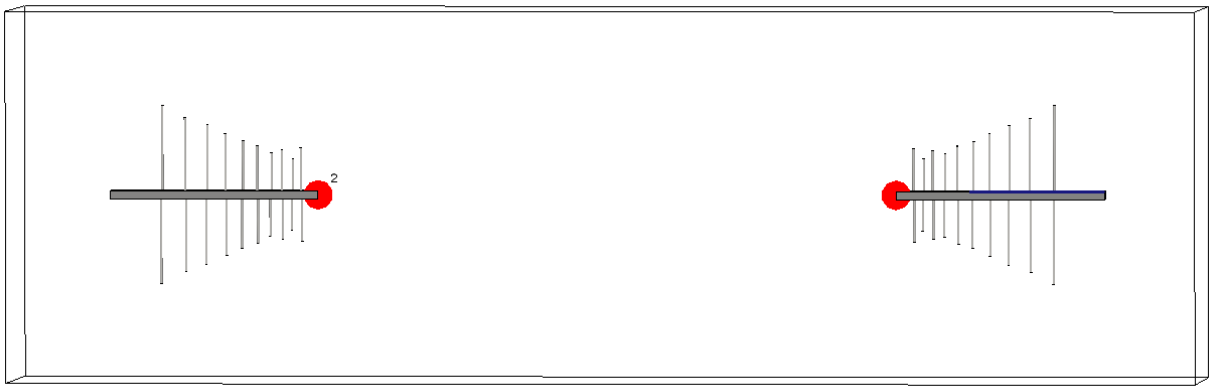

Figure 44. Top-view of the measurement test setup modelled in CST simulation software.

After estimating the distance R between the two antennas in simulation, the actual measurement setup for the two-antenna method was created. A distance of 1.5 meters was considered for the distance between the two antennas to be used for the actual measurement setup. The two-identical antennas were mounted on two separate wooden stands and were placed at the same height in such a way that both the antennas faced each other. The wooden stands with the antennas were separated by R=1.5 meters, that was obtained from simulation. The power transferred from antenna-1 to antenna-2 was measured using an FSH8 Rohde & Schwarz spectrum analyzer. The value obtained from the spectrum analyzer was then used to calculate the realized gain of the antenna using equation (17).

Figure 45 shows the comparison of the measured and the simulated S21 or the power transferred from antenna-1 to antenna-2. The plot is an evidence of the good agreement obtained between the measured and simulated results. The values from this plot were then used to calculate the realized gain of the antenna. Figure 46 shows the comparison of the simulated and measured realized gain of the AUT. The plot shows good agreement between the

measurement and simulation results. The graphs present reasonably high gain in the UHF reception range from 470 MHz to 790 MHz. The antenna demonstrates a high-rejection capability in the LTE-800 MHz and GSM-900 MHz band as expected.

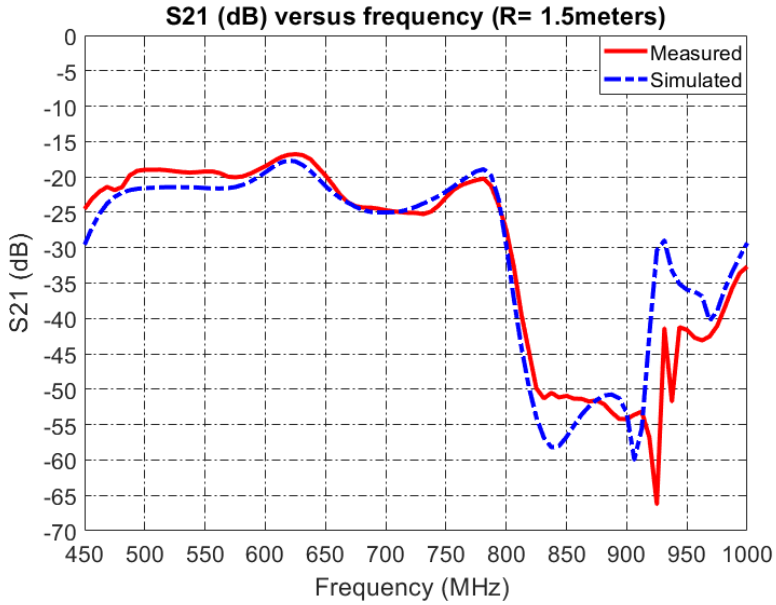

Figure 45. Measured and simulated S21 of the AUT.

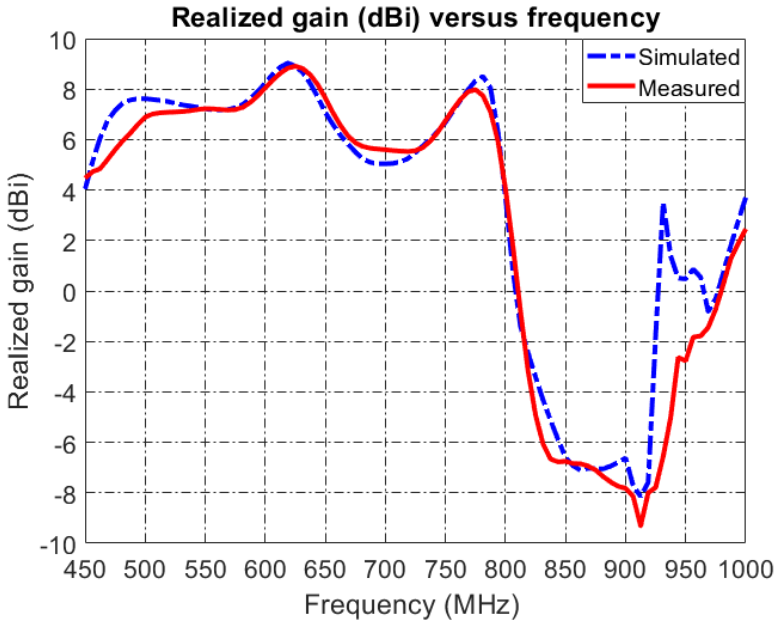

Figure 46. Measured and simulated realized gain of the AUT.

6.5 Conclusion

An improvement of the two-antenna method is presented in this paper using measurements and simulations. This paper also proposes a useful technique using CST simulation to estimate the distance between the identical antennas to be considered for the measurement setup in order to achieve accurate measurement results. The realized gain of the AUT obtained using simulation and measurement demonstrates a good agreement. The LPDAs and PLPDAs discussed in chapters so far, are linearly polarized. However, several satellite applications require circularly polarized antennas to eliminate the polarization mismatch loss. Although, circular polarization can be obtained through LPDA by using orthogonal LPDAs, but these designs are complex as well as bulky. Therefore, patch antennas are considered as good candidate for such applications where circular polarization is required. They are relatively easier to design and fabricate. Therefore, Chapter 7 focusses on designing circularly polarized elliptical patch antennas for GPS and Iridium applications.

Chapter 7 Dual-band Circularly polarized antenna

Circularly polarized antennas are very effective in avoiding polarization mismatch losses and thus improve the connection reliability between satellite communication devices. This chapter presents a compact and cost-efficient design of elliptical edge-fed circularly-polarized dual-band patch antenna that facilitates Global Positioning System (GPS) and Iridium applications like search and rescue operations. The design of a circularly-polarized antenna is a challenging task and requires special feeding like the edge-fed technique. The proposed antenna is modelled in CST Microwave Studio environment and is optimized using an innovative algorithm called Parallel Surrogate Model Assisted Differential Evolution for Antenna Synthesis. It has also been fabricated using Rogers RT 5880LZ laminate and exhibits a behavior in good agreement with the simulated results. The antenna has small dimensions and provides low S_{11}, a realized gain above 5 dBi and satisfactory axial ratio in both L1 GPS and Iridium bands. **A significant part of this chapter has already been published in a conference [143].**

7.1 Introduction

In the past decade, there has been a rapid development in the field of satellite communications that led to an increasing demand for compact and cost-efficient wireless devices. The use of miniaturized antennas can significantly reduce the size of wireless devices. Some applications for such antennas are search and rescue operations, fire-fighting, military, health monitoring systems and space applications [112]. However, the reduction of the antenna size can be a complex problem because it degrades the antenna performance [113]. Another issue that increases the complexity of these wireless communications systems is battery life. The antenna performance has a significant impact on the battery consumption of such systems. A low

performance antenna consumes more power in order to maintain the radiated power at a desired level and may lead to shorter battery life [114].

In satellite communications, antennas are utilized for both, transmission and reception. Unmatched polarization of transmitting and receiving antennas may lead to significant polarization mismatch losses. However, this problem can be overcome by using circularly polarized antennas [115]. Since most of the satellite antennas transmit circularly polarized waves, the use of circularly polarized antennas at the receiving end provides reception at higher level than that of a linearly polarized antenna. Moreover, by using linearly polarized antennas, the connection might be lost if the user moves to a position where there is no direct line of sight [114]. On the contrary, the use of circularly polarized antennas eliminates the requirement for antennas being in direct line of sight. Due to these advantages, mobile satellite communication systems, including Global Positioning System (GPS) and Iridium, utilize circularly polarized antennas.

Circular polarization can normally be achieved using a crossed dipole, a helix or a microstrip patch antenna. Microstrip patch antennas, provide several advantages like low profile, compact size, light weight and low cost in manufacture, and therefore they are good candidates for providing circular polarization [116]. There have been studies, where microstrip patch antennas with circular polarization were used for rescue operations [117], health monitoring systems [118], fire-fighting operations [119], and military applications [120]. Microstrip patch antennas have also been used for several EMC applications like those described in [121] and [122]. They are extensively used for dual-band applications like C and X bands described in [123], L and C band given in [124], L and X band given in [125], Wi-Fi bands (2.44 GHz and 5.51 GHz) given in [126], and finally L1 and L2 GPS bands given in [127]. A novel dual-band fractal monopole patch antenna for operation in 700 MHz and 2600 MHz Long Term Evolution (LTE) bands is proposed in [128], where 24% size reduction is achieved in the optimized design compared to the initial standard quarter-wave resonant monopole by using Particle Swarm Optimization (PSO). A miniaturized dual-band head-implanted antenna design is presented in [129] for medical implant communication services (MICS) and industrial, scientific and medical (ISM) applications. Circularly polarized microstrip wearable patch antennas have also been designed for GPS in [130, 131]. Furthermore, antennas operating in the GPS and/or

Iridium band have been proposed in [132] using a square patch as well as in [112] and [114] using a rectangular patch. An analysis on the performance of an elliptical patch antenna has been presented in [133], while its resonant circuit is studied in [134]. Elliptical patch antennas have also been used for ultra-wideband communications as presented in [135]. However, the design of an elliptical patch antenna for operation in the GPS and Iridium bands is a challenging task due to the unique characteristics of the elliptical patch geometry. In fact, the advantage of using an elliptical patch, instead of using a square patch (like the one used in [132]) or a rectangular patch (like the one used in [112] and [114]), is that it is easier to obtain circular polarization.

Due to the rapid development of wireless communications, the demand for utilizing a single antenna to support multiple operating frequencies has intensely been increased. A similar study is presented in [136], where four novel Fibonacci-type antennas are proposed for operation in GSM-900 MHz band and also in an extended band from 3.2GHz to 11.9 GHz with single, dual and triple band-notched characteristics. Several innovative patch antenna designs have been proposed for wearable and implantable applications as shown in [137-139].

After investigating the possibilities of using circularly-polarized patch antennas for satellite communications, an effort is made in this chapter to optimize an elliptical edge-fed circularly-polarized dual-band patch antenna that operates in both L1 GPS (1.563–1.587 GHz) and Iridium (1.616–1.626 GHz) bands and can be used for wearable applications. The antenna is required to provide, in both bands, S_{11} equal to or below –10 dB and realized gain (RG) equal to or above 5 dBi, which is higher compared to conventional square, rectangular and circular patch antennas. Studies performed in [140] suggest that GPS receivers work satisfactorily even when using linearly polarized antennas in urban environments due to multipath propagation. So, in the L1 GPS band, a more relaxed constraint may be applied for the axial ratio (AR), which is thus required not greater than 15 dB for this band. In the Iridium band, where nearly circular polarization is required, AR must be equal to or below 5 dB. All these requirements are summarized in Table 13.

Table 13. Antenna optimization requirements.

Parameter	Requirement	Description
1st band range	1.563 – 1.587 GHz	L1 GPS band
2nd band range	1.616 – 1.626 GHz	Iridium band
S_{11}	≤ –10 dB	in both bands
RG	≥ 5 dBi	in both bands
AR	≤ 15 dB	in the L1 GPS band
AR	≤ 5 dB	in the Iridium band

7.2 Antenna Geometry

A methodology to design dual-resonant elliptical patch antennas has been proposed in [141]. According to this methodology, approximate equations are used to calculate the lengths *a* and *b* of the semi-major axis and the semi-minor axis, respectively, while the elliptical patch is considered to be fed by an SMA probe located on the ellipse perimeter at 45° from the major axis. In fact, the parameters *a* and *b* determine the lowest resonant frequency and the highest resonant frequency, respectively, while the ratio *a*/*b* defines the antenna AR. Due to the use of approximate equations, the resonant frequencies are expected to deviate from their respective desired values. To verify this frequency deviation, the methodology given in [141] is applied for the center frequencies of the L1 GPS and Iridium bands, i.e., 1.575 and 1.621 GHz.

Actually, the two resonant frequencies represent the operating frequencies of the even and odd dominant (TM_{11}) modes of the elliptical patch. These frequencies can be determined by using approximate expressions of the Mathieu functions [141, 142], which in turn depend on the elliptical patch eccentricity defined as

$$e = \sqrt{1-\left(b/a\right)^2} \tag{18}$$

For the even dominant mode, the Mathieu function is given as

$$\begin{cases} q_{11}^{e} = -0.0049e + 3.7888e^{2} - 0.7228e^{3} + 2.2314e^{4}, \\ 0.05 \le e \le 0.55, \\ q_{11}^{e} = -0.1379 - 1.3138e + 3.9307e^{2} + 0.4056/(1-e), \\ 0.55 \le e \le 0.95, \end{cases} \tag{19}$$

while, for the odd dominant mode, it is given as

$$\begin{cases} q_{11}^{o} = -0.0063e + 3.8316e^{2} - 1.1351e^{3} + 5.2229e^{4}, \\ 0.05 \le e \le 0.45, \\ q_{11}^{o} = -1.2014 - 1.6271e + 2.1684e^{2} + 1.3089/(1-e), \\ 0.45 \le e \le 0.95. \end{cases} \tag{20}$$

By making a simple graphical representation of (2) and (3) for eccentricity intervals [0.05, 0.45], [0.45, 0.55] and [0.55, 0.95], it seems that $q_{11}^{e} < q_{11}^{o}$ for every value of e in the entire interval [0.05, 0.95]. The frequencies of the even and odd dominant modes are given in GHz [30], respectively, by:

$$f_{11}^{e} = \frac{15}{\pi a_{eff} e}\sqrt{\frac{q_{11}^{e}}{\varepsilon_r}} \tag{21}$$

And

$$f_{11}^{o} = \frac{15}{\pi a_{eff} e}\sqrt{\frac{q_{11}^{o}}{\varepsilon_r}} \tag{22}$$

In the above expressions, ε_r is the electric permittivity of the substrate, while a_{eff} is called effective semi-major axis and is used in calculations instead of a to compensate for the fringing field at the edge of the elliptical patch. This parameter is approximated by:

$$a_{eff} = \left[a^2 + \frac{ha}{0.3525\pi\varepsilon_r} \left\{ \ln\left(\frac{a}{2h} \right) + 1.41\varepsilon_r + 1.77 + \frac{h}{a}(0.268\varepsilon_r + 1.65) \right\} \right]^{\frac{1}{2}} \quad (23)$$

where h is the thickness of the substrate. It must be noted that a, a_{eff}, b and h are all in cm in (4), (5) and (6). By dividing (4) by (5), we get:

$$\frac{q_{11}^e}{q_{11}^o} = \left(\frac{f_{11}^e}{f_{11}^o} \right)^2 \quad (24)$$

Since $q_{11}^e < q_{11}^o$, from (7) we derive that $f_{11}^e < f_{11}^o$. Therefore, f_{11}^e represents the lowest resonant frequency (i.e., the center frequency 1.575 GHz of the L1 GPS band), while f_{11}^o represents the highest resonant frequency (i.e., the center frequency 1.621 GHz of the Iridium band).

To find the values of a and b, first we need to calculate the value of e. Considering that $0.05 \leq e \leq 0.45$, q_{11}^e and q_{11}^o are calculated from the first expressions of (2) and (3), respectively. By substituting the values of f_{11}^e and f_{11}^o as well as the first expressions of (2) and (3) in (7), we derive $e = 0.3282$. This value is considered to be valid, because it resides in the interval [0.05, 0.45].

To give the reader the complete calculation process of e, we describe below what would be the next steps if the value of e did not reside in the above interval. In such a case, we consider that $0.45 \leq e \leq 0.55$, which means that q_{11}^e is calculated from the first expression of (2) and q_{11}^o from the second expression of (3). By substituting these expressions as well as the values of f_{11}^e and f_{11}^o in (7), we derive the value of e, which must reside in the interval [0.45, 0.55]. If not, we finally consider that $0.55 \leq e \leq 0.95$, which means that q_{11}^e and q_{11}^o are calculated from the second expressions of (2) and (3), respectively. By substituting these expressions as well as the values of f_{11}^e and f_{11}^o in (7), we derive the value of e, which must reside in the interval [0.55, 0.95].

After e has been found and using certain values for ε_r and h, a_{eff} can be found from either (4) or (5). Then, from (6), we calculate the value of a. Finally, from (1), we find the value of b. Using the above value of e = 0.3282 and considering a substrate with ε_r = 2 and h = 2.54 mm (the selection of such values for ε_r and h will be explained below), we get a = 37.9 mm and b = 35.8 mm.

The antenna geometry extracted by this methodology is modeled in CST Microwave Studio (CST MWS) using copper thickness equal to 0.035mm and analyzed using the time domain solver of CST MWS, which employs the finite integration technique, with an accuracy of –50 dB for the frequency domain signals. From this analysis, the values of S_{11} are extracted in the frequency range 1.4-1.8 GHz (which includes the L1 GPS and Iridium bands). The graphical representation of S_{11} shown in Figure 47 verifies the creation of deviations from the center frequencies of both bands. In fact, the deviations are so high that the resonances overlap and merge into a single resonance at an intermediate frequency, without satisfying the requirement for S_{11} (see Table 13). Therefore, an optimization of the antenna geometry is necessary to compensate for these frequency deviations, while some geometry modifications are required to further improve the antenna behavior according to the above requirements.

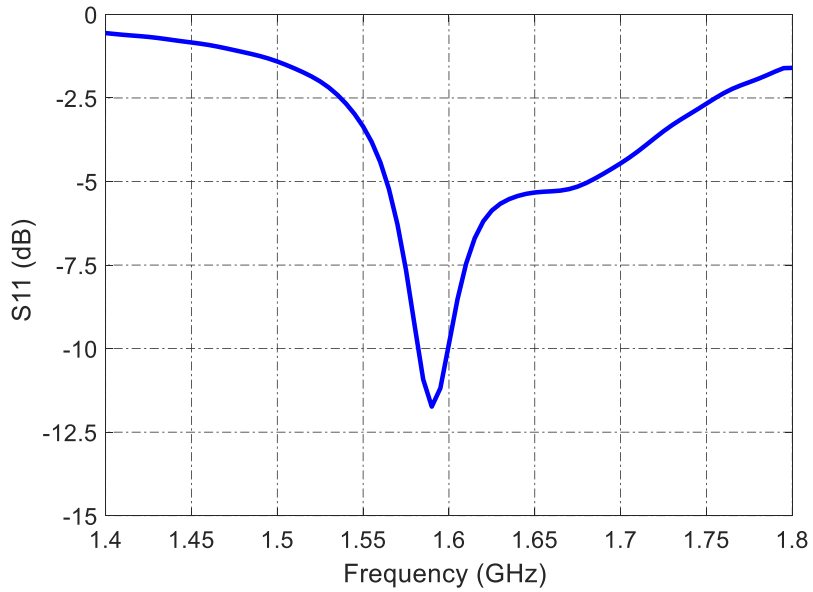

Figure 47. S11 of the simulated initial geometry designed according to the methodology given in [141].

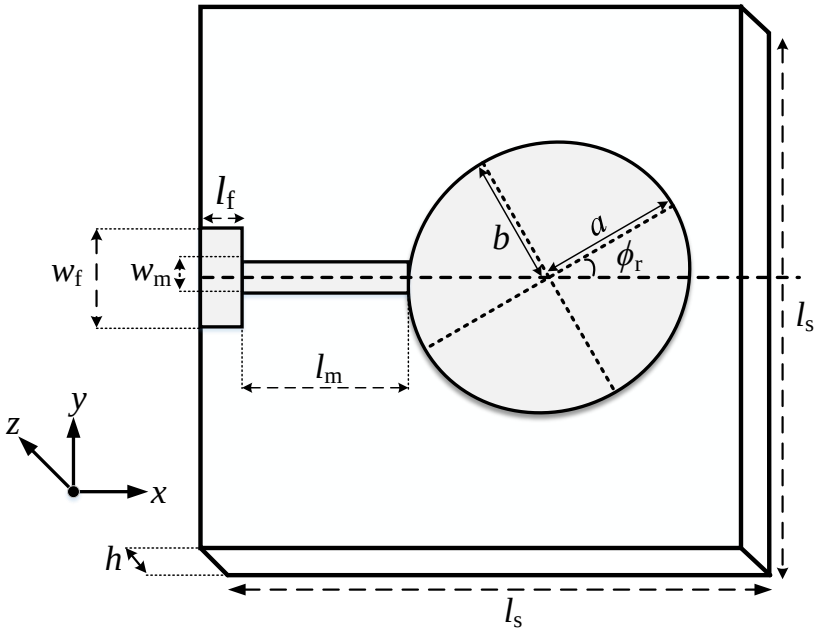

Figure 48. Schematic diagram of the proposed elliptical patch antenna.

The proposed antenna geometry (see Figure 48) is composed of a dielectric substrate, an elliptical conducting patch and a ground plane, while a feeding line and a matching line are introduced in this geometry. The substrate is defined by its electric permittivity ε_r and its thickness h, and is considered to be square-shaped with side length l_s. The elliptical patch is defined by the parameters a and b. The ground plane is of the same dimensions as the substrate. Finally, the feeding line and the matching line are defined by their lengths, respectively expressed as l_f and l_m, and their widths, respectively expressed as w_f and w_m. These two lines are parallel to each other but not parallel to the major axis of the elliptical patch. Thus, an azimuth angle ϕ_r is formed between the common axis of the two lines and the major axis of the patch. It is also obvious from Figure 48 that the patch is edge-fed. In comparison with the geometry given in [141], the proposed geometry induces more degrees of freedom due to 8 adjustable parameters (i.e., a, b, l_m, w_m, l_f, w_f, ϕ_r and l_s under optimization, considering that ε_r and h have fixed values) and therefore has the potential to concurrently satisfy all the above requirements (given in Table 13). A preliminary investigation of this geometry has been made in [143] without any optimization of the antenna behavior. The substrate used for the proposed antenna is Rogers RT/duroid 5880LZ laminate with $\varepsilon_r = 2$ and $h = 2.54$ mm (0.1 inch), unlike the usual FR4 substrate, which has $\varepsilon_r = 4.4$ and $h = 1.6$ mm. Since, the substrate used here has

a lower permittivity and a higher thickness compared to the FR4 substrate, greater bandwidth in both L1 GPS and Iridium bands is expected.

The antenna is modelled in CST MWS. The model consists of approximately 750000 mesh cells (the model changes dimensions during the optimization and thus the meshing size changes too). The antenna feeding is modelled by using a waveguide port at the edge of the feeding line. The full wave analysis is performed by applying the time domain solver of CST MWS with an accuracy of –50 dB for the frequency domain signals. The CST model of the proposed antenna is shown in Figure 49 (a) and the fabricated antenna in Figure 49 (b).

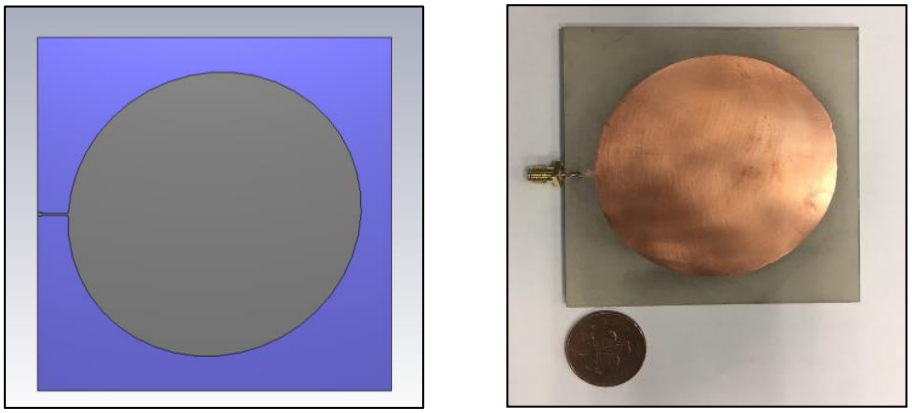

Figure 49. (a) CST model and (b) fabricated version of the proposed antenna.

7.3 Optimization using PSADEA

The optimization of the proposed antenna is a challenging task, because the antenna has to concurrently satisfy all the requirements of Table 13 in two bands. In general, antennas have been optimized so far by using either local optimization or global optimization methods. The success of local optimization methods depends on the quality of the initial design employed to start the optimization process. Consequently, such methods are not always able to satisfy all the predefined requirements. On the other hand, the use of global optimization methods, such as PSO, is costly in terms of computational time, because a large amount of fitness evaluations is required by such methods in order to converge. In addition, when full wave analysis is required (using the CST MWS in our problem) for every fitness evaluation, the computational cost is extremely increased.

The Surrogate Model Assisted Differential Evolution for Antenna Synthesis (SADEA) algorithm [144-146] is capable of obtaining comparable or better quality designs compared to standard global optimization techniques and with around 3 to 20 times efficiency improvement for antenna design cases [144], [147], [148]. The essential elements in the SADEA family are the Gaussian process surrogate modeling, the differential evolution search and the surrogate model-aware evolutionary search framework [144]. The Gaussian process is used to construct computationally cheap surrogate models, thus approximating the performance of computationally expensive simulations. Differential evolution is used to carry out global optimization. The key challenge for all surrogate-based optimization techniques is the appropriate balance between handling surrogate model prediction uncertainty (to avoid being trapped in local optima or wrong convergence) and reducing the number of real computationally expensive evaluations (to improve the efficiency). In the SADEA family, this is addressed by the surrogate model-aware evolutionary search framework [149].

In this chapter, the state-of-the-art parallel SADEA (PSADEA) algorithm is employed [145, 146]. Compared to the standard SADEA, PSADEA employs complementary differential evolution mutation strategies and reinforcement learning techniques, thus achieving an additional efficiency improvement of about 1.5 to 3 times, even in the sequential mode, as well as a further improvement in the solution quality [145, 146].

To help the optimization process converge faster, upper and lower boundaries must be defined for every optimization parameter. The optimal values of a and b are expected to deviate at most ±40% from their typical values (i.e., a = 37.9 mm and b = 35.8 mm) derived by the methodology given in [141]. The values of l_m and l_f are expected to be found between 0.5 mm, which is considered to be the smallest feasible fabricated copper size, and 48 mm, which is equal to a quarter of the wavelength at the lowest frequency of interest (1.563 GHz), considering that the maximum variation of voltage, current, or impedance takes place along a quarter-wavelength line. To have sufficient tolerance in achieving impedance matching, the values of w_m and w_f are expected to be found between 0.5 mm and 10 mm. The optimal value of ϕ_r is expected to deviate at most ±40% from its typical value (i.e., 45°) [141]. The boundaries of l_s are dynamically adjusted at the end of every iteration of the optimization process. Since the substrate must be larger in length along x-axis and y-axis (see Figure 48), the lower

boundary of l_s is considered to be equal to $l_{m,cur} + l_{f,cur} + 2a_{cur}$, where $l_{m,cur}$, $l_{f,cur}$ and a_{cur} are the current values of l_m, l_f and a, respectively, at the end of every iteration of the optimization process. Finally, the upper boundary of l_s is arbitrarily considered to be 40% greater than its lower boundary. All these boundaries are summarized in Table 14.

For every set of values of a, b, l_m, w_m, l_f, w_f, ϕ_r and l_s tested by the PSADEA algorithm, the antenna is analyzed by applying the CST MWS and the values of S_{11} (in dB), RG (in dBi) and AR (in dB) are extracted for 7 uniformly distributed frequency samples of the L1 GPS band with 4 MHz sampling step and for 3 uniformly distributed frequency samples of the Iridium band with 5 MHz sampling step. These values of S_{11}, RG and AR are used to calculate a fitness function, which is properly formulated according to all the above requirements (given in Table 13) and is subject to global minimization by the PSADEA algorithm. The fitness function formula is given below:

$$\text{fit} = -\text{RG}_{\min} + \max(S_{11\max}, -10) + \max(\text{AR}_{\text{Gmax}}, 15) + \max(\text{AR}_{\text{Imax}}, 5). \tag{25}$$

In (8), $\text{RG}_{\min}$ and $S_{11\max}$ represent the minimum RG and the maximum S_{11} found respectively over the 10 frequency samples of both bands, while AR_{Gmax} and AR_{Imax} represent the maximum values of AR found respectively over the 7 frequency samples of the L1 GPS band and over the 3 frequency samples of the Iridium band. The use of max(.) terms in the fitness formula ensures that, after the desired values of $S_{11\max}$, AR_{Gmax} and AR_{Imax} are reached, any improvement on them will not affect the fitness value, and the algorithm will solely focus on the maximization of $\text{RG}_{\min}$.

Table 14. Boundaries of optimized parameters.

Parameter	**Lower Boundary**	**Upper Boundary**
A	22.7 mm	53.1 mm
B	21.5 mm	50.1 mm
l_m	0.5 mm	48 mm
w_m	0.5 mm	10 mm
l_f	0.5 mm	48 mm
w_f	0.5 mm	10 mm
ϕ_r	27°	63°
l_s	$l_{m,cur} + l_{f,cur} + 2a_{cur}$	$1.4\times(l_{m,cur} + l_{f,cur} + 2a_{cur})$

Table 15. Optimized parameters of the proposed antenna geometry.

Parameter	Value
a	39.6 mm
b	37.4 mm
l_m	7.1 mm
w_m	0.5 mm
l_f	1.1 mm
w_f	1.0 mm
ϕ_r	30.9 degrees
l_s	94.3 mm

7.4 Results

The optimized antenna geometry extracted by the PSADEA algorithm is shown in Table 15. To validate the simulation results, the optimized antenna was fabricated by using Rogers 5880 LZ laminate substrate provided by Rogers Corporation. The feeding was implemented by applying at the edge of the substrate an SMA connector, which was soldered to the feeding line of the patch antenna. A picture of the fabricated antenna is shown in Figure 49 (b). The electromagnetic characteristics of the fabricated antenna were experimentally measured in an anechoic chamber of the National Physical Laboratory (NPL) of the U.K. and compared to those of the simulated antenna. The comparison in terms of S_{11}, RG and AR is shown respectively in Figures 50, 51 and 52. From Figure 50 it is evident that both the simulated and fabricated antennas fulfill the requirement for S_{11} in both bands. Figure 51 presents the left-hand circular polarization (LHCP) RG and the right-hand circular polarization (RHCP) RG of both the simulated and fabricated antennas. It is obvious that the antenna has RHCP, since the RHCP RG is much greater than the LHCP RG in both bands. Also, as shown in Figure 52, the antenna has better circular polarization in the Iridium band than in the L1 GPS band. Nevertheless, the requirements initially set for AR are fully met in both bands. AR can further be improved by implementing a simple C-type single feed technique on stacked microstrip antennas as presented in [150]. Finally, great similarity between the radiation patterns of the simulated and the fabricated antenna can be seen in Figure 53.

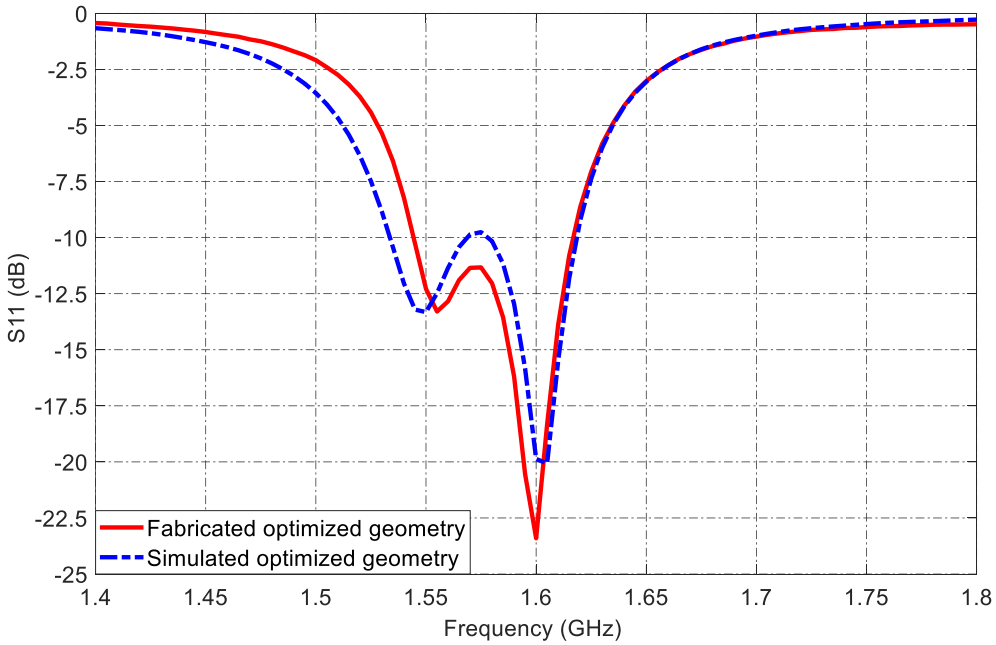

Figure 50. S11 of the simulated optimized geometry and the fabricated optimized geometry.

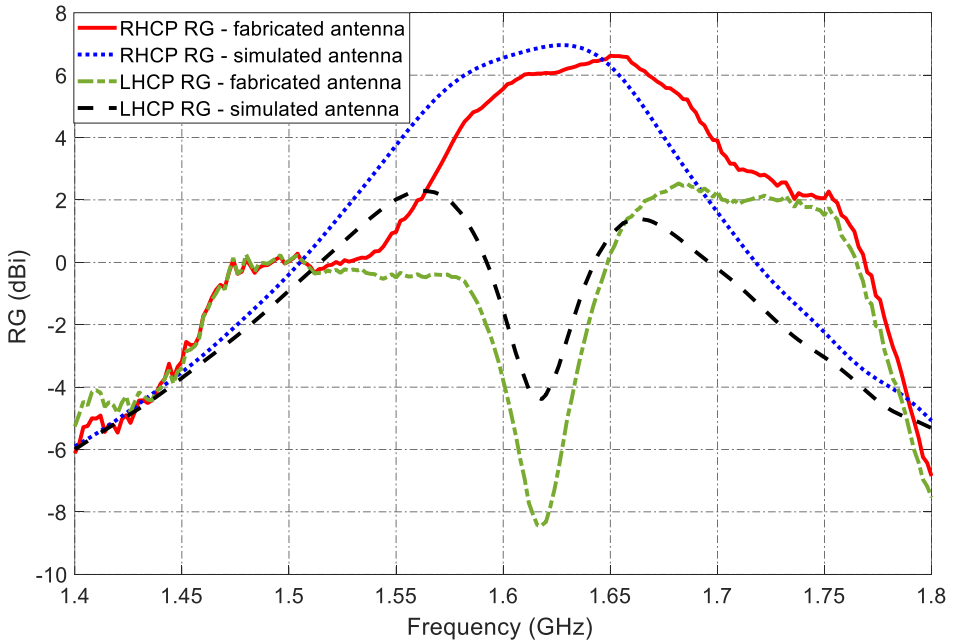

Figure 51. RHCP and LHCP realized gain of the simulated optimized geometry and the fabricated optimized geometry.

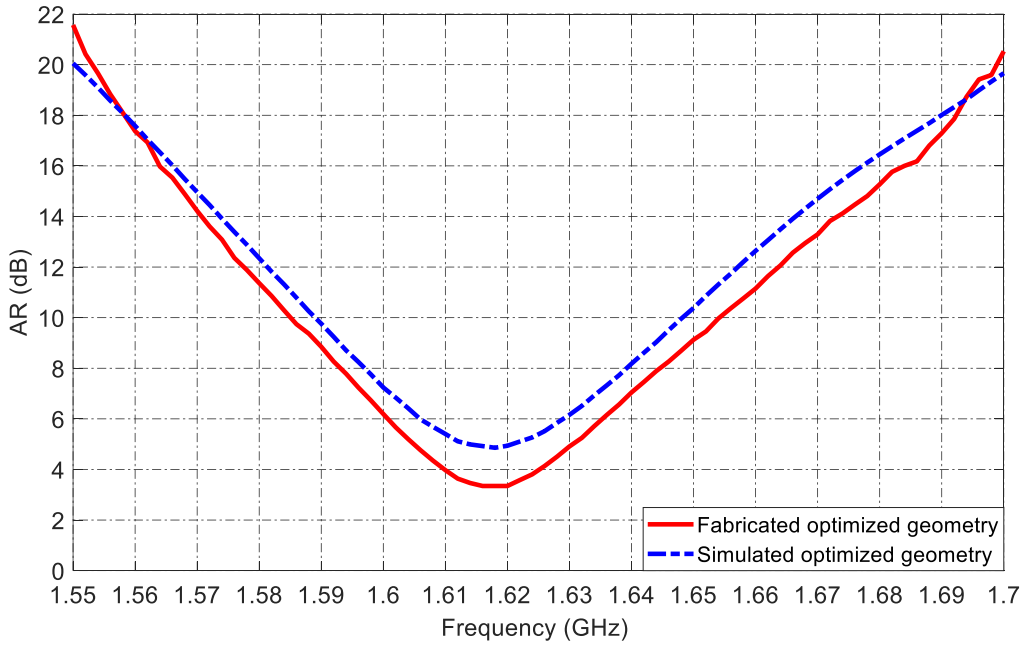

Figure 52. Axial ratio of the simulated optimized geometry and the fabricated optimized geometry.

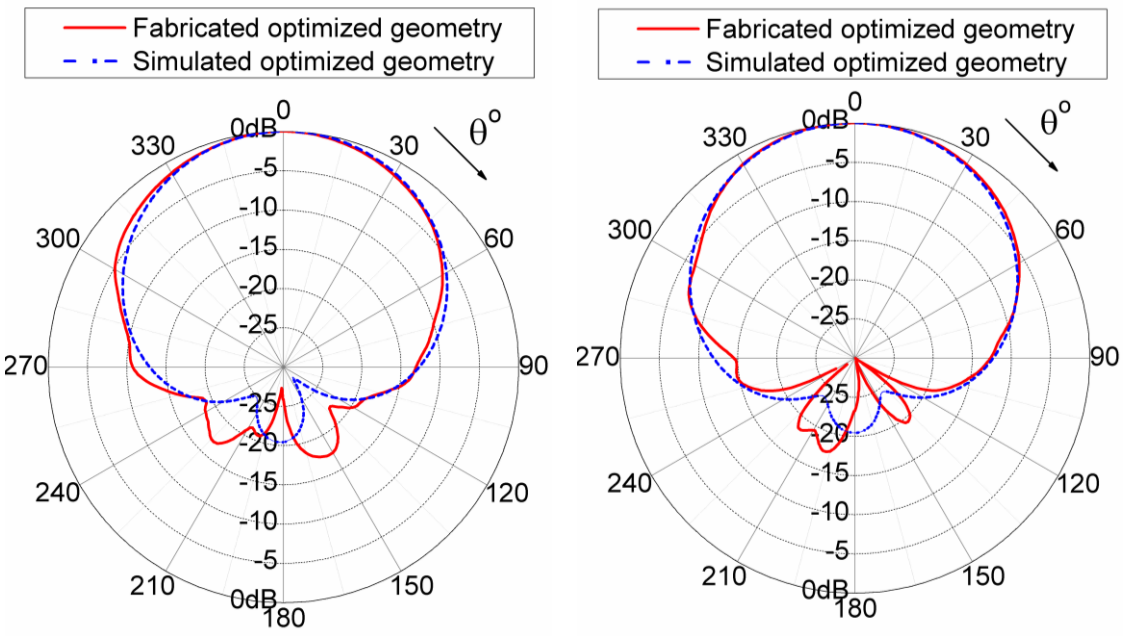

(a) (b)

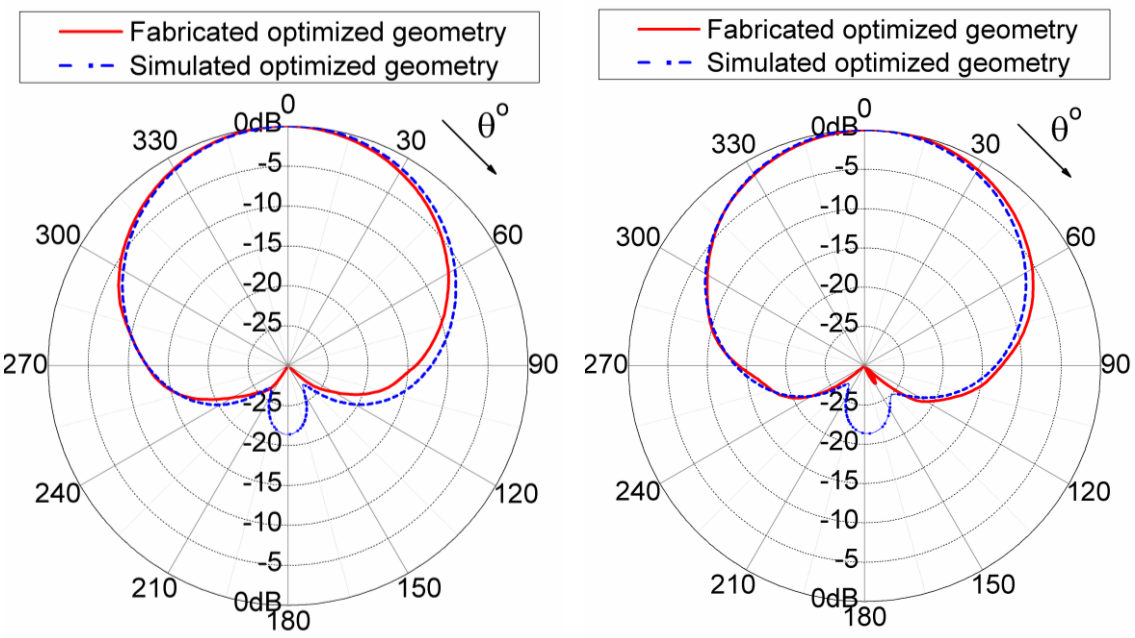

(c) (d)

Figure 53. Normalized radiation patterns of the simulated optimized antenna and the fabricated optimized antenna (a) for ϕ = 0o at 1.575 GHz, (b) for ϕ = 90o at 1.575 GHz, (c) for ϕ = 0o at 1.621 GHz, and (d) for ϕ = 90o at 1.621 GHz.

Figure 54. Polarization measurements - orientation #1.

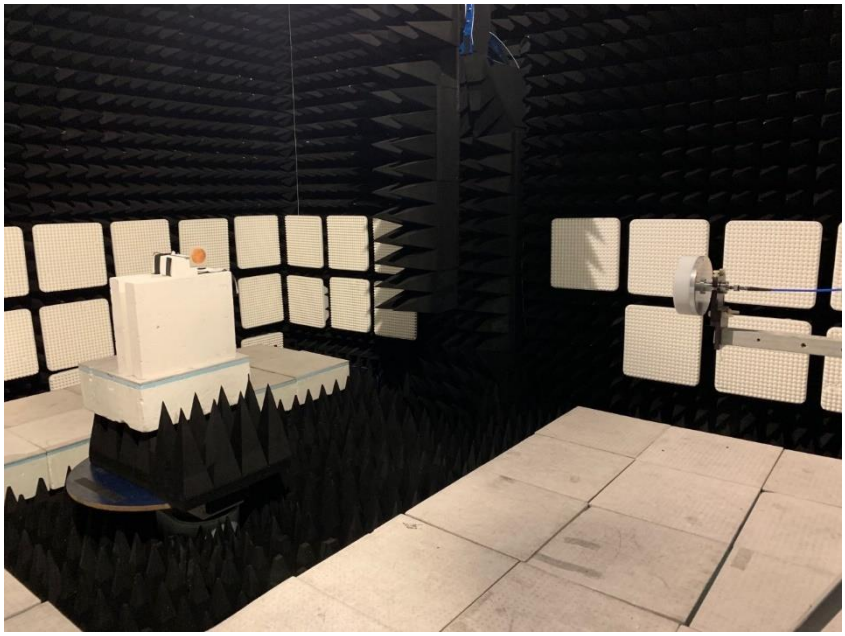

Figure 55. Polarization measurements-orientation #2.

Figures 54 and 55 show different orientations in which the proposed antenna was placed in order to obtain LHCP and RHCP measurements.

7.5 Conclusion

A dual-resonant elliptical patch antenna suitable for L1 GPS and Iridium applications has been optimized by using a state-of-the-art optimization technique called PSADEA. The optimized antenna is well-matched to a 50 Ω feeding source and provides RHCP with sufficient RG and AR in both bands according to the specified requirements. After all these, the proposed antenna may be considered as a good candidate for dual-band reception in wearable satellite applications. Finally, PSADEA is a robust technique capable of solving complex antenna design problems, which are subject to multiple requirements.

Chapter 8 Radio propagation and coverage prediction

8.1 Necessity of propagation prediction and modelling

The last four decades have demonstrated a rapid development in the mobile communications as well as in digital broadcasting leading to an increase in number of end-users and increased demands for high quality-of-service (QoS). Mobile communications have observed transition from 1G to 5G services, while on the other hand broadcasting services have observed a switchover from analog to digital giving rise to new technologies like Digital Video Broadcasting (DVB-T/T2) and digital radio – Digital Audio Broadcasting (DAB). The transition of these technologies is a challenging task which makes it significant for radio engineers to develop systems that aid to these transitions and to meet the end-user requirements at minimal costs. Propagation prediction plays an important role as it provides radio engineers with an estimate of how radio waves propagate when obstacles are introduced. This provides a good estimation of the optimal placement of broadcasting and/or base stations to provide the best coverage with minimal interference, thereby improving QoS. Designing a model for the propagation channel which predicts the received signal strength provides significant information to radio engineers.

Several propagation models have been developed that predict the coverage at a required location. In addition to this, there are propagation models that can predict the path loss, shadowing and multi-path propagation and fading. The International Telecommunications Union (ITU) have been introduced by the United Nations (UN) and has the responsibility to maintain a database of telecommunication recommendations. For the purpose of propagation prediction and modelling, some of the most commonly used propagation models recommended by the ITU are P.1546 and P.526. Both these models are empirical models, where P.1546 is a

method for point-to-area prediction for terrestrial services in the frequency range of 30 MHz to 3 GHz, whereas P.526 is a method for propagation by diffraction.

8.2 Radio propagation terminology

8.2.1 Free-space propagation

Radio waves propagate in free space at the speed of light (approximately 3 x 10^8 m/s) from a source into the surrounding area. Ideally, free space is a vacuum, however, a clear air can also be considered as a close approximation to this [151]. For mathematical analysis, an isotropic antenna which radiates power equally in all directions is considered as a reference. Therefore, in the case of an isotropic antenna acting as a transmitter or receiver free space path (FSPL) can be mathematically expressed as:

$$FSPL = 32.44 + 20\log d + 20\log f \tag{26}$$

Where,

FSPL= free space path loss in dB

d = path length in km

f = frequency in MHz

The link loss is measuring of the difference of the transmitted power and the received power on a point-to-point system. The link loss can be measured as:

$$Link\ Loss = FSPL - G_t - G_r + L_m \tag{27}$$

where,

FSPL = free space loss in dB
G_t = Gain of transmitting antenna in dBi (relative to the reference isotropic antenna)
G_r = Gain of receiving antenna in dBi
L_m = miscellaneous losses in dB (connector loss and feeder loss)

8.2.2 Equivalent isotropic radiated power

Generally, in radio systems, the transmission performance is mostly measured in terms of Effective Radiated Power (ERP). The calculation of ERP for any station is performed with the assumption that it is calculated with respect to the half-wave dipole as the reference antenna. ERP determines the excess power radiated by the antenna system when compared to the case where the simple half-wave dipole is considered for transmission [151, 152] . The power received by the antenna can also be represented as:

$$P_r = P_t - link\ loss \tag{28}$$

$$P_r = P_t + G_t + G_r - L_m - FSPL \tag{29}$$

ERP is the sum of power transmitted and the power radiated by an antenna, including the miscellaneous losses. Therefore, the ERP can be mathematically expressed in dB as:

$$ERP = P_t + G_t - L_m \tag{30}$$

ERP is also represented as W, dBW or dBm. Transmitted power and the received power in the above equations is expressed in terms of dBW or dBm.

If the isotropic source antenna is considered as the reference instead of the half-wave dipole, ERP is then referred to as Equivalent Isotropic Radiated Power (EIRP). The gain of the dipole compared to the isotropic antenna is approximately 2.15 dB and thus EIRP can be mathematically expressed as:

$$EIRP\,(dBW) = ERP + 2.15 \tag{31}$$

8.2.3 Relation between power density and electric field strength

Point-to-area is a term referred when transmission is performed by a central antenna to receivers that are spread throughout an area. This area is referred to as the coverage area. Radio

broadcasting, television broadcasting, (bi-directional) digital mobile communications are some most common examples of point-to-area transmission. In order to predict television broadcasting coverage , it is important to assume that the receiving antennas are placed on the rooftop of buildings or houses at around 10m higher. In addition to this, the receiving antennas should be highly directional and should also point towards the transmitting station in order to receive sufficient signal. However, in case of television broadcasting the received signal level by the receiving antennas should be approximately -50 dBm to ensure clear picture delivery to the consumers. This signal level is higher compared to other transmissions as the bandwidth of television is around 8 MHz which is wider compared to other transmitting systems. The power density is directly proportional to the electric field (V/m) and the magnetic field (A/m) of the electromagnetic wave. The power density (P_d) of an electromagnetic wave can be mathematically expressed as:

$$P_d = E \times H \, (W / m^2) \tag{32}$$

In the case of free-space propagation, intrinsic impedance is defined as the ratio of the electric field and the magnetic. This ratio is mathematically expressed as:

$$E = 120\pi H \tag{33}$$

Thus, the power density can be expressed in terms of electric field as:

$$P_d = \frac{E^2}{120\pi} \tag{34}$$

Therefore, the electric field can also be calculated using the power density as:

$$E\,(V / m) = \sqrt{P_d 120\pi} = \sqrt{\frac{P_t G_t}{4\pi r^2} 120\pi} = \sqrt{\frac{30 P_t G_t}{r}} \tag{35}$$

where, electric field is measured in V/m and the distance ‘r’ is measured in meters. However, the electric field strengths measured for radio propagation are usually very small and thus μV/m is commonly used. Also, the distances are usually large in case of radio propagation predictions

and thus they are usually measured in kilometers (km). Therefore, the above equation can be transformed in order to find the electric field strength in μV/m as:

$$E(\mu V/m) = 5480\frac{\sqrt{P_t G_t}}{d} \tag{36}$$

Furthermore, in order to simplify the calculation of electric field strength, P_tG_t can be assumed as 1000 W transmitted through a half-wave dipole, which results in the simplified value of P_tG_t of 1640. Thus, the above equation is transformed as:

$$E(\mu V/m) = 5480\frac{\sqrt{1640}}{d} = \frac{222000}{d} \tag{37}$$

The electric field strengths are usually expressed in logarithmic units and thus can be expressed as:

$$E(dB\mu V/m) = 20\log\left(\frac{222000}{d}\right) = 106.9 - 20\log d \tag{38}$$

d= distance in km

Furthermore, the received power by an isotropic antenna in dBm can also be calculated using the electric field strength as:

$$P_r(dBm) = E(dB\mu V/m) - 20\log f(MHz) - 77.2 \tag{39}$$

8.2.4 Line-of-sight (LOS) and non-line-of-sight (NLOS) propagation

Unlike, high frequency (HF) waves which are little affected by obstructions, the very-high frequency (VHF) and ultra-high frequency (UHF) waves can get seriously affected by obstacles, atmospheric changes, reflections and diffractions due to buildings, vegetation and other objects. LOS propagation is a phenomenon where the radio waves travel from the transmitting antenna to the receiving antenna in a straight line without any obstacles in

between. Mobile communications, FM radio and satellite transmissions are the most common examples where LOS propagation is used.

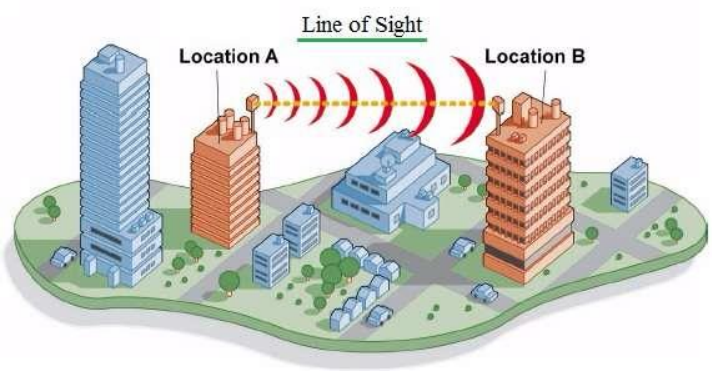

Figure 56. LOS propagation (http://www.rfwireless-world.com/Terminology/LOS-vs-NLOS-wireless-channel.html).

Unlike LOS, the NLOS propagation occurs when the there is an obstruction in the propagation path between the transmitting antenna and the receiving antenna. In such cases, the signal is received by the receiving antennas after undergoing several reflections or diffractions and thus an attenuated signal is received at the receiving end. NLOS can also be useful in the case of mobile communications where the signal transmitted from a base station can reach the user at ground level after undergoing several reflections and/or diffractions on buildings and other obstacles as shown in figure 57 [153].

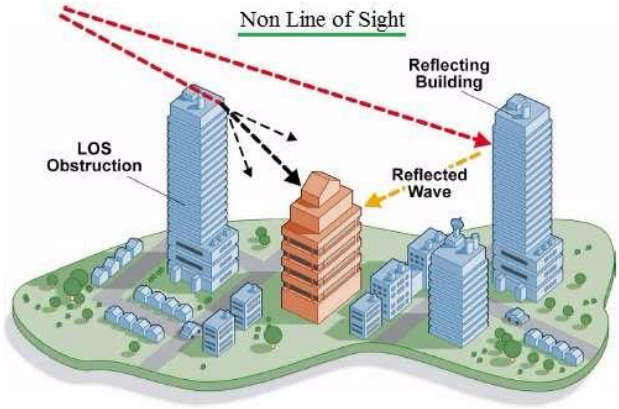

Figure 57. NLOS propagation(http://www.rfwireless-world.com/Terminology/LOS-vs-NLOS-wireless-channel.html).

8.3 Fresnel zones and clearance requirements

The Fresnel ellipsoid is an ellipsoid that surrounds the radio propagation path between the transmitting and receiving points. The operating frequency and the distance between the transmitting and receiving antenna plays a significant role in determining the size of the Fresnel ellipsoid. The signal from the transmitting antenna can travel to the receiving antenna in a direct path or through several reflections or diffractions. Fresnel zones play an important role in calculating the losses due to reflections and diffractions. These zones are referred as F1, F2, F3 and so on as shown in Figure 58. Usually, the first three Fresnel zones are used for calculations, however, there is no specific limit for the number of Fresnel zones that exist between a transmitter and a receiver.

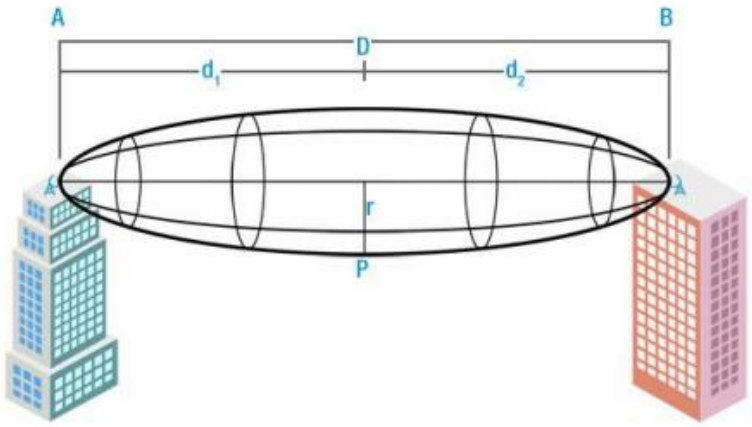

Figure 58. Fresnel zones between the transmitter and receiver [151].

As suggested in [151], zero diffraction loss can be obtained if the Fresnel parameter "v" is not more than -0.8. The radius of the first Fresnel zone is mathematically expressed as:

$$R = \sqrt{\frac{\lambda d_1 d_2}{d_1 + d_2}} \tag{40}$$

where,

λ = wavelength of the signal

$D = d_1 + d_2$ =distance between the transmitter and the receiver in km.

Therefore, in terms of frequency in MHz, the expression can be rewritten as:

$$R = 550\sqrt{\frac{d_1 d_2}{(d_1 + d_2) f}} \tag{41}$$

The value of the radius will be maximum if $d_1=d_2=d/2$, hence the maximum radius can be expressed as:

$$R_{\max} = 275\sqrt{\frac{d}{f}} \tag{42}$$

The radius of the Fresnel zone provides information about the Fresnel zone clearance level. If the ratio of the radius of the Fresnel zone and its clearance from obstacles is more than 60%, it is concluded that the transmitter is in LOS with the receiver with no diffraction loss.

8.4 Diffraction through obstacles

The radio propagation path between the transmitter and the receiver is not always LOS. Radio engineers also need to predict the signal strength in the shadow of obstacles. Obstacles cause diffraction and predicting the signal strength in such cases is a very challenging task. Therefore, this section will introduce to the types of diffraction and mathematical models that can be used to predict signal strength in such cases.

8.4.1 Single knife-edge diffraction

A simple case where the receiver lies in the shadow of a perfectly absorbing obstacle is defined as a knife-edge and the diffraction caused to radio waves by this knife-edge is termed as knife-edge diffraction. Figure 59 shows the case where a radio wave transmitted by the transmitter towards the receiver hits perpendicular to the knife-edge. In such cases, the signal strength can be predicted in the obstacle shadow relative to the case without obstacle. Diffraction loss is

defined as the ratio of the signal strength without the obstacle to the signal strength with the obstacle. Two factors that significantly affect diffraction loss are the geometry of the path and the frequency of operation. All the factors responsible for the diffraction loss can be combined in a single parameter, which is known as Fresnel parameter.

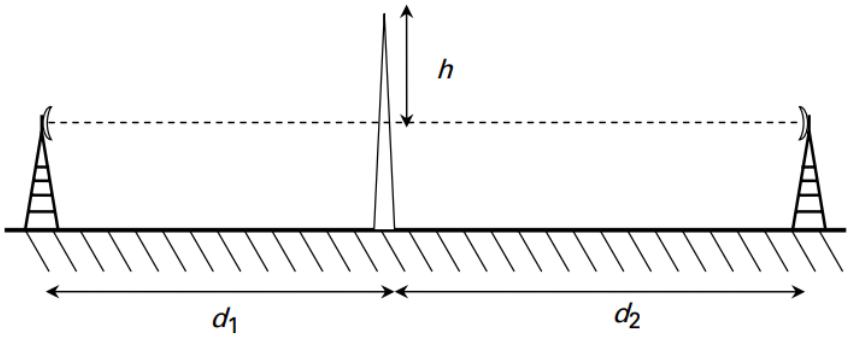

Figure 59. Knife-edge diffraction geometry [151].

The Fresnel parameter "v" is mathematically expressed as:

$$v = h\sqrt{\frac{2}{\lambda}\left(\frac{1}{d_1}+\frac{1}{d_2}\right)} \tag{43}$$

The diffraction loss is approximated in terms of Fresnel parameter as:

$$Diffraction\ Loss\,(dB) = 6.9 + 20\log\left(\sqrt{(v-0.1)^2+1}+v-0.1\right) \tag{44}$$

This relation is also shown in Figure 60.

This graph suggests that diffraction loss is 6 dB when the Fresnel parameter is 0. It states that, the signal strength will be reduced by 6 dB as the receiver approaches to the shadow boundary of an obstacle. Also, the Fresnel parameter must be approximately -0.8 in order to ignore the diffraction loss as it gets reduced to zero.

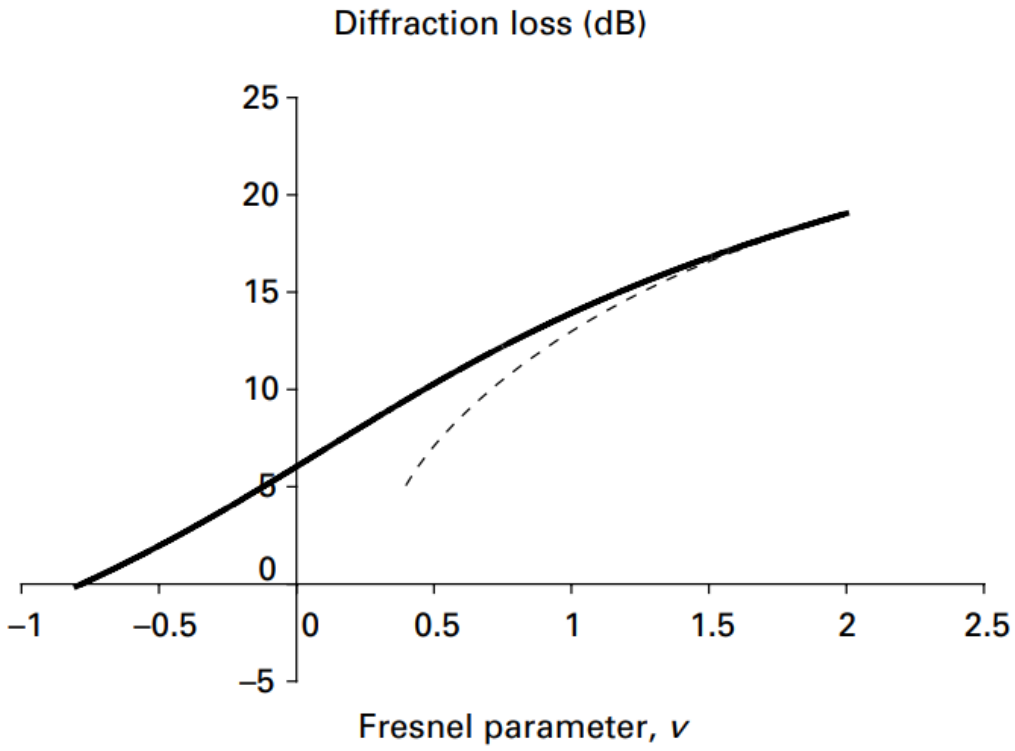

Figure 60. Relation of diffraction loss in dB as a function of the Fresnel parameter [151].

However, in cases where the receiver point is deep in the shadow of an obstacle, then the diffraction loss can be expressed as:

$$Diffraction\,loss\,(dB) = 13 + 20\log v \tag{45}$$

The above equation predicts the diffraction loss accurately for cases where v > 1.5.

The mathematical expression to calculate the Fresnel parameter clearly suggests that the Fresnel parameter is directly proportional to the height "h" shown in Figure 59 and directly proportional to the square root of frequency "f". This suggests that if the frequency is low, then the Fresnel parameter will be low as well. Thus, for the case of radio waves, the lower frequencies will be able to penetrate deeper in the obstacle shadow. Figure 61 shows the relation of the Fresnel parameter and relative signal strength (in dB).

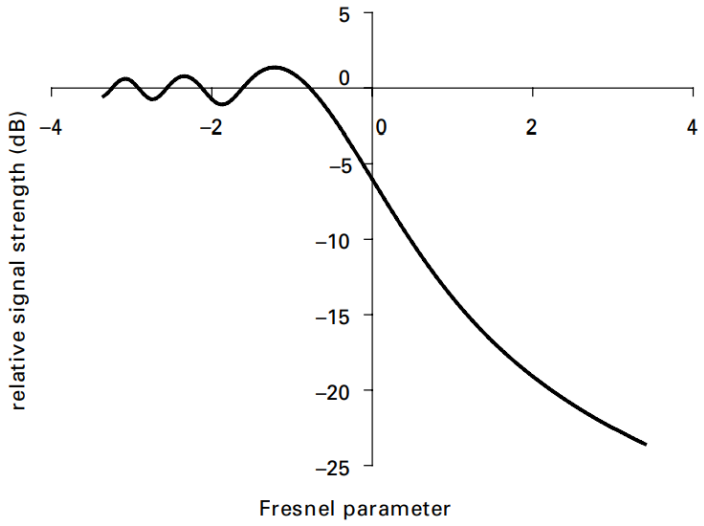

Figure 61. Relative signal strength (in dB) versus Fresnel parameter [151].

8.4.2 Multiple knife-edge diffraction

The introduction of a second or more knife edges in the shadow of a single-knife edge, makes it challenging to predict the additional loss introduced by the second knife-edge. The calculation then requires the evaluation of a two-dimensional integral of Fresnel equation in the case of two knife-edges. Similarly, for the cases where there are n knife edges, the evaluation of n-dimensional integral is required. These calculations are very complex and thus several approximation methods are used like the Bullington method [154], the Deygout method [155] and the Epstein-Peterson method [156]. A comparison of these three approximate models are shown in the next section.

8.4.2.1 The Bullington method

The Bullington method tries to reduce multiple-knife edges to a single knife-edge. This is done by extending lines from the transmitter and the receiver through the tip of the knife-edges that form the maximum angle of elevation. The intersection of these two lines is the location of an imaginary equivalent single knife-edge. Then, calculations can be performed by using the equations for a single knife-edge. However, [157] suggests that any other knife edges with

lower angle of elevation are ignored, and thus ignoring the knife edges may lead to underestimating the diffraction loss. The Bullington method of approximation can be visualised in Figure 62.

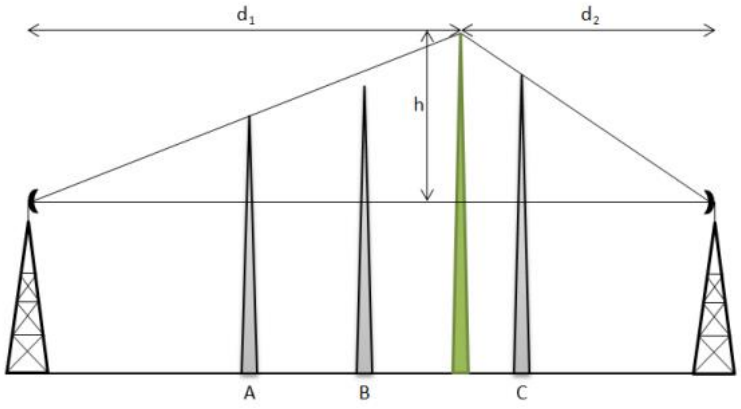

Figure 62. The Bullington model approximation [151].

8.4.2.2 The Epstein-Peterson method

The Epstein-Peterson method approximates the multiple knife-edge scenario by multiple hops as shown in Figure 63. The computation of total diffraction loss is done by the addition of losses caused due to every diffracting edge of the hop. The single-knife edge equations are used in this approximation method. This method provides better accuracy compared to the Bullington approximation method, however, it has the drawback of overestimating the path loss [151, 156].

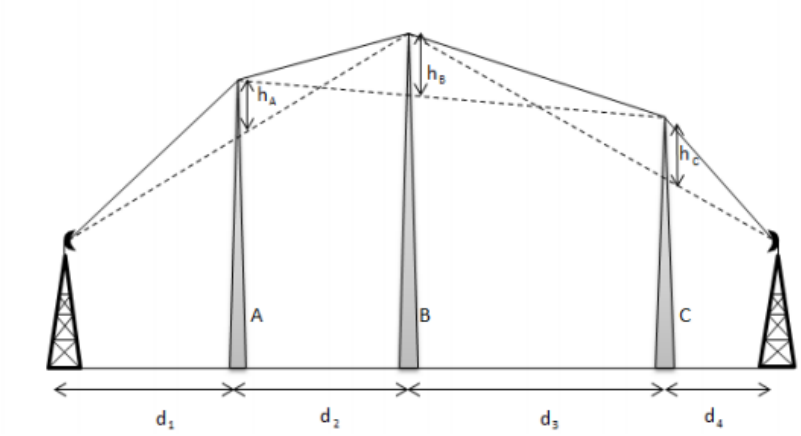

Figure 63. Epstein-Peterson method of approximation [151].

8.4.2.3 The Deygout method

The Deygout method is similar to the Epstein-Peterson method. However, the results obtained from the Epstein-Peterson method and the Deygout method are different. In this method, first step is to detect the most dominant edge. In other words, the obstacle with the largest Fresnel parameter value is the most dominant edge. The diffraction loss due to this obstacle is then calculated assuming that it was the only edge present. Followed by this calculation, the dominant edge divides the path into two sub-paths. The calculation of this sub-path is performed by following the Epstein-Peterson method. After calculating all the sub-path losses, the total diffraction loss is calculated by adding the diffraction loss of the dominant edge and all the sub-path losses [151, 155].

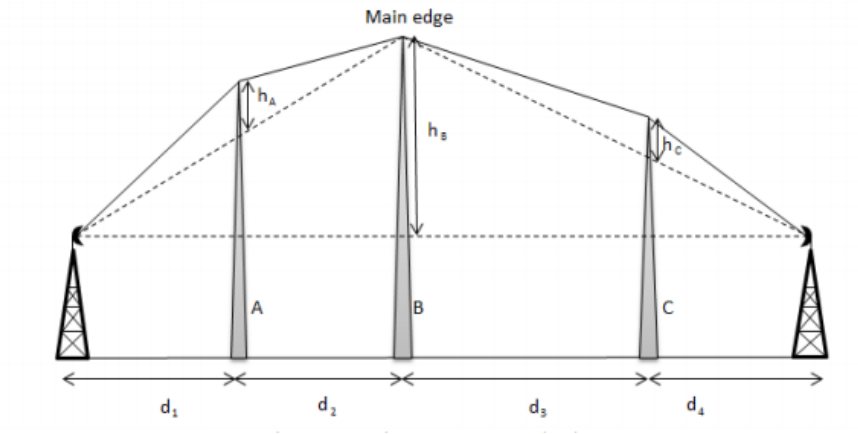

Figure 64. The Deygout method of approximation [151].

8.5 Path loss prediction models

The path loss of a radio wave is usually characterised using empirical radio propagation models that make use of the data obtained by measurements and observation in various types of scenarios. The propagation models that are used in ICS Telecom software and Radio Mobile are described in this section.

8.5.1 The Longley Rice model

The Longley Rice Model, also known as Irregular Terrain Model (ITM) was developed by the National Telecommunications and Information Administration – Institute for Telecommunication Sciences (NTIA-ITS). In USA, the Federal Communications Commission (FCC) standardized this model to be used for TV broadcasting channel allocation applications. This model can be used for radio propagation in the frequency range from 20 MHz to 20 GHz, for distances between 200 km to 5000 km and heights between 0.5m to 3000m. It is based on electromagnetic theory and statistical analysis of terrain features and radio measurements. It is formulated to predict median attenuation of radio signals as a function of distance as well as the losses introduced due to refraction and clutter. The parameters that are required for this model are: 1. Frequency, 2. ERP (Effective Radiated Power), 3. Height of the antenna, 4. Antenna polarization, 5. Refractivity, 6. Permittivity, 7. Conductivity of the surface, 8. Earth's curvature and 9. Situation and time variability [158, 159].

8.5.2 The Okumura-Hata-Davidson Model

The Okumura-Hata-Davidson model is derived originally from Okumura-Hata [160] in order to provide wider range of input parameters like height, distance and frequency. The path loss can be calculated using Okumura-Hata-Davidson model using mathematical equations shown in [158] as:

$$PL_{OHD} = PL_{Hata} + A(h_1, d_{km}) - S_1(d_{km}) - S_2(h_1, d_{km}) - S_3(f_{MHz}) - S_4(f_{MHz}, d_{km}) \quad (46)$$

Where,

PL_{OHD} = path loss by Okumura-Hata-Davidson model

PL_{Hata} = path loss by Okumura-Hata model

h = height in meters

f = frequency in MHz

d = distance in km

$$PL_{Hata} = 69.55 + 26.16\log f_{MHz} - 13.82\log h_1 - a(h_2) + (44.9 - 6.55\log h_1)\cdot \log d_{km} \tag{47}$$

where, $a(h_2)$ represents mobile antenna height correction factor and can be mathematically presented as:

$$a(h_2) = \begin{cases} (1.1\log f_{MHz} - 0.7)\cdot h_2 - 1.56\log f_{MHz} + 0.8, \\ \text{for medium / small city, quasi-open area} \\ 8.29(\log(1.54h_2))^2 - 1.1, \\ \text{for large city and } f_c \le 300MHz \\ 3.2(\log(11.75h_2))^2 - 4.97, \\ \text{for large city and } f_c \ge 300MHz \end{cases} \tag{48}$$

The expressions of other parameters involved in the path loss equation are:

$$A(h_1, d_{km}) = \begin{cases} 0, \text{ when } d_{km} < 20 \\ 0.62137(d_{km} - 20\left[0.5 + 015\log\left(\frac{h_1}{121.92}\right)\right], \text{ when } 20 < d_{km} < 300 \end{cases} \tag{49}$$

$$S_1(d_{km}) = \begin{cases} 0, d_{km} < 64.38 \\ 0.174(d_{km} - 64.38), \text{ when } 64.38 \le d_{km} < 300 \end{cases} \tag{50}$$

$$S_2(h_1, d_{km}) = 0.00784\left|\log\left(\frac{9.92}{d_{km}}\right)\right|(h_1 - 300), \text{ when } h_1 > 300m \tag{51}$$

$$S_3(f_{MHz}) = \frac{f_{MHz}}{250}\log\left(\frac{1500}{f_{MHz}}\right) \tag{52}$$

$$S_4(f_{MHz}, d_{km}) = \left[0.112\log\left(\frac{1500}{f_{MHz}}\right)\right](d_{km} - 64.38), \text{ when } d_{km} > 6439km \tag{53}$$

In the above equations, the carrier frequency can range from 30 MHz to 1500 MHz; base station antenna height can vary from 20m to 2500m; mobile station antenna height can vary from 1 m

to 10m and the distance of transmission can vary from 1 km to 3000 km. The terms “A” and “S_1” are used for distance extension of 300km. The correction factor for base station antenna height “h1” is referred as S_2. Lastly, the correction factors responsible to extend the frequencies upto 1500 MHz are “S_3” and “S_4”.
At the receiving antenna, the expression of the electric field strength is:

$$E(dB\mu V/m) = ERP(dBW) - PL_{OHD}(dB) + 20\log f_{MHz} + 109.35 \quad (54)$$

8.5.3 The ITU-R P.1546 model

The ITU-R P.1546 is a propagation model recommended by International Telecommunications Union (ITU). This model applies to prediction of point to area transmission in the frequency range from 30 MHz to 3000 MHz for terrestrial service applications. It performs the interpolation or extrapolation of empirical data obtained for field strength as a function of path distance, antenna height and the percentage of time. There are some conditions that are implied for this model:

1. It should be noted that the propagation curves that present field strength values are for 1 kW ERP and include several input parameters. Additionally, the data collected was the result of measurements performed in two climate seasons and therefore, considerable difference can be seen if measurements are performed in other climatic conditions.

2. The maximum field strength values are valid only if the specific conditions are used.

3. The minimum value of the effective receiver mobile station antenna height should be 10m above the ground around the mobile station antenna.

4. For this model, the loss from transmitter to receiver is not equal to the loss from receiver to transmitter, and thus it suggests that this is a non-symmetrical model.

8.5.4 The ITU-R 525/526 model

ITU-R 525/526, also known as “Propagation by Diffraction”, uses the free-space path loss (FSPL) equation as described in ITU-R525 recommendation and as stated in equation 26. This model is recommended to use for DVB-T/T2 transmission with the combination of Deygout 94 diffraction model as it considers the three dominant obstructions in the Fresnel zone for the calculations.

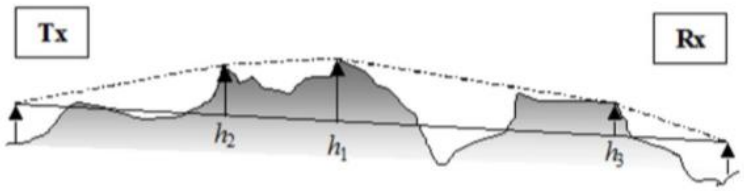

Figure 65. Three dominant obstructions considered in ITU-R P.525/526 with Deygout 94 mode [151].

8.6 Measurement campaigns

In total, two measurement campaigns were carried out from 2017-2019 in order to determine the electric field strengths at different points from broadcasting transmitters. Both the measurements were carried out in Huddersfield, UK. This section provides details about the transmitters involved in these campaigns.

8.6.1 Emley Moor DTV transmitting station

Emley Moor DTV transmitting station, also known as the Arqiva tower, is the tallest free-standing structure in the United Kingdom. It is 330.4m tall and is located in Emley, 7.2 miles from the University of Huddersfield. The geographical coordinates of this station are **Lat. N53.612049° Long W1.664439°.** It can cover almost all the major parts of Northern England with the help of a number of relays. The campaign involved measuring received signal strength from this transmitting station at four different locations in Huddersfield: 1. Castle Hill, Huddersfield (Lat. N53622312°, Long. W1.772157°) at the ground level, 2. Castle Hill Victoria top platform at 35m above the ground, 3. Holme Moss (Lat. N53.531919°, Long. W1.852700°) and 4. Greenhead park. The measurement points were selected such that all of them provided LOS path to the transmitting station in Emley Moor. A picture of the Emley moor broadcasting tower is shown in Figure 66.

Figure 66. Emley Moor broadcasting tower.

Emley Moor broadcasting tower provides several TV and radio services which are listed below:

8.6.1.1 Analogue Radio (FM) services

Table 16. Analog radio FM services provided by Emley Moor broadcasting station.

Frequency (MHz)	Radiated power (kW)	Service
105.1	2.55	Capital Yorkshire
106.2	2.35	Heart Yorkshire

8.6.1.2 Digital radio (DAB) services

Table 17. Digital radio DAB services provided by Emley Moor broadcasting station.

Frequency (MHz)	Block	Radiated power (kW)	Operator
216.928	11A	10	Sound Digital
222.064	11D	8.5	Digital One
225.648	12B	10	BBC National DAB
229.072	12D	5	Leeds

8.6.1.3 DTV (DVB-T/DVB-T2) services

Table 18. DTV (DVB-T/DVB-T2 services provided by Emley Moor broadcasting station.

Frequency (MHz)	Channel	Radiated Power (kW)	Operator	System
562.000	32	54.8	COM7 (ARQ C)	DVB-T2
578.000	34	51.1	COM8 (ARQ D)	DVB-T2
634.000	41	174	PSB3 (BBC B)	DVB-T2
658.000	44	174	PSB2 (D3 & 4)	DVB-T
682.000	47	174	PSB1 (BBC A)	DVB-T
690.000	48	174	COM6 (ARQ B)	DVB-T
714.000	51	174	COM4 (SDN)	DVB-T
722.000	52	174	COM5 (ARQ A)	DVB-T
754.000	56	5	LTVmux	DVB-T

Table 19. System configurations of Emley Moor broadcasting station.

Frequency	Channel	Encoding	Modulation	Technology	Antenna	Electrical tilt
562.000	32	MPEG 4	256 QAM	Solid State	S1	NO
578.000	34	MPEG 4	256 QAM	Solid State	S1	NO
634.000	41	MPEG 4	256 QAM	IOT	S1	NO
658.000	44	MPEG 2	64 QAM	IOT	S1	NO
682.000	47	MPEG 2	64 QAM	IOT	S1	NO
690.000	48	MPEG 2	64 QAM	Solid State	S2	YES
714.000	51	MPEG 2	64 QAM	IOT	S2	YES
722.000	52	MPEG 2	64 QAM	Solid State	S2	YES
754.000	56	MPEG 2	QPSK	Solid State	DIR	NO

COM in the above table refers to commercial operators, PSB refers to the Public Service Broadcast that comprises of public stations. Some of the examples of PSB are BBC and ITV. DVB-T technology is used to transmit Standard Definition (SD) channels whereas the DVB-T2 technology is used to transmit High-Definition (HD) channels. IOT stands for inductive output tube, a technology that utilises valve power amplifiers for radio wave amplification. Solid state technology and the IOT technology in this station both provide an output power around 12kW-14kW. Therefore, for the simulation study, an average power of 13 kW was assumed for the calculations for both the cases.

This broadcasting station comprises of three antenna arrays: S1, S2 and S3. Mostly, S1 and S2 are used for transmission, while S3 array is kept on stand-by. These antenna array comprise of Katherein antenna panels in four directions. The transmitter antenna provides a gain of approximately 12.15 dBi, that is equivalent to 10 dBd, after including coaxial feeder loss. S1 array beams towards the horizon whereas S2 array implements a few degrees of downward electrical tilt.

8.6.2 Belmont DTV Transmitter

Belmont DTV transmitter is located on the B1225 route near Donnington of Bain in the Lincolnshire region. It is coordinated at Lat. N53.335844 Long. W0.171980 and is owned and operated by Arqiva. The antenna is located at 351.7m above sea level. It used to be one of the

tallest structures within the European Union with a height of 387.7m, however, in April 2010, the height of the antenna mast was shortened which lead to its reduced height of 351.7m. It is still the 14th highest structure in the European Union and is 2nd highest structure in the United Kingdom. It is responsible to provide digital TV, analogue and digital radio to the Lincolnshire, eastern Yorkshire, northern parts of Norfolk and a few parts of Nottinghamshire. After the switchover from analogue to digital, the Belmont transmitting station transmits at 50 kW for Mux A, 100 kW for Arqiva A & B and 150 kW for BBC. A picture of Belmont's transmitting tower is shown below:

Figure 67. Belmont transmitting station.

Figure 68. Antenna mast of the Belmont's transmitting tower.

The path profiles and the electric field strengths of the transmitted signal from this broadcasting station were measured at different locations, which are listed in the results section.

Some of the services provided by these transmitting stations are listed in the tables below:

8.6.2.1 UHF DTV services

Table 20. UHF DTV services provided by Belmont transmitting station.

Frequency (MHz)	UHF Channel	Radiated Power (kW)	Operator	System
482	22	150	BBC A	DVB-T
506	25	150	Digital 3 & 4	DVB-T
522	27	5	Local TV	DVB-T
530	28	150	BBC B	DVB-T2
545.833	30-	50	SDN	DVB-T
570	33	37.1	Arqiva C	DVB-T2
586	35	40.9	Arqiva D	DVB-T2
730	53	100	Arqiva A	DVB-T
786	60	100	Arqiva B	DVB-T

8.6.2.2 Analog Radio (FM VHF) services

Table 21. Analog radio-FM VHF services provided by Belmont transmitting station.

Frequency (MHz)	Radiated Power (kW)	Service
88.8	8	BBC Radio 2
90.9	8	BBC Radio 3
93.1	8	BBC Radio 4
94.9	3	BBC Radio Lincolnshire
98.3	8	BBC Radio 1
100.5	3.1	Classic FM
102.2	3.2	Lincs FM

8.6.2.3 Digital radio (DAB)

Table 22. Digital radio (DAB) services provided by the Belmont transmitting station.

Frequency (MHz)	Block	Radiated power (kW)	Service
215.072	12A	—	MuXCo Lincolnshire
216.928	11A	—	Sound Digital
222.064	11D	5	Digital One
225.648	12B	5	BBC National DAB

8.7 Simulation Setup

The results obtained from measurement campaigns were used to compare with the results obtained by simulation software using different propagation models like Longley Rice, Deygout 94, Epstein Peterson, Bullington model, ITU-R P.1546 and Okumura-Hata Davidson. Simulations were performed using three simulation softwares: 1. ATDI ICS Telecom (commercial software), 2. Radio Mobile (freeware software) and 3. Home developed propagation models in Matlab. The simulation setup is described in this section. All simulations were performed on an 8-core Intel i7-5960X processor at 3 GHz, with 64 GB RAM memory.

8.7.1 ICS Telecom

The measurement setup was duplicated in the ICS Telecom software by placing the Emley Moor station and other measurement points on the United Kingdom map with respective latitude and longitude coordinates.

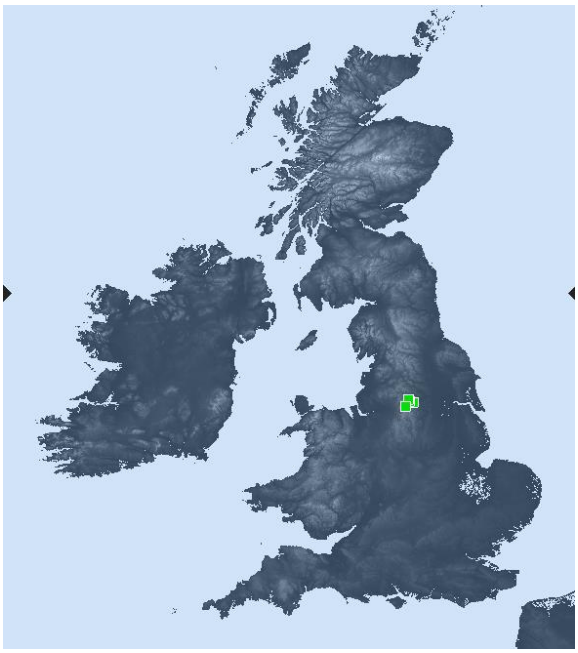

Figure 69. Emley Moor measurement campaign setup in ICS Telecom

It should be noted that before placing the stations on the ICS Telecom software, a digital 3D elevation model layer of ".GEO" format for the United Kingdom needs to be added to the project file. Additionally, the clutter file is also added to the project in order to provide the details of clutters including several obstacles like vegetation, buildings etc. to the ICS project. Both these layers will help in providing accurate simulation results. The Emley Moor transmitter configuration is setup in the software as shown in Figure 70.

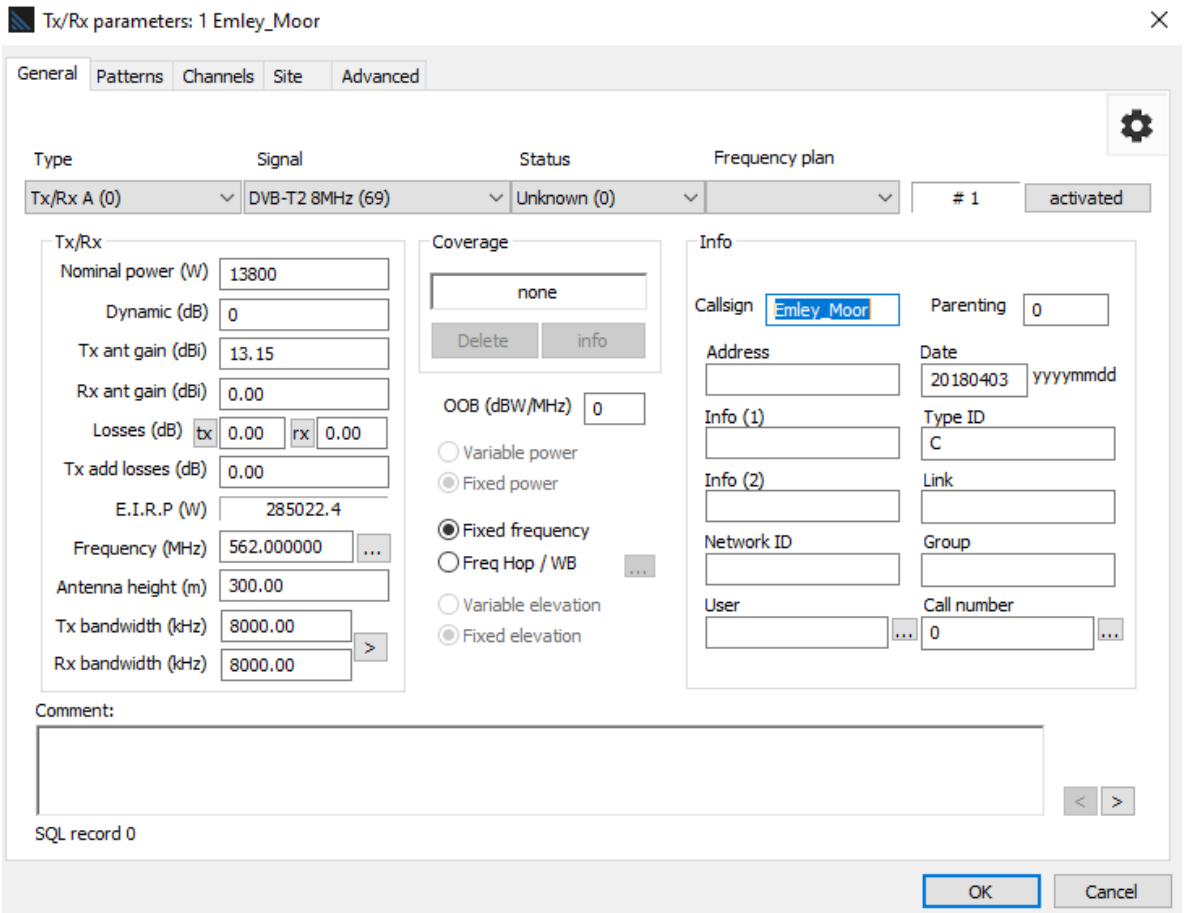

Figure 70. Emley Moor transmitting station configuration.

The actual transmitting antenna configurations were setup in the simulation software including its radiation patterns, gain and polarization. In this case, the nominal power was set to 13.8 kW and the antenna height of 300 m was selected. The frequency of interest and the propagation model can be selected as required. Additionally, this antenna was set to provide horizontal polarization for transmitting and receiving end and a gain of 13.15 dBi. The setup of antenna pattern in ICS software is shown in Figure 71 and it is omni-directional.

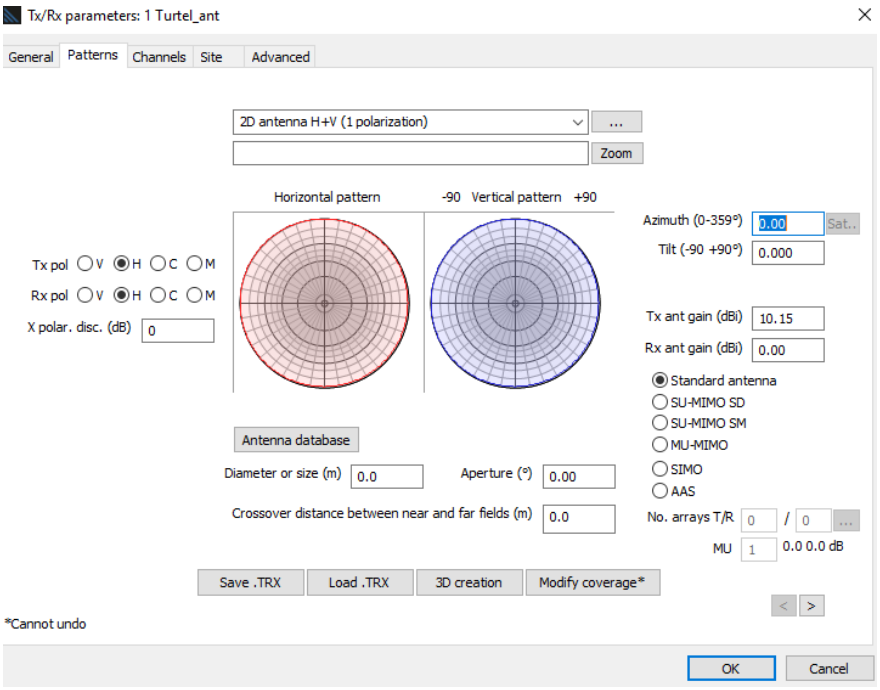

Figure 71. Setup for antenna pattern configuration in ICS.

Similar to Emley Moor configurations, the setup replicating the measurement campaign for Belmont broadcasting station was implemented in ICS Telecom as shown in Figure 72.

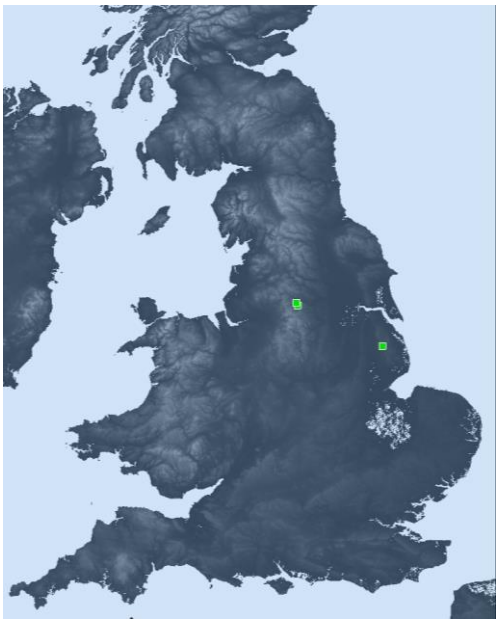

Figure 72. Belmont measurement campaign setup in ICS Telecom.

8.7.2 Radio mobile

One of the aspects of this study, is to compare ICS Telecom (a commercial software by ATDI) and Radio Mobile by simulating coverage using different propagation models. Therefore, a similar setup for Emley Moor TV transmitter and Belmont transmitter was implemented in the Radio Mobile software by adding both the transmitters and the measurement points on the United Kingdom map. The Radio Mobile software is a freeware that was introduced by Roger Coudé, a radio amateur from Canada. However, this software is capable to simulate and perform propagation calculations only by using NTIA-ITS Longley Rice Model (Irregular Terrain Model). On the other hand, ICS Telecom provides a wide range of propagation models to use for propagation calculations. A comparison of the propagation calculations using different propagation models in ICS Telecom and Radio Mobile with measurements is demonstrated in the results section. Radio Mobile makes use of elevation data that is made publicly available by NASA's SRTM mission.

8.7.3 Matlab algorithm for propagation prediction

Two matlab algorithms were developed previously by University of Huddersfield and Brunel University that perform calculations for path profiles using the Deygout and Epstein-Peterson propagation models. The idea of this collaboration was to compare the propagation models provided by ICS Telecom and Radio Mobile with the algorithms developed by the collaborators and the measurement data. Similar to Radio Mobile, these algorithms make use of the SRTM data for terrain elevation provided by the National Aeronautics and Space Administration (NASA) in order to estimate the path profile between two stations. These algorithms require the user to provide a few input parameters like: frequency of operation, transmitter power, height of the transmitting antenna, height of the receiving antenna, name of the transmitter, latitude and longitude of the transmitter and receiver.

The algorithm then performs calculations according to the propagation model selected after considering the number of knife-edges as well as the elevation conditions.

Furthermore, several calculations were performed similarly for both the measurement campaigns. The comparison of the results obtained from these algorithms is shown along with the comparison with results from ICS Telecom, Radio Mobile and actual measurement data in the next section.

8.8 Results and discussion

This section provides the comparison of the results obtained from the actual measurement campaign, ICS, Telecom, Radio Mobile and Matlab algorithms for the measurement campaigns: 1. Emley Moor transmitter, and 2. Belmont transmitter.

8.8.1 Emley Moor DTV transmitter

8.8.1.1 Electric field strength comparison at three locations

The signal strength of the Emley Moor transmitter was measured at: 1. Victoria Tower-Top of Castle Hill, 2. Greenhead Park and 3. Holme Moss. The signal strengths measured were in dBμV, thus they need to be converted to electric field strengths (dBμV/m). This can be done with the help of the antenna factor used for the reception. For this campaign, a 10-dipole Iskra P20 LPDA was used for reception. By adding the antenna factor to the measured signal strength, the electric field strength is calculated.

Table 23 shows the signal strength and electric field strength of the signal from Emley Moor broadcasting station at Victoria top of Castle Hill, Greenhead park and Holme Moss. The average transmitter power of 13 kW and an antenna gain of 12.5 dBi were considered for these measurements. The measurements were recorded at the three locations for 8 TV channels ranging from 562 MHz to 754 MHz.

In table 23, column 2 shows the details of the transmitter and the channel number and its respective center frequency. The table suggests that very strong signal is received from Emley Moor tower to all the three locations. However, it is observed that electric field strength is higher in the case of Victoria Tower and Holme Moss compared to Greenhead park. The reason for this is because Castle Hill and Holme Moss are situated high above the ground level and thus receive higher electric field strength compared to Greenhead park.

Table 23. Measured electric field strength of the signal from Emley Moor broadcasting station to the 3 locations in Huddersfield region.

No.	Transmitter Emley Moor DTV LAT 53.612049 N LONG 1.664439 W Altitude 256.0 m Average power 13 kW, antenna gain 12.5 dBi Antenna height 537m a.s.l, 300m a.g.	Antenna correction factor for Iskra P20 Log-Periodic with 2m LMR200 cable and N connector (dB/m)	Victoria Tower - Top (7.20km, 279° H, -2.16° V) Antenna height 307m a.s.l / 34.3m above ground LAT 53.622245 N LONG 1.772236 W		Greenhead Park (9.61km, 295° H, -2.5° V) Antenna height 140.3m a.s.l / 2m above ground LAT 53.648782 N LONG 1.796412 W		Holme Moss (15.3km, 234° H, -0.26° V) Antenna height 502.3m a.s.l / 2m above ground LAT 53.531919 N LONG 1.852700 W	
			Signal Strength (dB µV)	Electric Field Strength (dBµV/m)	Signal Strength (dB µV)	Electric Field Strength (dBµV/m)	Signal Strength (dB µV)	Electric Field Strength (dBµV/m)
1	Channel 32 562 MHz	19.3	85.7	105.0	75.5	94.8	85.3	104.6
2	Channel 34 578 MHz	19.5	85.9	105.4	79.2	98.7	82.6	102.1
3	Channel 41 634 MHz	20.2	84.0	104.2	78.8	99.0	83.2	103.4
4	Channel 44 658 MHz	20.7	88.0	108.7	78.5	99.2	83.8	104.5
5	Channel 48 690 MHz	21.4	92.3	113.7	82.3	103.7	79.9	101.3
6	Channel 51 714 MHz	21.6	89.9	111.5	80.9	102.5	77.2	98.8
7	Channel 52 722 MHz	21.6	87.4	109.0	81.8	103.4	75.9	97.5

8.8.1.2 Emley Moor to Victoria Tower (Castle Hill top)

This section presents: 1. comparison of the electric field strength to the free-space calculations and 2. comparison of path profiles using ICS Telecom, Radio Mobile and Matlab algorithm from Emley Moor to Victoria tower.

8.8.1.2.1 Electric field strength comparison with free-space

Table 24. Comparison of measured electric field strengths and free-space loss at Victoria tower top.

No.	Channels Emley Moor DTV DVB-T/T2 LAT.: 53.612049 N LONG.: 1.64439 W Altitude 256m	Frequency	E(dBµV/m) received at Victoria Tower Top		Difference (dB)
			Measurements	Free space	
1	Channel 32	562 MHz	105	110.9	-5.9
2	Channel 34	578 MHz	105.4	110.9	-5.5
3	Channel 41	634 MHz	104.2	110.9	-6.7
4	Channel 44	658 MHz	108.7	110.9	-2.2
5	Channel 48	690 MHz	113.7	110.9	2.8
6	Channel 51	714 MHz	111.5	110.9	0.6
7	Channel 52	722 MHz	109	110.9	-1.9

The comparison of the electric field strength with free-space loss is shown in Table 24. Data from table 24, shows that a weaker signal is obtained from channel 32, channel 34 and channel 41 compared to the other channels with higher frequencies. The possible reason for this may be due to the different antenna systems involved in broadcasting. In this case, S1 and S2 array are used for broadcasting for DTV broadcasting. It is known that the S2 antenna array provides

a slight electrical down tilt while the S1 antenna array points the beam to the horizontal direction.

8.8.1.2.2 Path profile comparison

The path profiles from Emley Moor tower to Victoria tower simulated in Radio Mobile, ICS Telecom, and matlab are shown in Figures 73, 74 and 75 respectively.

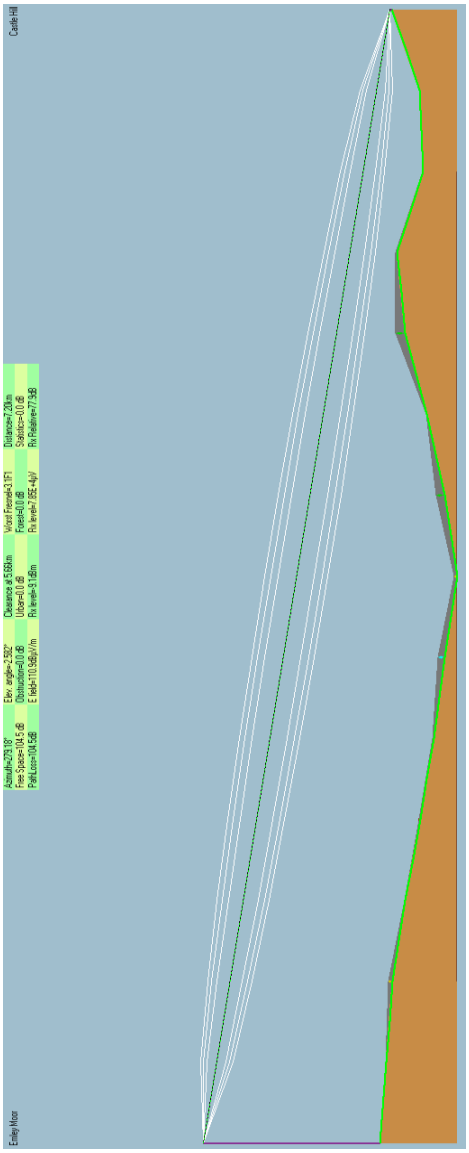

Figure 73. Path profile from Emley Moor to Victoria tower top in Radio Mobile.

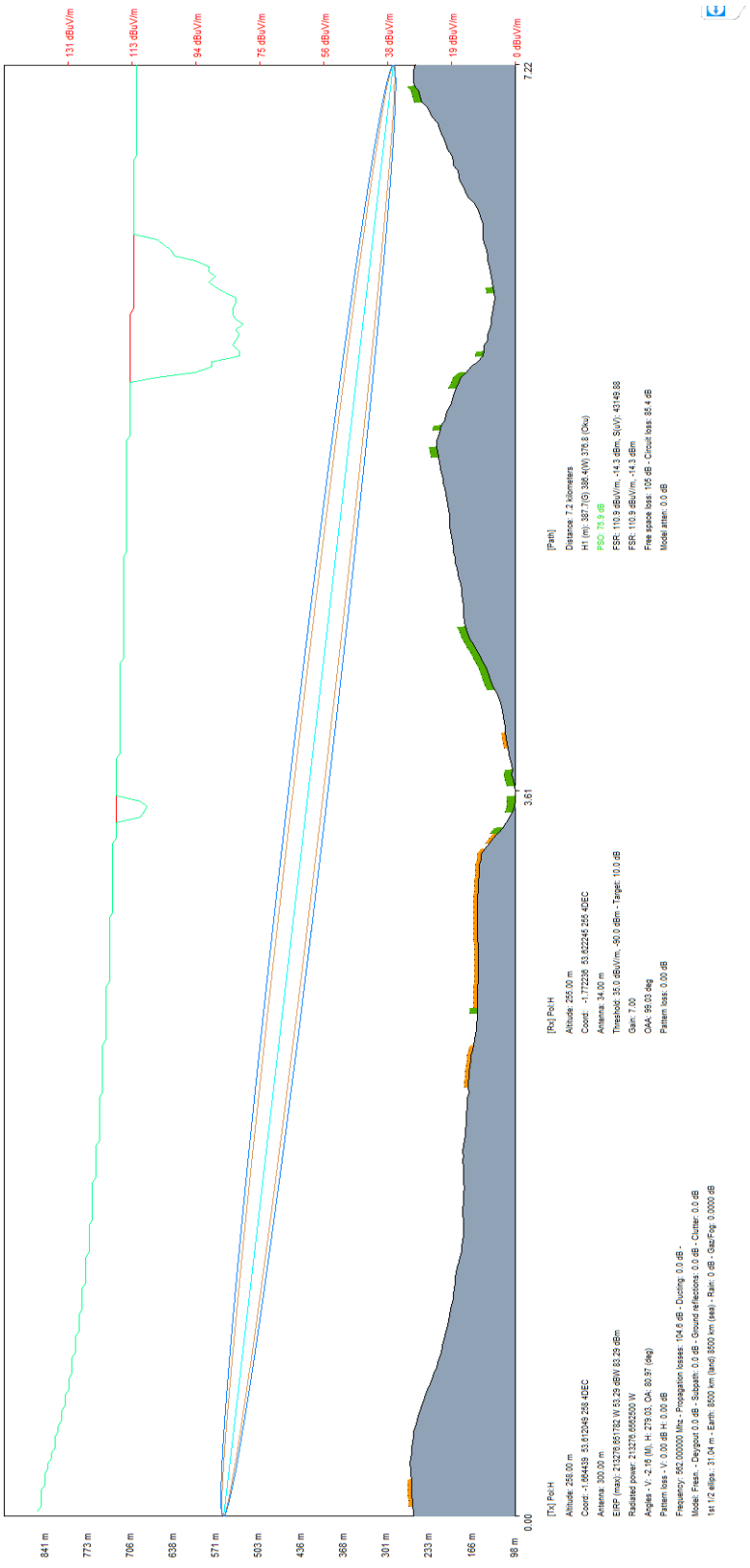

Figure 74. Path profile from Emley Moor to Victoria tower top in ICS Telecom.

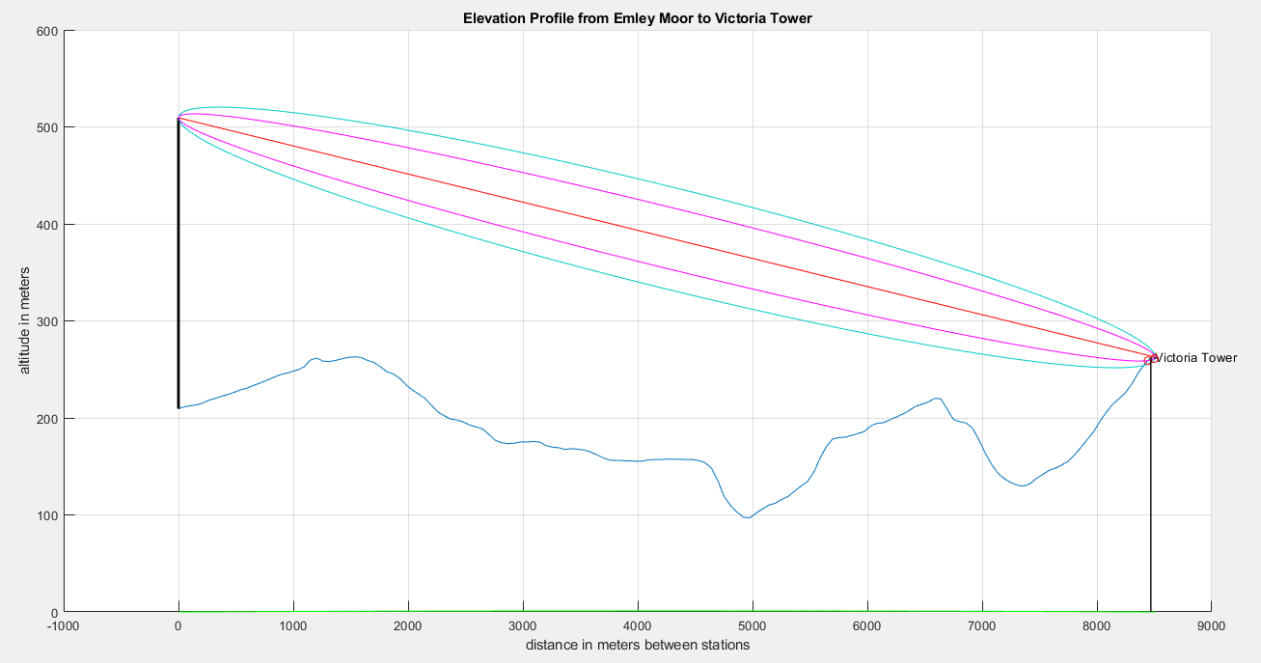

Figure 75. Path profile from Emley Moor to Victoria tower top using Matlab.

The path profiles from Figure 73, 74 and 75 suggest that all three simulations predict the path profile between Emley Moor and Victoria Tower correctly. They clearly demonstrate that there are no obstacles in their path and thus propagation in this case can be suggested to follow LOS. Thus, all three simulations present elevation data accurately.

8.8.1.3 Emley Moor to Holme Moss

Similar to the previous section, this section also presents: 1. Comparisons of electric field strength and free-space field-strength and 2. Comparison of path profiles from the Emley Moor broadcasting station to Holme Moss.

8.8.1.3.1 Actual electric field strength comparison with free-space

Table 25. Comparison of the measured electric field strength with free space field-strength at Holme Moss.

No.	Channels Emley Moor DTV DVB-T/T2 LAT.: 53.612049 N LONG.: 1.64439 W, Altitude 256m	Frequency	E(dBμV/m) received at Holme Moss		Difference (dB)
			Measurements	Free-space	
1	Channel 32	562 MHz	104.6	104.3	0.3
2	Channel 34	578 MHz	102.1	104.3	-2.2
3	Channel 41	634 MHz	103.4	104.3	-0.9
4	Channel 44	658 MHz	104.5	104.3	0.2
5	Channel 48	690 MHz	101.3	104.3	-3.0
6	Channel 51	714 MHz	98.8	104.3	-5.5
7	Channel 52	722 MHz	97.5	104.3	-6.8

In this case of reception at Holme Moss, the observation is completely opposite as compared to the reception at Victoria Tower. It was observed that stronger signals were received for Channels 32, 34, 41 and 44 compared to the remaining channels. The reason for this is that S1 antenna array does not provide any electrical tilt and thus the beam faces the horizontal direction. It is well known that Holme Moss is positioned in a straight line to the Emley Moor tower without practically any tilt.

8.8.1.3.2 Path profile comparison

The path profiles from Emley Moor tower to Victoria tower simulated in Radio Mobile software, ICS Telecom and matlab algorithm is shown in Figure 76, 77 and 78 respectively.

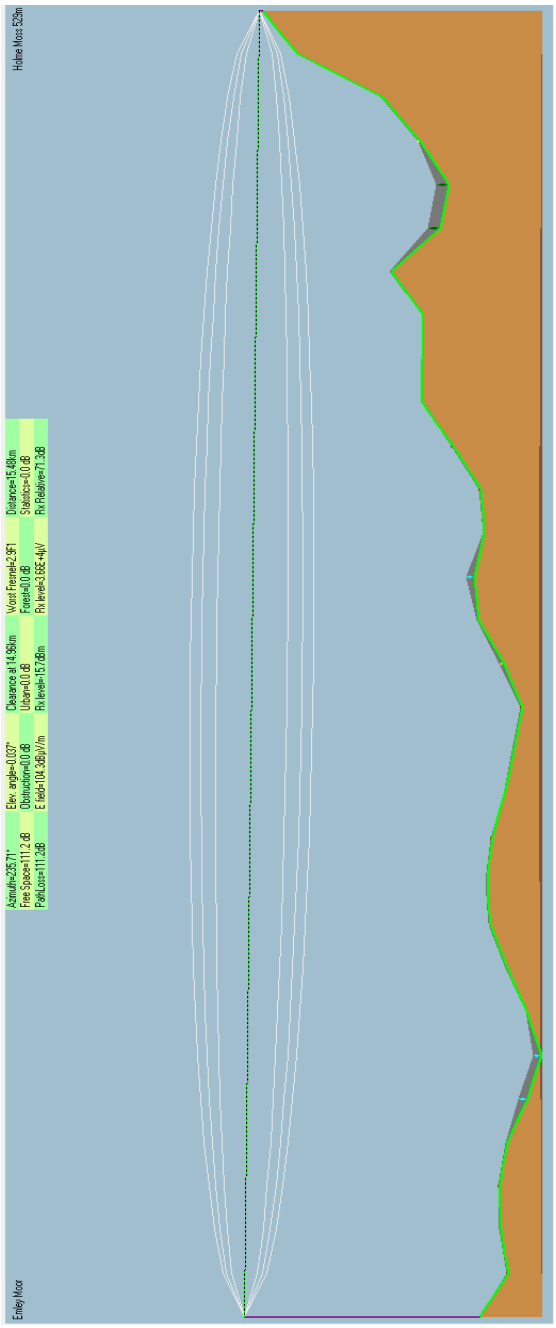

Figure 76. Path profile from Emley Moor to Holme Moss in Radio Mobile.

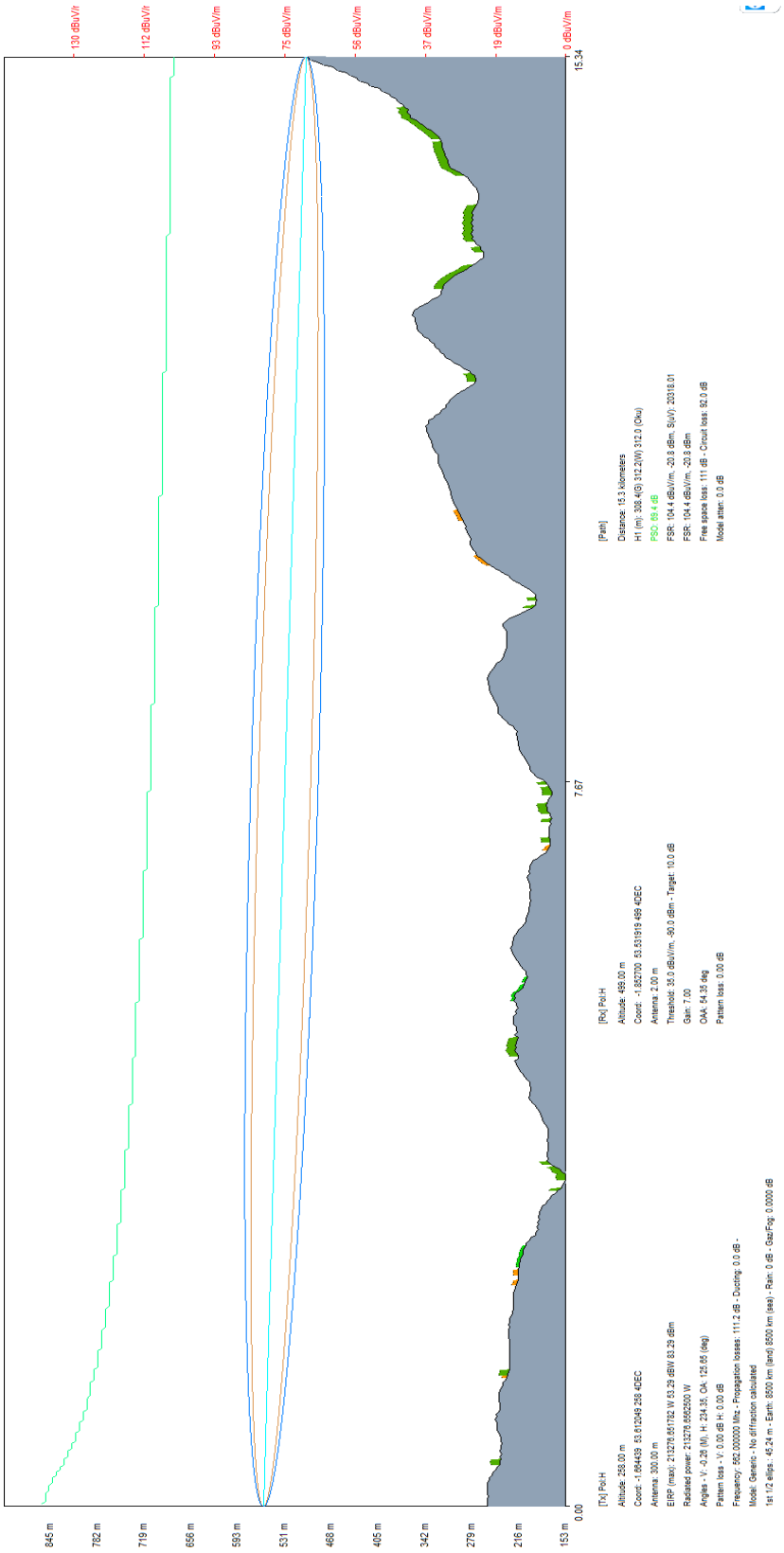

Figure 77. Path profile from Emley Moor to Holme Moss in ICS Telecom.

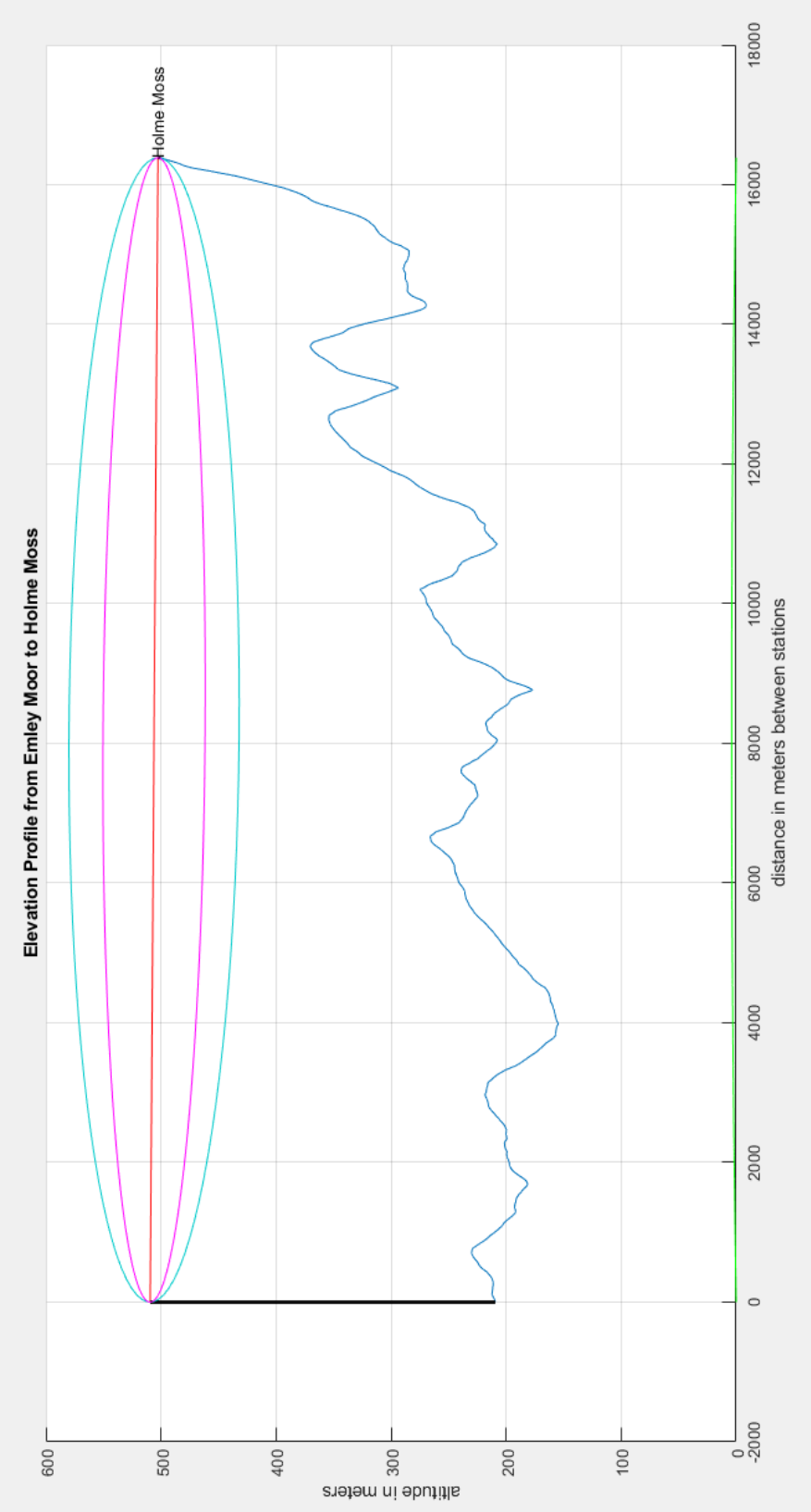

Figure 78. Path profile from Emley Moor to Holme Moss using Matlab.

The path profiles predicted by Radio Mobile, ICS Telecom and Matlab algorithm from Emley Moor to Holme Moss suggests that the no obstacles are observed between their path and thus they demonstrate LOS propagation. Also, it is observed that there is almost no electrical tilt (approximately 0.26 degrees) between them and thus they face horizontally straight to each other.

8.8.1.4 Emley Moor to Greenhead park

This section provides: 1. Comparison of electric field strength and free-space field-strength and 2. Comparison of path profiles from Emley Moor broadcasting station to Greenhead Park.

8.8.1.4.1 Electric field strength comparison with free-space

Table 26. Comparison of the measured electric field strength with the free-space and other simulated values obtained by other propagation models.

No.	Channels Emley Moor DTV DVB-T/T2 LAT.: 53.612049 N LONG.: 1.64439 W Altitude 256m	Frequency	E(dBμV/m) received at Victoria Tower Top			
			Measurements	Free space	Longley-Rice (ICS Telecom)	Deygout 94 (ICS Telecom)
1	Channel 32	562 MHz	94.8	108.4	81.6	99.3
2	Channel 34	578 MHz	98.7	108.4	81.2	99.3
3	Channel 41	634 MHz	99.0	108.4	79.9	99.2
4	Channel 44	658 MHz	99.2	108.4	79.4	99.1
5	Channel 48	690 MHz	103.7	108.4	78.8	99.0
6	Channel 51	714 MHz	102.5	108.4	78.3	99.0
7	Channel 52	722 MHz	103.4	108.4	78.1	99.0

Table 26 suggests that the Electric field strength values predicted by Deygout 94 are closer to the measured electric field strength values, while Longley-Rice model has a higher difference in the values compared to the Deygout 94.

8.8.1.4.2 Path profile comparison

The path profiles from Emley Moor tower to Greenhead Park simulated in Radio Mobile, ICS Telecom and Matlab are shown in Figure 79, 80 and 81 respectively.

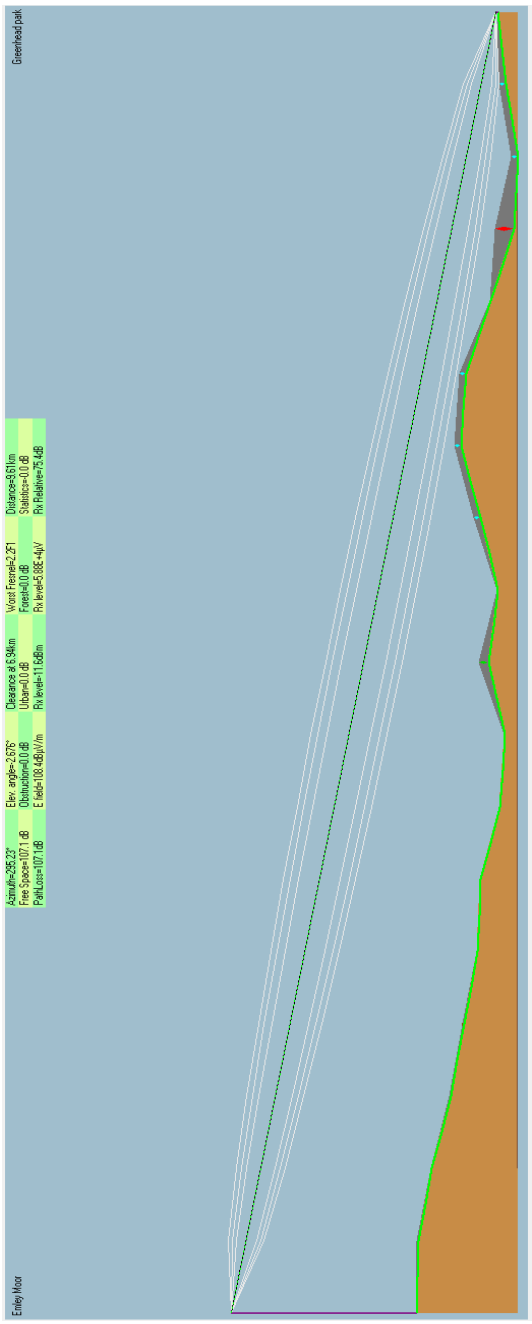

Figure 79. Path profile from Emley Moor to Holme Moss using Radio Mobile.

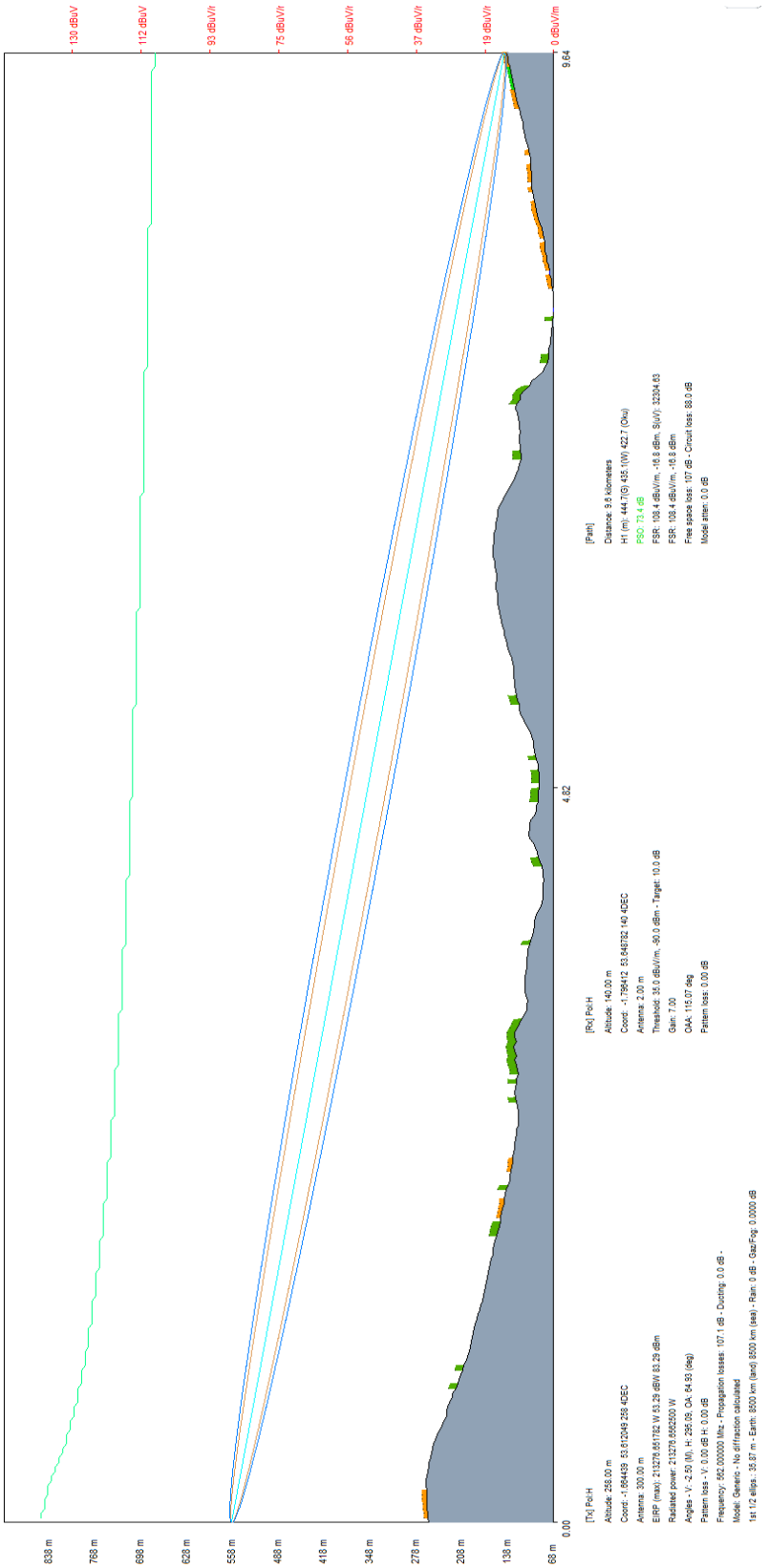

Figure 80. Path profile from Emley Moor to Holme Moss using ICS Telecom.

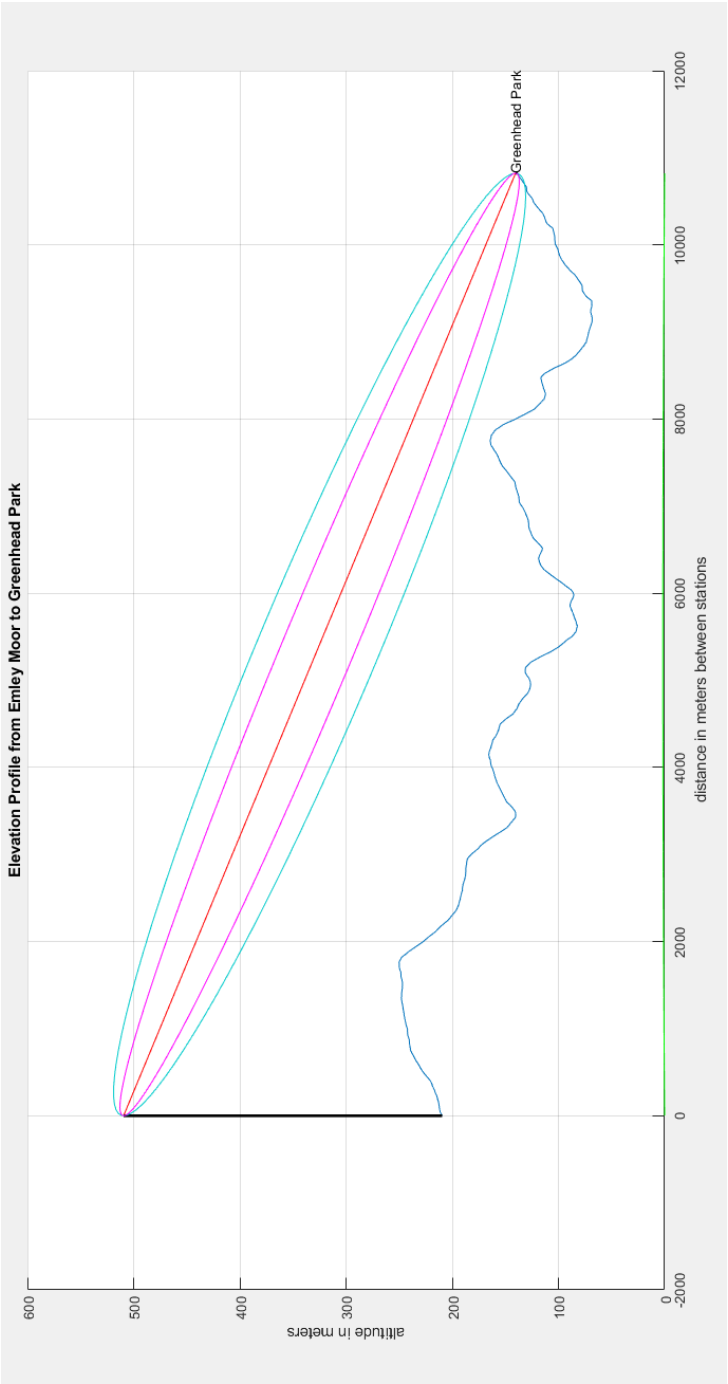

Figure 81. Path profile from Emley Moor to Holme Moss using Matlab algorithm.

The path profile predicted by Radio Mobile, ICS Telecom and Matlab algorithm suggests that LOS propagation is observed as there are no obstacles in their path. Additionally, a downward electrical tilt is observed between them.

8.8.1.5 Emley Moor transmitter coverage

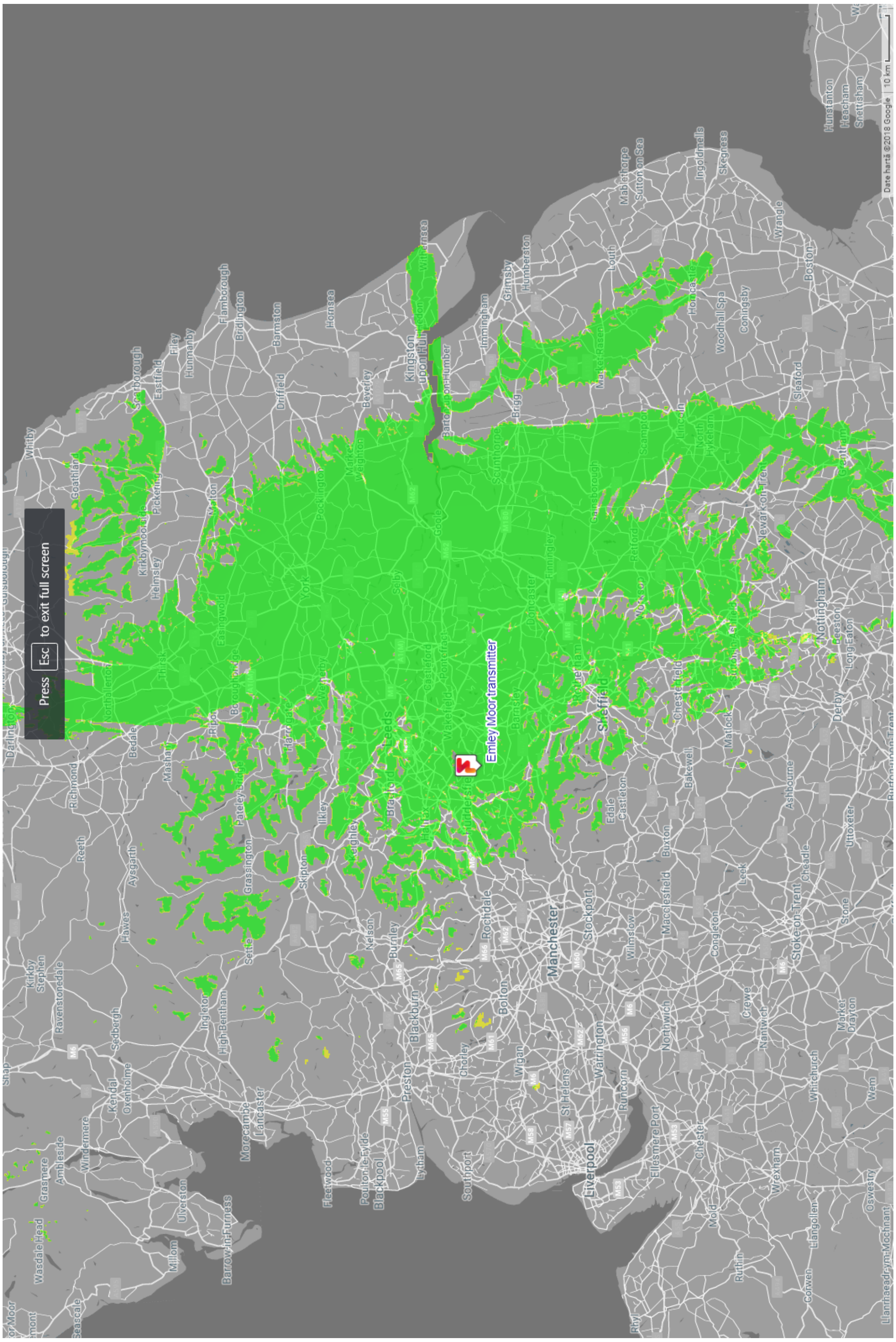

Figure 82. Official UK coverage provided by Freeview TV web source [161].

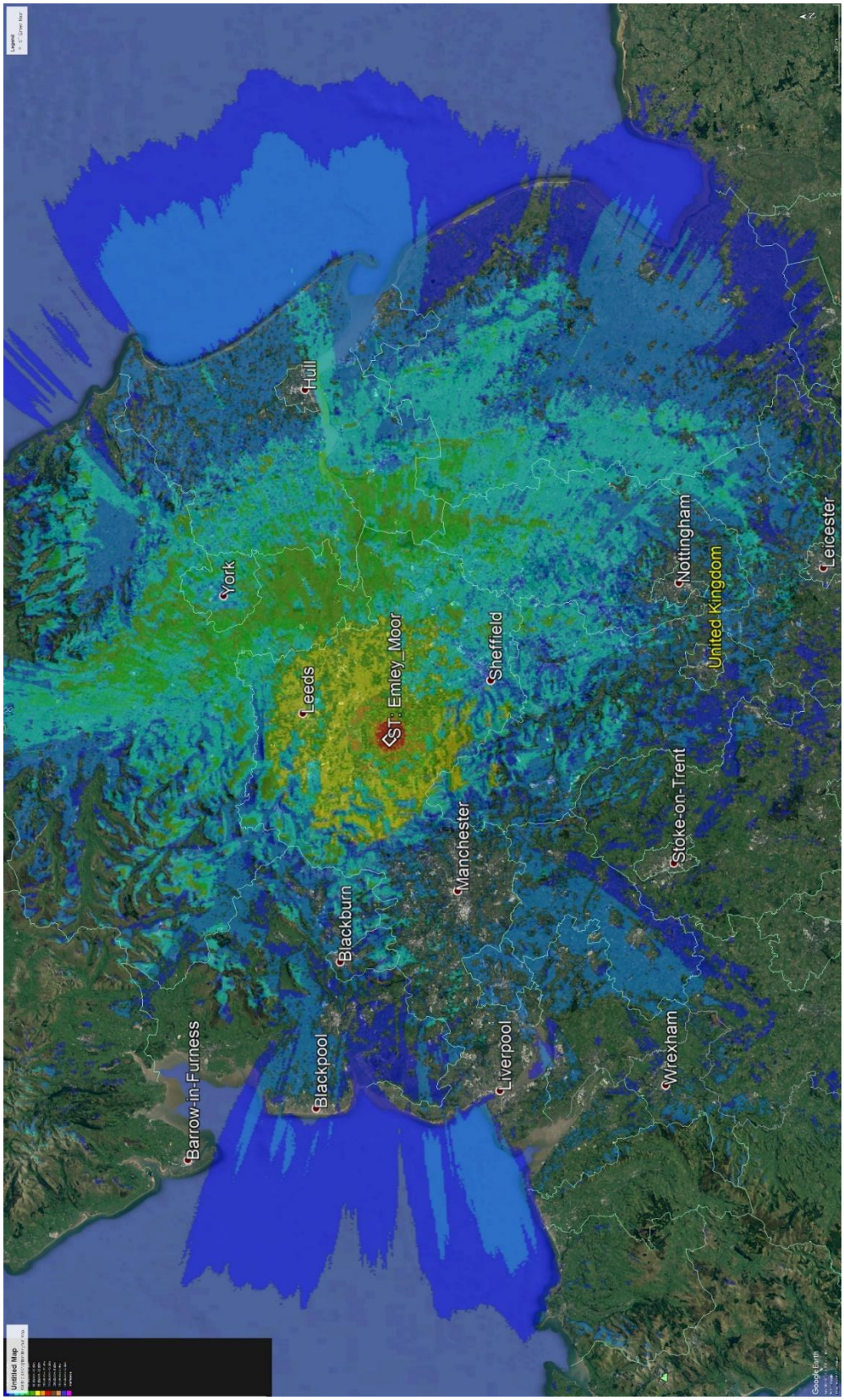

Figure 83. Predicted Emley Moor transmitter coverage using Deygout 94 (threshold as 45 dBµV/m)..

Figure 82 shows the official coverage of the Emley Moor transmitter released by Freeview web source. Freeview is one of the UK's brand that provides DTV services in major parts of the country. This image was used to compare it with the Emley Moor transmitter coverage predicted by the ICS Telecom software. Deygout 94 model was used to predict this coverage. The simulation also included sub path attenuation loss in order to improve the simulation accuracy. Furthermore, for this simulation, Fresnel significant fraction of 0.6 was considered. The coverage was calculated from 175 kms from the Emley Moor transmitter in all the directions, where the reception threshold was set to 45 dBμV/m as shown in Figure 83. The zones with red, orange and yellow colour represent area that receives strong electric field whereas the zones with white and blue colour represents lowest reception of electric field strength. After comparing Figure 82 and Figure 83, it can be stated that the predicted coverage of Emley Moor transmitter resembles very close to the official coverage provided by Freeview. It can also be concluded that the Emley Moor transmitter covers almost all the parts of Yorkshire and Lancashire, in addition to some parts of Lincolnshire, Teesside and Northumberland.

8.8.2 Belmont Transmitter

8.8.2.1 Electric field strength comparison at 2 locations

The signal strength of the Belmont transmitter was measured at: 1. Victoria Tower, and 2. Greenhead Park. The signal strengths measured were in dBµV, thus they need to be converted into electric field strengths (dBµV/m). This can be done with the help of antenna correction factor of the receiving antenna. For this campaign, a 10-dipole Iskra P20 LPDA was used for reception. By adding the antenna factor to the measured signal strength, the electric field strength is calculated.

Table 27. Measured signal strength and electric field strength from Belmont transmitter in Huddersfield region.

No.	Transmitter Belmont DTV LAT 53.335844 N LONG 0.171980 W Altitude 128.0 m Average power 10kW, antenna gain 17.15 dBi Antenna height 480m a.s.l, 352m a.g.	Antenna correction factor for Iskra P20 Log-Periodic with 2m LMR200 cable and N connector (dB/m)	Victoria Tower - Top (110.9km, 287°H, -0.47°V) Antenna height 307m a.s.l / 34.3m above ground LAT 53.622245 N LONG 1.772236 W		Greenhead Park (113.5km, 288°H, -0.55° V) Antenna height 140.3m a.s.l / 2m above ground LAT 53.648782 N LONG 1.796412 W	
			Signal Strength (dB µV)	Electric Field Strength (dBµV/m)	Signal Strength (dB µV)	Electric Field Strength (dBµV/m)
1	Channel 22 482 MHz	17.84	60.3	78.1	30.6	48.4
2	Channel 25 506 MHz	18.13	62.2	80.3	32.5	50.6
3	Channel 28 530 MHz	18.52	62.7	81.2	32.0	50.5
4	Channel 60 786 MHz	21.41	57.8	79.2	29.2	50.6

8.8.2.2 Comparison of measured and simulated electric field strength

8.8.2.2.1 Belmont station to Victoria tower

Table 28. Comparison of the measured electric field strength to the simulated values from Belmont station to Victoria tower.

No.	Channels Belmont DTV DVB-T2 LAT.: 53.335844 N LONG.: 0.171980 W Altitude 128m	Frequency	E(dBuV/m) received at Victoria Tower Top						
			Measurements	Free-space	Longley-Rice (Radio Mobile)	Longley-Rice (ICS Telecom)	Deygout 94 (ICS Telecom)	Deygout 94 (Matlab)	Epstein-Peterson (Matlab)
1	Channel 22	482 MHz	78.1	91.1	77.3	77.9	79.0	78.8	78.6
2	Channel 25	506 MHz	80.3	91.1	77.3	78.0	79.1	78.8	78.6
3	Channel 28	530 MHz	81.2	91.1	77.3	78.2	79.1	78.8	78.6
4	Channel 60	786 MHz	79.2	91.1	77.1	80.0	79.3	78.7	78.5

Table 28 suggests that the measurements and simulations were performed for four channels: 22, 25, 28 and 60 with centre frequencies of 482 MHz, 506 MHz, 530 MHz and 786 MHz respectively. It is observed that the simulated results obtained from all the propagation models were very close to the measured data. Further analysis on this data is performed by calculating the difference between the measured and the other simulated values. This error difference provided a good estimate on which model is closer to the measured data.

Table 29. Difference error between the measured and simulated electric field strength values from Belmont station to Victoria Tower.

No.	Channels Belmont DTV DVB-T2 LAT.: 53.335844 N LONG.: 0.171980 W, Altitude 128m	Frequency	Difference to measurements to Victoria Tower (dB)					
			Free-space	Longley-Rice (Radio Mobile)	Longley-Rice (ICS Telecom)	Deygout 94 (ICS Telecom)	Deygout 94 (Matlab)	Epstein-Peterson (Matlab)
1	Channel 22	482 MHz	-13.0	0.8	0.2	-0.9	-0.7	-5.0
2	Channel 25	506 MHz	-10.8	3.0	2.3	1.2	1.5	1.7
3	Channel 28	530 MHz	-9.9	3.9	3.0	2.1	2.4	2.6
4	Channel 60	786 MHz	-11.9	2.1	2.1	-0.1	2.5	0.7
Average Difference			**-11.4**	**2.5**	**1.9**	**0.6**	**1.4**	**0.0**
Standard Deviation			**1.2**	**1.1**	**1.0**	**1.2**	**1.3**	**3.0**

The difference of the measured values and the simulated values is shown in Table 29. This table suggests that since the error values are small, the simulations are in good agreement with the measurements. However, it is difficult to make an assertion on the best propagation model. Epstein-Peterson model in Matlab showed an average difference of 0, and thus provides a good prediction for this scenario. On the other hand, Radio Mobile and ICS Telecom simulations provided low standard deviations and also provide good estimate of the electric field strength values.

8.8.2.2.2 Belmont station to Greenhead park

Table 30. Comparison of the measured electric field strength to the simulated values from Belmont station to Greenhead park.

No.	Channels Belmont DTV DVB-T2 LAT.: 53.335844 N LONG.: 0.171980 W, Altitude 128m	Frequency	E(dBμV/m) received at Greenhead Park						
			Measurements	Free-space	Longley-Rice (Radio Mobile)	Longley-Rice (ICS Telecom)	Deygout 94 (ICS Telecom)	Deygout 94 (Matlab)	Epstein-Peterson (Matlab)
1	Channel 22	482 MHz	48.4	90.9	49.7	17.3	50.7	70.7	65.5
2	Channel 25	506 MHz	50.6	90.9	49.4	17.1	50.5	70.6	65.3
3	Channel 28	530 MHz	50.5	90.9	49.1	16.9	50.3	70.5	65.1
4	Channel 60	786 MHz	50.6	90.9	46.8	15.1	48.6	66.4	64.6

Table 30 shows the comparison of the electric field strength values of Belmont DTV transmitter at Greenhead park. Compared to Emley Moor transmitter, the electric field strength value at Greenhead park was lower because of the larger distance between Belmont and Greenhead park. Also, it was observed that Longley-Rice model in ICS Telecom could not predict the correct electric field strength values. One of the possible reasons for this is because the large

distance between the two points had a significant impact on Longley-Rice calculations (in ICS Telecom) and thus it overestimated the path loss that lead to the incorrect prediction.

On the other hand, it was observed that the Matlab algorithms showed higher values than the measured data because both the algorithms could not successfully detect all the knife-edges between their path due to which they underestimated the path loss.

Longley-Rice model in Radio Mobile and Deygout 94 in ICS Telecom were the only propagation models that could predict the electric field strength values closer to the measurements. However, a better estimation of the accuracy was obtained by calculating the difference between the measurements and simulations as shown in Table 31.

Table 31. Comparison in the difference between measurement and simulations for the electric field strength of Belmont DTV transmitter measured at Greenhead park.

No.	Channels Belmont DTV DVB-T2 LAT.: 53.335844 N LONG.: 0.171980 W, Altitude 128m	Frequency	Difference to measurements for Greenhead Park (dB)					
			Free-space	Longley-Rice (Radio Mobile)	Longley-Rice (ICS Telecom)	Deygout 94 (ICS Telecom)	Deygout 94 (Matlab)	Epstein-Peterson (Matlab)
1	Channel 22	482 MHz	-42.5	-1.3	31.1	-2.3	22.3	17.1
2	Channel 25	506 MHz	-40.3	1.2	33.5	0.1	20.0	14.7
3	Channel 28	530 MHz	-40.4	1.4	33.6	0.2	20.0	14.6
4	Channel 60	786 MHz	-40.3	3.8	35.5	2.0	15.8	14.0
Average Difference			**-40.9**	**1.3**	**33.4**	**0.0**	**19.5**	**15.1**
Standard Deviation			**0.9**	**1.8**	**1.6**	**1.5**	**2.3**	**1.2**

Table 31 suggests that Deygout 94 in ICS Telecom demonstrated lowest average difference as well as lower standard deviation. Thus, it can be stated that Deygout 94 provides the best estimate of the electric field strength values in this scenario followed by Longley-Rice in Radio Mobile also showing promising results.

8.8.2.3 Path profile comparison

8.8.2.3.1 Belmont station to Victoria tower

The path profiles from Belmont transmitting station to Victoria tower simulated in Radio Mobile, ICS Telecom and matlab are shown in Figures 84, 85 and 86 respectively.

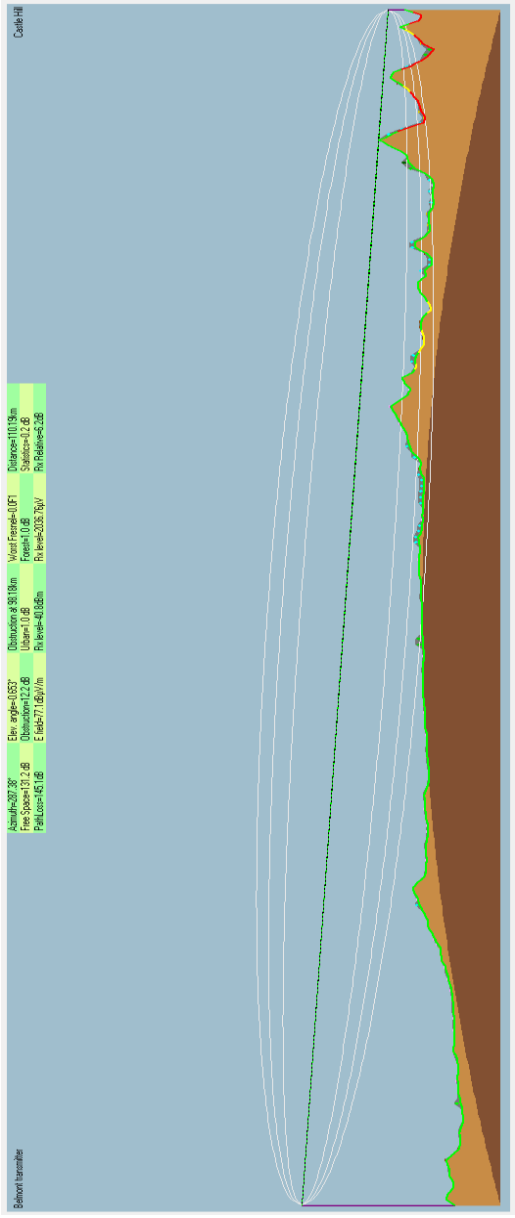

Figure 84. Path profile from Belmont station to Victoria tower using Radio Mobile.

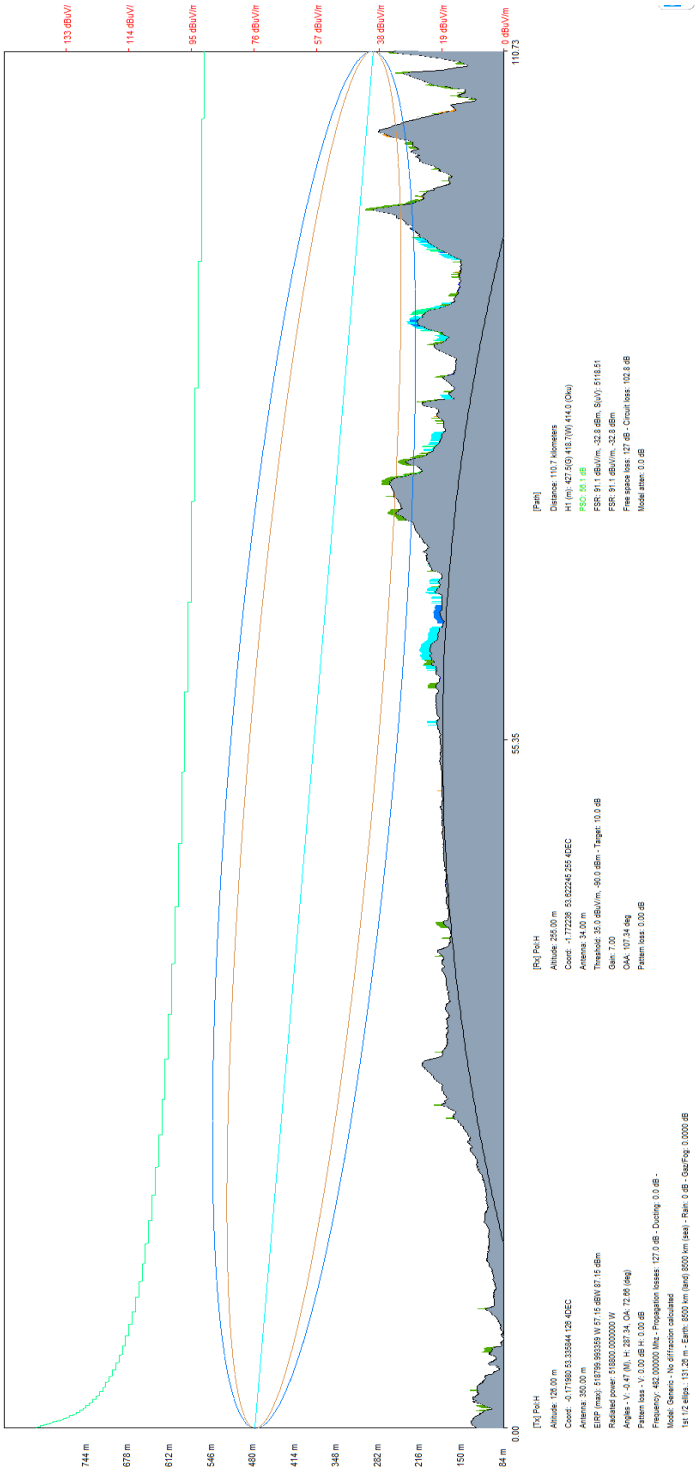

Figure 85. Path profile from Belmont station to Victoria tower using ICS Telecom.

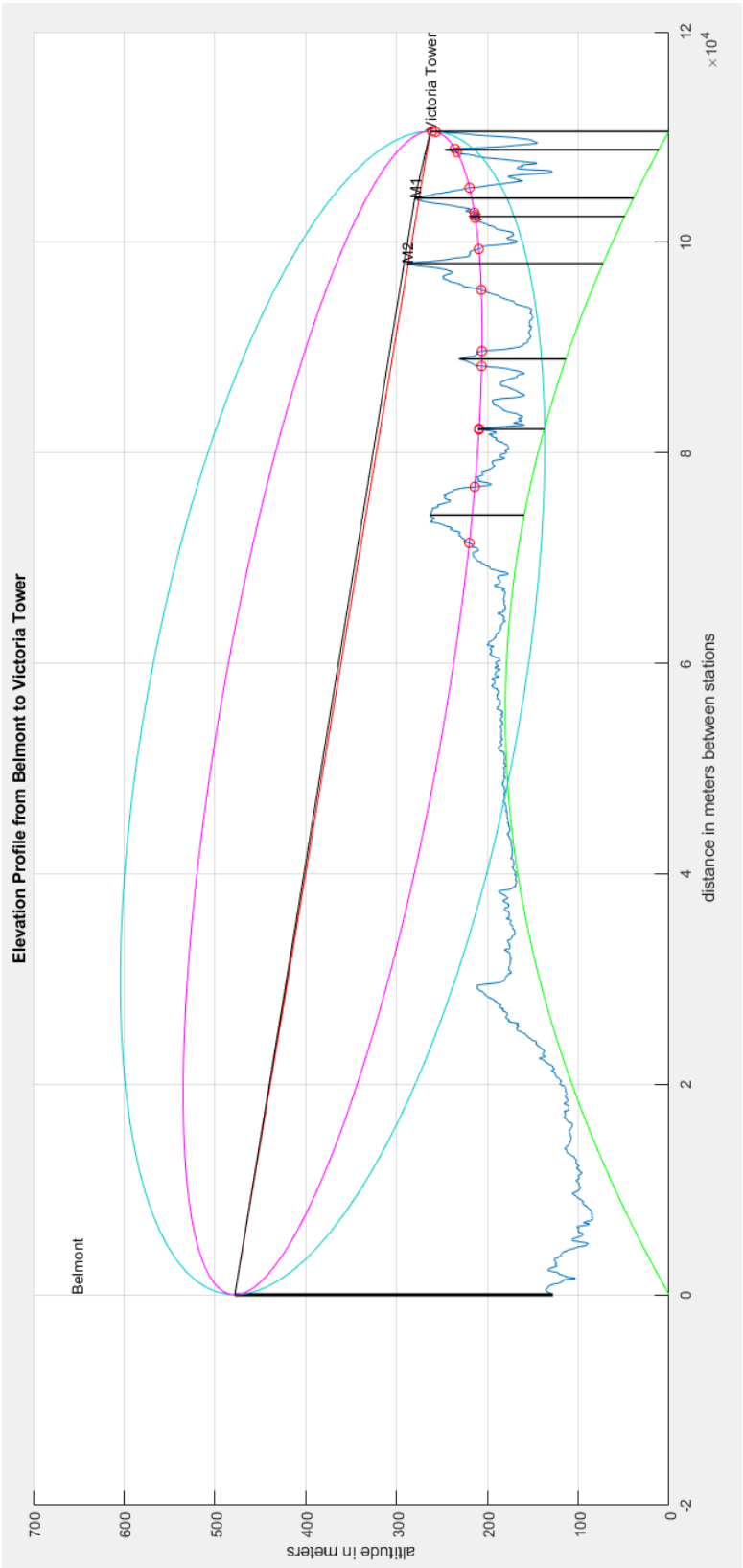

Figure 86. Path profile from Belmont station to Victoria tower using Matlab algorithm.

Figure 84, 85 and 86 shows the path profiles generated by Radio Mobile, ICS Telecom and Matlab algorithm respectively. These figures suggest that detection of multiple-knife edges was observed. Figure 84 suggests that the propagation by diffraction is occurred due to the multiple knife-edges and the obstacles in the Fresnel zone contributed for the loss of 12.2 dB.

Figure 85 demonstrates the multiple knife-edges detection with high details. The reason for this increased accuracy is because ICS Telecom also takes elevation model into the account. The figure suggests that obstacles in the Fresnel zone as well as the clutter in this case significantly contributes to the loss. Figure 86 also demonstrates the capability of the Matlab algorithm to detect the multiple knife-edges. However, ICS Telecom shows the path profile with good accuracy and details.

8.8.2.3.2 Belmont station to Greenhead park

The path profiles from Belmont to Greenhead park simulated in Radio Mobile, ICS Telecom, and matlab are shown in Figures 87, 88 and 89 respectively.

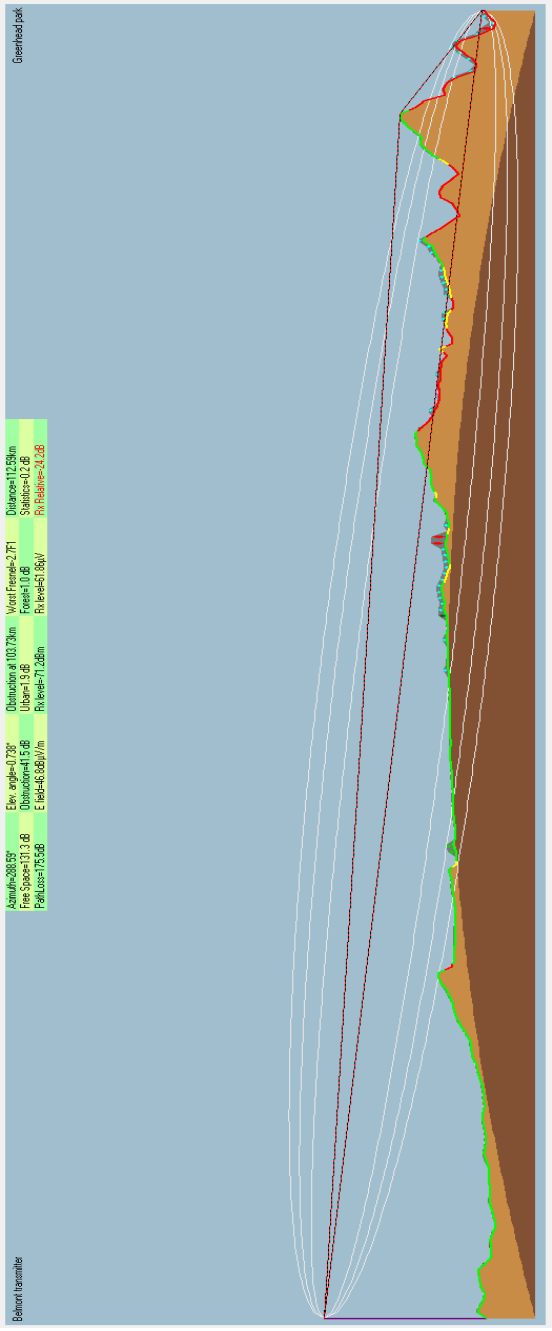

Figure 87. Path profile from Belmont station to Greenhead park using Radio Mobile.

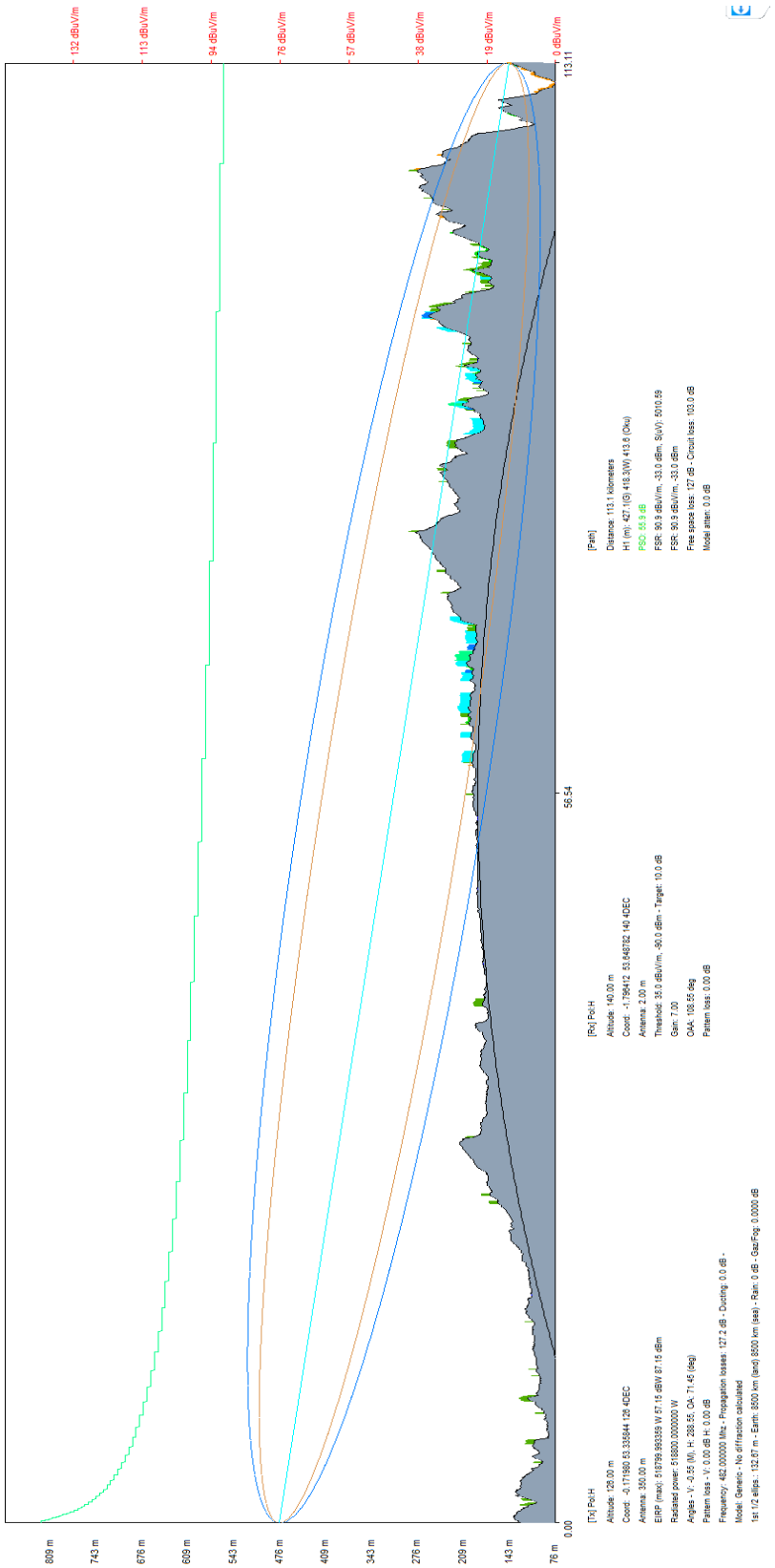

Figure 88. Path profile from Belmont station to Greenhead park using ICS Telecom.

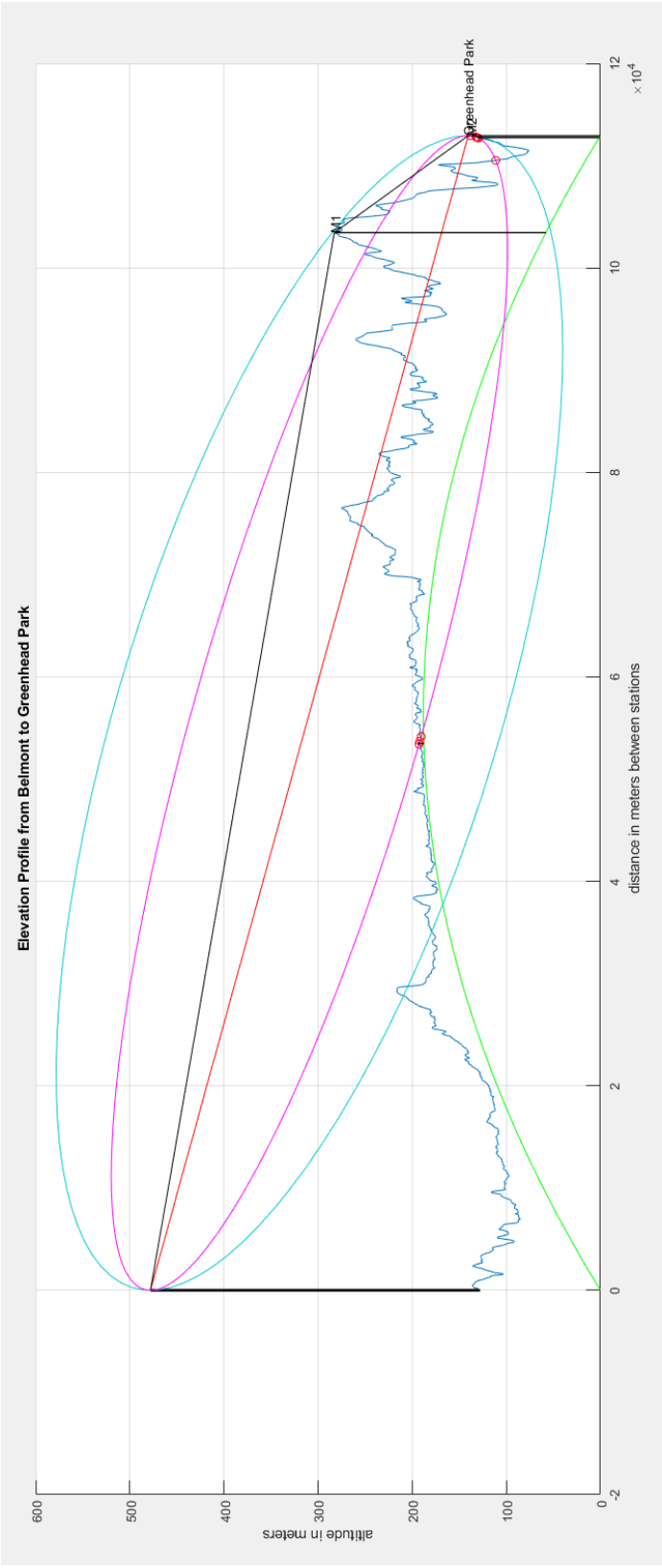

Figure 89. Path profile from Belmont station to Greenhead park using Matlab algorithm

Figure 87, 88 and 89 shows the path profile from Belmont transmitter to Greenhead park calculated by Radio Mobile, ICS Telecom and Matlab algorithms. All the three figures suggest that a significant knife-edge is detected near the signal reception point. This knife-edge blocks the path between the Belmont transmitter and the Greenhead park resulting in high loss, thereby leading to weaker signal reception. Longley-Rice model in Radio Mobile predicts this loss to be as high as 41.5 dB. Figure 88, showing the results obtained in ICS Telecom, provides better details regarding the clutter information and detected knife-edges. It not only detects the multiple knife-edges but also suggests that the earth's curvature also make a significant impact on propagation calculation using Longley-Rice model and thus overestimated the path loss. Figure 89, demonstrating the path profile by Matlab algorithm, suggests that the algorithm failed to identify all the knife-edges. It could identify only the most significant knife-edge which lead it to underestimate the path loss, thereby providing higher electric field strength values compared to the measured data.

8.9 Conclusion

This chapter discusses the study of radio propagation and coverage prediction for two transmitters locations: 1. Emley Moor, and 3. Belmont. A comparison of the measured electric field strength with simulated values calculated using several propagation models in ICS Telecom, Radio Mobile and Matlab is presented in this chapter. Longley-Rice and Deygout 94 provided the best results, though, Epstein-Peterson model in Matlab also showed promising results in some cases. Additionally, the path profile calculated by the three softwares suggests that ICS Telecom could predict the path profiles precisely with high details by considering vegetation, clutter and earth's curvature in the calculation. While, radio Mobile showed promising results, the path profile predicted by Matlab missed to detect several knife edges. The coverage of Emley Moor transmitter was also predicted closely to the official coverage released by Freeview TV.

Chapter 9 Conclusion

9.1 Research summary

In this research, a thorough investigation on designing LPDAs is carried out. Followed by designing traditional LPDAs, novel antenna designs are proposed to solve the interference problem caused due to the coexistence of the UHF TV band and the LTE-800 MHz band. A cost-efficient antenna with better performance than the ones available in the market is proposed, that eradicates the necessity of using external filters. This provides a useful design methodology of the antennas that will be required after the clearance of the 700 MHz band. Furthermore, this research also compares different optimisation algorithms available in CST software to optimize a 10-dipole LPDA. However, the size of LPDAs can be quite big when it needs to cover a wide range of frequencies for wideband measurements as well as EMC measurement applications. Therefore, this thesis also addresses the requirement to reduce the size of LPDAs by implementing the concept on PCB to develop PLPDAs. In addition to this, it also presents a review of several miniaturization techniques that have been proposed by several researchers. A novel wideband PLPDA with a triangular longest dipole is presented in this paper that can cover frequencies in the range from 0.4 GHz to 8 GHz. The proposed antenna provides flat gain as well as highly directional characteristics. Gain measurements are very challenging and often multiple measurements need to be performed with different separation distances between two identical antennas while implementing the two-antenna method. A simulation-assisted gain determination technique is proposed in this study, where the measurement setup is exactly duplicated in the simulation software. Several simulations are then carried out with different separation distances between the antennas. In this way, the distance that provides accurate gain is selected for the measurement. This provides a time-efficient as well as accurate technique to determine the gain of an antenna using the two-antenna method, where the measurements can be carried out in a single trial. As a case-study,

a 10-dipole LPDA with LTE-800 protection is selected to validate the technique. This research also deals with circularly polarized antennas for satellite applications like search and rescue operations. An investigation of elliptical patch antennas is carried out and an edge-fed dual-band elliptical patch with circular polarization is proposed in this thesis for GPS-L1 and Iridium applications. The simulated results were validated using the measurements performed in an anechoic chamber at NPL, Teddington. The optimization of this antenna was performed using the state-of-the-art PSADEA algorithm developed by Wrexham Glyndwr University. The concept of elliptical patch antenna design was implemented also to design an antenna for UWB system for RTLS applications. The proposed antenna was used for a localisation system developed by DecaWave Limited, to increase the localisation range from 75m to 250m. A study on radio propagation coverage prediction is also performed in this work. Three measurement campaigns were carried out, one in the Republic of North Macedonia and Greece and two in the United Kingdom. These measurements involved measuring the electric field strength of the transmitters at different points around the transmitter. The locations of the transmitter and the measurement points were duplicated in the ICS Telecom and Radio Mobile (radio planning softwares). The simulations were performed using several propagation models. A comparative study on the measured and simulated results was performed in order to determine the prediction accuracy of the models. Furthermore, path profiles from the transmitters to specific points were predicted by these models. Lastly, the coverage of Emley Moor broadcasting station was predicted using ICS Telecom software and then compared with the official coverage released by Freeview TV.

9.2 Future work

- The work presented in this thesis presents novel LPDAs for UHF TV reception that can reject LTE-800 and GSM-900 frequency band to mitigate with the interference caused because of the coexistence of the UHF TV and mobile communication spectrum. However, with the evolution of mobile communication technology from 4G to 5G, the clearance of the 700 MHz band is also proposed. Therefore, there is a requirement to design new antennas that can receive UHF TV signals rejecting 700 MHz band, LTE-800 and GSM-900 MHz band to reduce interference. The novel technique proposed in

this thesis ca be used to design such antennas without using any external filters. This provides a cost-efficient as well as relatively high-performance solution compared to the conventional commercial products available in the market.

- An array of several LPDAs operating at VHF and UHF frequencies can be used for detecting and positioning stealth airplanes for military applications. Currently most of these radar systems use separate arrays of VHF and UHF Yagis to detect and position such planes. However, a combined array of LPDAs can be designed that can operate both in VHF and UHF through a single array of antennas. This will reduce the size of the radar systems and will make it hard to detect.
- Also, there is very limited literature on PLPDAs that cover a wide frequency range from 0.4 GHz to 8 GHz. Therefore, further investigation of bandwidth and gain enhancement of such antennas with size reduction is required. Several miniaturization techniques that include capacitive and resistive loading need to be investigated to further reduce the size of PLPDAs. Moreover, EMC and several other antenna measurements require wideband reference antennas that can cover wide range of frequencies. For such applications, wideband PLPDAs with wide bandwidth can be designed that can provide flat gain and highly directional characteristics.
- PLPDAs and band-rejection techniques can also be used to design antennas for wideband applications for Sub-6 GHz, 28 GHz, and mmWave frequency bands.
- Additionally, investigations of designing PLPDAs with stacked PCBs are also required as that may lead to a further reducing the size of antennas. The hybrid printed Yagi-Uda and PLPDA can also be implemented to increase the gain of the PLPDA by using additional reflectors and directors.
- Dual-band patch antennas for GPS and Iridium applications have been proposed in this thesis. However, there is a need for patch antennas that can provide tri-band or quad-band characteristics. Furthermore, electromagnetically coupled antennas, metamaterials and leaky wave antennas need to be investigated as they are promising solutions for Terahertz (THz) applications. Machine learning can be integrated with the antenna design process to develop novel antennas with minimal computational time using evolutionary algorithms.

- There is also a need for Multiple Input Multiple Output (MIMO) and beamforming antennas and with the introduction of 5G and future 6G mobile technologies, there is a requirement for designing antennas for mobile phones that can operate in all of GSM, 3G, 4G, 5G and future 6G frequency bands. These antennas will be part of our future investigations.
- There are several on-going trials for deploying 5G technologies in urban as well as rural areas in different countries. This requires radio engineers to study propagation of 5G waves as well as to determine the placement of base stations and repeaters so that the deployment can be performed at minimal cost without compromising the quality of service. Radio planning softwares are intensively used by frequency regulatory organizations like Ofcom. Therefore, research on 5G deployment planning and propagation modelling will be essential in the future.

References

[1] *Gsma.com, 2019. [Online]. Available: https://www.gsma.com/spectrum/wp-content/uploads/2012/07/700MHz-800MHz-band-UK.pdf.*

[2] *Department for Business Innovation & Skills and Department of Culture, Media and Sport (June 2009), "Digital Britain: Final Report". .*

[3] *"Digital UK | 700MHz clearance", Digitaluk.co.uk, 2019. [Online]. Available: http://www.digitaluk.co.uk/operations/700mhz_clearance.*

[4] *Digitaluk.co.uk, 2019. [Online]. Available: http://www.digitaluk.co.uk/data/assets/pdf_file/0006/94308/Digital_UK_Spectrum_factsheet_May_2018.pdf. [Accessed: 28- Oct- 2019].*

[5] Z. D. Zaharis, C. Skeberis, T. D. Xenos, P. I. Lazaridis, and D. I. Stratakis, "IWO-based synthesis of log-periodic dipole array," in *2014 International Conference on Telecommunications and Multimedia (TEMU)*, 2014: IEEE, pp. 150-154.

[6] P. I. Lazaridis *et al.*, "Comparison of evolutionary algorithms for LPDA antenna optimization," *Radio Science,* vol. 51, no. 8, pp. 1377-1384, 2016.

[7] G. A. Casula, P. Maxia, G. Mazzarella, and G. Montisci, "Design of a printed log-periodic dipole array for ultra-wideband applications," *Progress In Electromagnetics Research,* vol. 38, pp. 15-26, 2013.

[8] C. A. Balanis, *Antenna theory: analysis and design*. John wiley & sons, 2016.

[9] R. L. Carrel, "Analysis and design of the log-periodic dipole antenna," ILLINOIS UNIV AT URBANA ELECTRICAL ENGINEERING RESEARCH LAB, 1961.

[10] Y. Huang and K. Boyle, *Antennas: from theory to practice*. John Wiley & Sons, 2008.

[11] R. Carrel, "The design of log-periodic dipole antennas," in *1958 IRE International Convention Record*, 1966, vol. 9: IEEE, pp. 61-75.

[12] K. Mistry, P. Lazaridis, Z. D. Zaharis, T. D. Xenos, and I. Glover, "Optimization of log-periodic dipole antenna with LTE band-rejection," presented at the Loughborough Antenna Propagation Conference (LAPC), Loughborough, UK, 2017.

[13] Z. D. Zaharis, C. Skeberis, P. I. Lazaridis, and T. D. Xenos, "Optimal wideband LPDA design for efficient multimedia content delivery over emerging mobile computing systems," *IEEE Systems Journal,* vol. 10, no. 2, pp. 831-838, 2015.

[14] M. N. A Karim, M. K. Abd Rahim, H. A. Majid, O. B. Ayop, M. Abu, and F. Zubir, "Log periodic fractal Koch antenna for UHF band applications," *Progress In Electromagnetics Research,* vol. 100, pp. 201-218, 2010.

[15] P. I. Lazaridis, Z. D. Zaharis, C. Skeberis, T. Xenos, E. Tziris, and P. Gallion, "Optimal design of UHF TV band log-periodic antenna using invasive weed optimization," in *2014 4th International Conference on Wireless Communications, Vehicular Technology, Information Theory and Aerospace & Electronic Systems (VITAE)*, 2014: IEEE, pp. 1-5.

[16] T. Weiland, M. Timm, and I. Munteanu, "A practical guide to 3-D simulation," *IEEE Microwave Magazine,* vol. 9, no. 6, pp. 62-75, 2008.

[17] D. Lim, Y.-S. Ong, Y. Jin, and B. Sendhoff, "Trusted evolutionary algorithm," in *2006 IEEE International Conference on Evolutionary Computation*, 2006: IEEE, pp. 149-156.

[18] S. Xu, X. Zou, W. Liu, X. Wang, H. Zhu, and T. Zhao, "Research of Particle Swarm Optimization algorithm based on Nelder-Mead simplex and its application on partial discharge parameter recognition," in *2010 IEEE International Power Modulator and High Voltage Conference*, 2010: IEEE, pp. 719-722.

[19] N. Hansen and A. Ostermeier, "Completely derandomized self-adaptation in evolution strategies," *Evolutionary computation,* vol. 9, no. 2, pp. 159-195, 2001.

[20] E. BouDaher and A. Hoorfar, "Electromagnetic optimization using mixed-parameter and multiobjective covariance matrix adaptation evolution strategy," *IEEE Transactions on Antennas and Propagation,* vol. 63, no. 4, pp. 1712-1724, 2015.

[21] J. M. Kovitz and Y. Rahmat-Samii, "A comparative study between CMA evolution strategies and Particle Swarm Optimization for antenna applications," in *2013 US National Committee of URSI National Radio Science Meeting (USNC-URSI NRSM)*, 2013: IEEE, pp. 1-1.

[22] A. A. Awotunde, "Estimation of well test parameters using global optimization techniques," *Journal of Petroleum Science and Engineering,* vol. 125, pp. 269-277, 2015.

[23] European Parliament Resolution. (2008). *EPR 2008/2009 (INI), "Reaping the full benefits of the digital dividend in Europe: A common approach to the use of the spectrum released by the digital switchover", September, 2008*.

[24] *EU COM(2009) 586, "Transforming the digital dividend into social benefits and economic growth", October, 2009*.

[25] Dec. 2010/267/EU. *"On harmonised technical conditions of use in the 790-862 MHz frequency band for terrestrial systems capable of providing electronic communications services in the European Union", May, 2010*.

[26] M. Ferrante, G. Fusco, E. Restuccia, M. Celidonio, P. Masullo, and L. Pulcini, "Experimental results on the coexistence of TV broadcasting service with LTE mobile systems in the 800 MHz band," in *2014 Euro Med Telco Conference (EMTC)*, 2014: IEEE, pp. 1-6.

[27] WRC Resolution 232 [COM5/10]. *"Use of the frequency band 694-790 MHz by the mobile, except aeronautical mobile, service in Region 1 and related studies", Geneva, 2012*.

[28] *Final Acts-WRC-12, ITU-R, Geneva, Switzerland, 2012*.

[29] *Provisional Final Acts-WRC-15, ITU-R, Geneva, Switzerland, 2015*.

[30] M. Fuentes, C. Garcia-Pardo, E. Garro, D. Gomez-Barquero, and N. Cardona, "Coexistence of digital terrestrial television and next generation cellular networks in the 700 MHz band," *IEEE Wireless Communications,* vol. 21, no. 6, pp. 63-69, 2014.

[31] N. Andrea, "Improvements of antennas, particularly logperiodic antennas " Patent EP2549587B1, 2013.

[32] N. Barbano and H. Hochman, "Antenna boom and feed line structure," Patent US3550144A, 1970.

[33] Z. D. Zaharis, I. P. Gravas, P. I. Lazaridis, I. A. Glover, C. S. Antonopoulos, and T. D. Xenos, "Optimal LTE-protected LPDA design for DVB-T reception using particle swarm optimization with velocity mutation," *IEEE Transactions on Antennas and Propagation,* vol. 66, no. 8, pp. 3926-3935, 2018.

[34] K. Mistry, P. Lazaridis, T. H. Lo, Z. D. Zaharis, I. Glover, and B. Liu, "A novel design of a 10-dipole log-periodic antenna with LTE-800 and GSM-900 band rejection," in *IEEE MTT-S International Conference on Numerical Electromagnetic and Multiphysics Modeling and Optimization*, 2019: Institute of Electrical and Electronics Engineers Inc.

[35] Y. Li, F. Yang, J. OuYang, and H. Zhou, "Yagi-Uda antenna optimization based on invasive weed optimization method," *Electromagnetics,* vol. 31, no. 8, pp. 571-577, 2011.

[36] A. R. R. Mallahzadeh, H. Oraizi, and Z. Davoodi-Rad, "Application of the invasive weed optimization technique for antenna configurations," *Progress in Electromagnetics Research,* vol. 79, pp. 137-150, 2008.

[37] S. Pal, A. Basak, and S. Das, "Linear antenna array synthesis with modified invasive weed optimisation algorithm," *International Journal of Bio-Inspired Computation,* vol. 3, no. 4, pp. 238-251, 2011.

[38] S. Sedighy, A. Mallahzadeh, M. Soleimani, and J. Rashed-Mohassel, "Optimization of printed Yagi antenna using invasive weed optimization (IWO)," *IEEE Antennas and Wireless Propagation Letters,* vol. 9, pp. 1275-1278, 2010.

[39] Z. D. Zaharis, P. I. Lazaridis, J. Cosmas, C. Skeberis, and T. D. Xenos, "Synthesis of a near-optimal high-gain antenna array with main lobe tilting and null filling using Taguchi initialized invasive weed optimization," *IEEE Transactions on Broadcasting,* vol. 60, no. 1, pp. 120-127, 2014.

[40] M. F. Pantoja, A. R. Bretones, F. G. Ruiz, S. Garcia, and R. G. Martin, "Particle-Swarm optimization in antenna design: Optimization of log-periodic dipole arrays," *IEEE Antennas and Propagation Magazine,* vol. 49, no. 4, pp. 34-47, 2007.

[41] R. Golubovic and D. Oclan, "Antenna Optimization Using Particle Swarm Optimization Algorithm," *Journal of Automatic Control,* vol. 16, 1, pp. 21-24, 2006.

[42] Z. D. Zaharis, D. G. Kampitaki, P. I. Lazaridis, A. I. Papastergiou, and P. B. Gallion, "On the design of multifrequency dividers suitable for GSM; DCS/PCS/UMTS applications by using a particle swarm optimization-based technique," *Microwave and Optical Technology Letters,* vol. 49, no. 9, pp. 2138-2144, 2007.

[43] Z. D. Zaharis, C. Skeberis, T. D. Xenos, P. I. Lazaridis, and J. Cosmas, "Design of a novel antenna array beamformer using neural networks trained by modified adaptive

dispersion invasive weed optimization based data," *IEEE Transactions on Broadcasting,* vol. 59, no. 3, pp. 455-460, 2013.

[44] Z. D. Zaharis *et al.*, "Exponential log-periodic antenna design using improved particle swarm optimization with velocity mutation," *IEEE Transactions on Magnetics,* vol. 53, no. 6, pp. 1-4, 2017.

[45] Q. He, H. Gan, and D. Jiao, "Explicit time-domain finite-element method stabilized for an arbitrarily large time step," *IEEE Transactions on Antennas and Propagation,* vol. 60, no. 11, pp. 5240-5250, 2012.

[46] M. Gaffar and D. Jiao, "An explicit and unconditionally stable FDTD method for electromagnetic analysis," *IEEE Transactions on Microwave Theory and Techniques,* vol. 62, no. 11, pp. 2538-2550, 2014.

[47] J. Osburn, "'EMC antenna parameters and their relationships' ITEM June 1997," ed.

[48] F. Lin, Y. Qi, J. Fan, and Y.-C. Jiao, "0.7–20-GHz dual-polarized bilateral tapered slot antenna for EMC measurements," *IEEE Transactions on Electromagnetic Compatibility,* vol. 56, no. 6, pp. 1271-1275, 2014.

[49] M. G. Aram, H. Tahmasbi, and H. Aliakbarian, "An ultra-wideband miniaturized printed dipole antenna for EMC measurements," in *2017 International Symposium on Electromagnetic Compatibility-EMC EUROPE*, 2017: IEEE, pp. 1-4.

[50] Q. Wu, X. Ding, and D. Su, "A compact dipole antenna with curved reflector for 1.0–4.2 GHz EMC measurement," *IEEE Transactions on Electromagnetic Compatibility,* vol. 57, no. 6, pp. 1289-1297, 2015.

[51] A. Chauloux, F. Colombel, M. Himdi, J.-L. Lasserre, and P. Pouliguen, "Low-return-loss printed log-periodic dipole antenna," *IEEE Antennas and Wireless Propagation Letters,* vol. 13, pp. 503-506, 2014.

[52] C. Campbell, I. Traboulay, M. Suthers, and H. Kneve, "Design of a stripline log-periodic dipole antenna," *IEEE Transactions on Antennas and Propagation,* vol. 25, no. 5, pp. 718-721, 1977.

[53] A. A. Gheethan and D. E. Anagnostou, "Reduced size planar log-periodic dipole arrays (LPDAs) using rectangular meander line elements," in *2008 IEEE Antennas and Propagation Society International Symposium*, 2008: IEEE, pp. 1-4.

[54] D. E. Anagnostou, J. Papapolymerou, M. M. Tentzeris, and C. G. Christodoulou, "A printed log-periodic Koch-dipole array (LPKDA)," *IEEE Antennas and Wireless Propagation Letters,* vol. 7, pp. 456-460, 2008.

[55] S. M. Hashemi, V. Nayyeri, M. Soleimani, and A.-R. Mallahzadeh, "Designing a compact-optimized planar dipole array antenna," *IEEE Antennas and Wireless Propagation Letters,* vol. 10, pp. 243-246, 2011.

[56] C. Yu *et al.*, "Ultrawideband printed log-periodic dipole antenna with multiple notched bands," *IEEE Transactions on Antennas and propagation,* vol. 59, no. 3, pp. 725-732, 2010.

[57] Z. Zaharis, D. Kampitaki, A. Papastergiou, A. Hatzigaidas, P. Lazaridis, and M. Spasos, "Optimal design of a linear antenna array under the restriction of uniform excitation distribution using a particle swarm optimization based method," *WSEAS Transactions on Communications,* vol. 6, no. 1, pp. 52-59, 2007.

[58] W.-T. Li, Y.-Q. Hei, and X.-W. Shi, "Pattern synthesis of conformal arrays by a modified particle swarm optimization," *Progress In Electromagnetics Research,* vol. 117, pp. 237-252, 2011.

[59] W.-C. Weng and C. T. Choi, "Optimal design of CPW slot antennas using Taguchi's method," *IEEE Transactions on Magnetics,* vol. 45, no. 3, pp. 1542-1545, 2009.

[60] N. Nemri, A. Smida, R. Ghayoula, H. Trabelsi, and A. Gharsallah, "Phase-only array beam control using a Taguchi optimization method," in *2011 11th Mediterranean Microwave Symposium (MMS)*, 2011: IEEE, pp. 97-100.

[61] N. Sheng, C. Liao, W. Lin, L. Chang, Q. Zhang, and H. Zhou, "A hybrid optimized algorithm based on EGO and Taguchi's method for solving expensive evaluation problems of antenna design," *Progress In Electromagnetics Research,* vol. 17, pp. 181-192, 2010.

[62] K. Mistry *et al.*, "Measurement, simulation and optimization of wideband log-periodic antennas," in *2017 XXXIInd General Assembly and Scientific Symposium of the International Union of Radio Science (URSI GASS)*, 2017: IEEE, pp. 1-4.

[63] K. K. Mistry *et al.*, "Time and Frequency Domain Simulation, Measurement and Optimization of Log-Periodic Antennas," *Wireless Personal Communications,* pp. 771-783, 2019.

[64] *FCC, FCC first report and order on ultra-wideband technology, 2002*.

[65] "ECC Decision of 24 March 2006 on the Harmonised Conditions forDevices using Ultra-Wideband (UWB) Technology in Bands Below10.6GHz 2006, ECC Std. [Online]. Available at: http://www.ero.dk/."

[66] J. Liang, C. C. Chiau, X. Chen, and C. G. Parini, "Study of a printed circular disc monopole antenna for UWB systems," *IEEE transactions on antennas and propagation,* vol. 53, no. 11, pp. 3500-3504, 2005.

[67] R. Azim, M. T. Islam, and N. Misran, "Compact tapered-shape slot antenna for UWB applications," *IEEE Antennas and Wireless Propagation Letters,* vol. 10, pp. 1190-1193, 2011.

[68] C.-L. Tsai and C.-L. Yang, "Novel compact eye-shaped UWB antennas," *IEEE Antennas and Wireless Propagation Letters,* vol. 11, pp. 184-187, 2012.

[69] A. K. Gautam, S. Yadav, and B. K. Kanaujia, "A CPW-fed compact UWB microstrip antenna," *IEEE Antennas and Wireless propagation letters,* vol. 12, pp. 151-154, 2013.

[70] J. Yeo and J. I. Lee, "Miniaturized LPDA antenna for portable direction finding applications," *ETRI journal,* vol. 34, no. 1, pp. 118-121, 2012.

[71] R. W. Harrison and M. Jessup, "A novel log periodic implementation of a 700 MHz–6 GHz slant polarised fixed-beam antenna array for direction finding applications," in *2012 42nd European Microwave Conference*, 2012: IEEE, pp. 727-730.

[72] X. Liang and Y. Chia, "New precision wideband direction finding antenna," *IEE Proceedings-Microwaves, Antennas and Propagation,* vol. 148, no. 6, pp. 363-364, 2001.

[73] D. Isbell, "Log periodic dipole arrays," *IRE transactions on antennas and propagation,* vol. 8, no. 3, pp. 260-267, 1960.

[74] V. Rumsey, "Frequency independent antennas," in *1958 IRE International Convention Record*, 1966, vol. 5: IEEE, pp. 114-118.

[75] R. DuHamel and F. Ore, "Logarithmically periodic antenna designs," in *1958 IRE International Convention Record*, 1966, vol. 6: IEEE, pp. 139-151.

[76] R. DuHamel and D. Isbell, "Broadband logarithmically periodic antenna structures," in *1958 IRE International Convention Record*, 1966, vol. 5: IEEE, pp. 119-128.

[77] A. Paul and I. Gupta, "An analysis of log periodic antenna with printed dipoles," *IEEE Transactions on Microwave Theory and Techniques,* vol. 29, no. 2, pp. 114-117, 1981.

[78] R. Pantoja and A. Sapienza, "A microwave printed planar log-periodic dipole array antenna," *IEEE Transactions on antennas and propagation,* vol. 35, no. 10, pp. 1176-1178, 1987.

[79] A. Kyei, D.-U. Sim, and Y.-B. Jung, "Compact log-periodic dipole array antenna with bandwidth-enhancement techniques for the low frequency band," *IET Microwaves, Antennas & Propagation,* vol. 11, no. 5, pp. 711-717, 2016.

[80] Q. Sun, J. Wang, J. Cui, J. Fu, C. Zhou, and E. Wang, "A compact printed log-periodic antenna with loaded stub," in *Proceedings of 2014 3rd Asia-Pacific Conference on Antennas and Propagation*, 2014: IEEE, pp. 593-595.

[81] J. Chen, J. Ludwig, and S. Lim, "Design of a compact log-periodic dipole array using T-shaped top loadings," *IEEE Antennas and Wireless Propagation Letters,* vol. 16, pp. 1585-1588, 2017.

[82] M. Pirai and H. HR, "Size reduction of microstrip LPDA antenna with top loading," *IEICE Electronics Express,* vol. 6, no. 21, pp. 1528-1534, 2009.

[83] J. Anguera, C. Puente, C. Borja, and J. Soler, "Fractal shaped antennas: A review," *Encyclopedia of RF and microwave engineering,* 2005.

[84] H. Oraizi, A. Amini, and M. K. Mehr, "Design of miniaturised UWB log-periodic end-fire antenna using several fractals with WLAN band-rejection," *IET Microwaves, Antennas & Propagation,* vol. 11, no. 2, pp. 193-202, 2017.

[85] J. P. Gianvittorio and Y. Rahmat-Samii, "Fractal antennas: A novel antenna miniaturization technique, and applications," *IEEE Antennas and Propagation magazine,* vol. 44, no. 1, pp. 20-36, 2002.

[86] J. Anguera, C. Puente, E. Martinez, and E. Rozan, "The fractal Hilbert monopole: A two-dimensional wire," *Microwave and Optical technology letters,* vol. 36, no. 2, pp. 102-104, 2003.

[87] A. Moallemizadeh, H. Hassani, and S. M. A. Nezhad, "Wide bandwidth and small size LPDA antenna," in *2012 6th European Conference on Antennas and Propagation (EUCAP)*, 2012: IEEE, pp. 1-3.

[88] M. J. Almalkawi, L. W. Cross, and K. A. Alshamaileh, "A transmission line circuit-oriented approach for miniaturization of a log-periodic dipole array (LPDA) antenna," in *2014 IEEE 57th International Midwest Symposium on Circuits and Systems (MWSCAS)*, 2014: IEEE, pp. 73-76.

[89] N. Rahman and M. Jamlos, "Miniaturized log periodic fractal koch antenna with c-shaped stub," in *2016 International Conference on Computer and Communication Engineering (ICCCE)*, 2016: IEEE, pp. 53-56.

[90] S. K. Jain, A. Shrivastava, and G. Shrivas, "Miniaturization of microstrip patch antenna using metamaterial loaded with SRR," in *2015 International Conference on Electromagnetics in Advanced Applications (ICEAA)*, 2015: IEEE, pp. 1224-1227.

[91] K. Anim and Y.-B. Jung, "Shortened log-periodic dipole antenna using printed dual-band dipole elements," *IEEE Transactions on Antennas and Propagation,* vol. 66, no. 12, pp. 6762-6771, 2018.

[92] M. Khandelwal, B. K. Kanaujia, and A. Gautam, "Low profile UWB log-periodic dipole antenna for wireless communication with notched band," *Microwave and Optical Technology Letters,* vol. 55, no. 12, pp. 2901-2906, 2013.

[93] X.-R. Li, M. Ye, and Q.-X. Chu, "Novel high gain printed log-periodic dipole antenna," in *2016 IEEE International Symposium on Antennas and Propagation (APSURSI)*, 2016: IEEE, pp. 1647-1648.

[94] L. Chang, S. He, J. Q. Zhang, and D. Li, "A compact dielectric-loaded log-periodic dipole array (LPDA) antenna," *IEEE Antennas and Wireless Propagation Letters,* vol. 16, pp. 2759-2762, 2017.

[95] G. Shin, M. Kong, S.-H. Lee, S.-T. Kim, and I.-J. Yoon, "Gain Characteristic Maintained, Miniaturized LPDA Antenna Using Partially Applied Folded Planar Helix Dipoles," *IEEE Access,* vol. 6, pp. 25874-25880, 2018.

[96] S. Eser and L. Sevgi, "Open-area test site (OATS) calibration," *IEEE Antennas and Propagation Magazine,* vol. 52, no. 3, pp. 204-212, 2010.

[97] G. E. Evans, "Antenna measurement techniques," *Norwood, MA, Artech House, Inc., 1990, 238 p.,* 1990.

[98] "CISPR 16-1-4, “Specification for radio disturbance and immunity measuring apparatus and methods - Part 1-4: Radio disturbance and immunity measuring apparatus - Antennas and test sites for radiated disturbance measurements,” IEC, 2012.."

[99] R. De Jough, M. Hajian, and L. Ligthart, "Antenna time-domain measurement techniques," *IEEE Antennas and Propagation Magazine,* vol. 39, no. 5, pp. 7-11, 1997.

[100] J. Krieger, E. Newman, and I. Gupta, "The single antenna method for the measurement of antenna gain and phase," *IEEE transactions on antennas and propagation,* vol. 54, no. 11, pp. 3562-3565, 2006.

[101] S. Loredo, G. Leon, S. Zapatero, and F. Las-Heras, "Measurement of low-gain antennas in non-anechoic test sites through wideband channel characterization and echo cancellation [Measurements Corner]," *IEEE Antennas and Propagation Magazine,* vol. 51, no. 1, pp. 128-135, 2009.

[102] C. Lemoine, E. Amador, P. Besnier, J. Sol, J.-M. Floc'h, and A. Laisné, "Statistical estimation of antenna gain from measurements carried out in a mode-stirred reverberation chamber," in *2011 XXXth URSI General Assembly and Scientific Symposium*, 2011: IEEE, pp. 1-4.

[103] B. A. Witvliet, E. van Maanen, M. J. Bentum, C. H. Slump, and R. Schiphorst, "Novel Method to measure the gain of UHF directional antennas using distance scan," in *The 8th European Conference on Antennas and Propagation (EuCAP 2014)*, 2014: IEEE, pp. 396-400.

[104] B. A. Witvliet *et al.*, "Mixed-path trans-horizon UHF measurements for P. 1546 propagation model verification," in *2011 IEEE-APS Topical Conference on Antennas and Propagation in Wireless Communications*, 2011: IEEE, pp. 303-306.

[105] B. Witvliet, "Airborne evaluation/verification of antenna patterns of broadcasting stations," in *18th International Wroclaw Symposium and Exhibition on Electromagnetic Compatibility, EMC 2006*, 2006.

[106] K. Harima, "Evaluating the effectiveness of applying the phase center for antenna measurements," in *2017 IEEE Conference on Antenna Measurements & Applications (CAMA)*, 2017: IEEE, pp. 61-64.

[107] K. Harima, "Accurate gain measurement for millimeter-wave horn and open-ended waveguide antennas," in *2012 International Symposium on Antennas and Propagation (ISAP)*, 2012: IEEE, pp. 1019-1022.

[108] K. Harima, "Accurate gain determination of LPDA by considering the phase center," *IEICE Electronics Express,* vol. 7, no. 23, pp. 1760-1765, 2010.

[109] P. Baumgartner, W. Renhart, O. Biro, and T. Bauernfeind, "Numerical Investigations of the Field Regions for Wire Based Antenna Systems," in *22nd International Conference on the Computation of Electromagnetic Fields*, 2019.

[110] P. Baumgartner, T. Bauernfeind, O. Biro, D. Kreindl, and W. Renhart, "Boundaries of the field regions: A simulation based approach," in *The 18th International IGTE Symposium on Numerical Field Calculation in Electrical Engineering-Abstracts*, 2018.

[111] H. T. Friis, "A note on a simple transmission formula," *Proceedings of the IRE,* vol. 34, no. 5, pp. 254-256, 1946.

[112] E. K. Kaivanto, M. Berg, E. Salonen, and P. De Maagt, "Wearable circularly polarized antenna for personal satellite communication and navigation," *IEEE Transactions on Antennas and Propagation,* vol. 59, no. 12, pp. 4490-4496, 2011.

[113] Q. Tan and D. Erricolo, "Comparison between printed folded monopole and inverted F antennas for wireless portable devices," in *2007 IEEE Antennas and Propagation Society International Symposium*, 2007: IEEE, pp. 4701-4704.

[114] H. Khaleel, *Innovation in wearable and flexible antennas*. Wit Press, 2014.

[115] F. Farzami, S. Khaledian, B. Smida, and D. Erricolo, "Reconfigurable linear/circular polarization rectangular waveguide filtenna," *IEEE Transactions on Antennas and Propagation,* vol. 66, no. 1, pp. 9-15, 2017.

[116] H. Jung and C. Seo, "Analysis of elliptical microstrip patch antenna considering attachment mode," *IEEE Transactions on Antennas and Propagation,* vol. 50, no. 6, pp. 888-890, 2002.

[117] D. Curone *et al.*, "Smart garments for emergency operators: the ProeTEX project," *IEEE Trans. Information Technology in Biomedicine,* vol. 14, no. 3, pp. 694-701, 2010.

[118] A. Alomainy, Y. Hao, and F. Pasveer, "Numerical and experimental evaluation of a compact sensor antenna for healthcare devices," *IEEE Transactions on Biomedical Circuits and Systems,* vol. 1, no. 4, pp. 242-249, 2007.

[119] L. Vallozzi, P. Van Torre, C. Hertleer, H. Rogier, M. Moeneclaey, and J. Verhaevert, "Wireless communication for firefighters using dual-polarized textile antennas integrated in their garment," *IEEE Transactions on Antennas and Propagation,* vol. 58, no. 4, pp. 1357-1368, 2010.

[120] P. Salonen and Y. Rahmat-Samii, "Textile antennas: Effects of antenna bending on input matching and impedance bandwidth," in *2006 First European Conference on Antennas and Propagation*, 2006: IEEE, pp. 1-5.

[121] K. K. Mistry, P. I. Lazaridis, Z. D. Zaharis, T. D. Xenos, E. N. Tziris, and I. A. Glover, "An optimal design of printed log-periodic antenna for L-band EMC applications," in *2018 IEEE International Symposium on Electromagnetic Compatibility and 2018 IEEE Asia-Pacific Symposium on Electromagnetic Compatibility (EMC/APEMC)*, 2018: IEEE, pp. 1150-1155.

[122] E. N. Tziris *et al.*, "Invasive weed optimized planar elliptical dipole antenna for ultra-wideband EMC applications," in *2018 IEEE International Symposium on Electromagnetic Compatibility and 2018 IEEE Asia-Pacific Symposium on Electromagnetic Compatibility (EMC/APEMC)*, 2018: IEEE, pp. 233-236.

[123] R. Pokuls, J. Uher, and D. Pozar, "Microstrip antennas for SAR applications," *IEEE Transactions on Antennas and Propagation,* vol. 46, no. 9, pp. 1289-1296, 1998.

[124] L. L. Shafai, W. A. Chamma, M. Barakat, P. C. Strickland, and G. Seguin, "Dual-band dual-polarized perforated microstrip antennas for SAR applications," *IEEE Transactions on Antennas and Propagation,* vol. 48, no. 1, pp. 58-66, 2000.

[125] F. Ferrero, C. Luxey, G. Jacquemod, and R. Staraj, "Dual-band circularly polarized microstrip antenna for satellite applications," *IEEE Antennas and Wireless Propagation Letters,* vol. 4, pp. 13-15, 2005.

[126] L. Lizzi, F. Viani, and A. Massa, "Dual-band spline-shaped PCB antenna for Wi-Fi applications," *IEEE Antennas and Wireless Propagation Letters,* vol. 8, pp. 616-619, 2009.

[127] R. Azaro, F. Natale, M. Donelli, E. Zeni, and A. Massa, "Synthesis of a prefractal dual-band monopolar antenna for GPS applications," *IEEE Antennas and Wireless Propagation Letters,* vol. 5, pp. 361-364, 2006.

[128] L. Lizzi and A. Massa, "Dual-band printed fractal monopole antenna for LTE applications," *IEEE Antennas and Wireless Propagation Letters,* vol. 10, pp. 760-763, 2011.

[129] A. Kiourti and K. S. Nikita, "Miniature scalp-implantable antennas for telemetry in the MICS and ISM bands: design, safety considerations and link budget analysis," *IEEE Transactions on Antennas and Propagation,* vol. 60, no. 8, pp. 3568-3575, 2012.

[130] P. Salonen, Y. Rahmat-Samii, M. Schaffrath, and M. Kivikoski, "Effect of textile materials on wearable antenna performance: A case study of GPS antennas," in *IEEE Antennas and Propagation Society Symposium, 2004.*, 2004, vol. 1: IEEE, pp. 459-462.

[131] L. Vallozzi, W. Vandendriessche, H. Rogier, C. Hertleer, and M. Scarpello, "Design of a protective garment GPS antenna," *Microwave and optical technology letters,* vol. 51, no. 6, pp. 1504-1508, 2009.

[132] A. Dierck, H. Rogier, and F. Declercq, "A wearable active antenna for global positioning system and satellite phone," *IEEE Transactions on Antennas and Propagation,* vol. 61, no. 2, pp. 532-538, 2012.

[133] S. Long, L. Shen, D. Schaubert, and F. Farrar, "An experimental study of the circular-polarized elliptical printed-circuit antenna," *IEEE transactions on Antennas and Propagation,* vol. 29, no. 1, pp. 95-99, 1981.

[134] S. Long and M. McAllister, "The impedance of an elliptical printed-circuit antenna," *IEEE Transactions on Antennas and Propagation,* vol. 30, no. 6, pp. 1197-1200, 1982.

[135] C.-Y. Huang and W.-C. Hsia, "Planar elliptical antenna for ultra-wideband communications," *Electronics Letters,* vol. 41, no. 6, pp. 296-297, 2005.

[136] K. Srivastava *et al.*, "Integrated GSM-UWB Fibonacci-type antennas with single, dual, and triple notched bands," *IET Microwaves, Antennas & Propagation,* vol. 12, no. 6, pp. 1004-1012, 2018.

[137] R. B. Simorangkir, A. Kiourti, and K. P. Esselle, "UWB wearable antenna with a full ground plane based on PDMS-embedded conductive fabric," *IEEE Antennas and Wireless Propagation Letters,* vol. 17, no. 3, pp. 493-496, 2018.

[138] A. Kiourti, "RFID Antennas for Body-Area Applications: From Wearables to Implants," *IEEE Antennas and Propagation Magazine,* vol. 60, no. 5, pp. 14-25, 2018.

[139] A. Kiourti, J. R. Costa, C. A. Fernandes, and K. S. Nikita, "A broadband implantable and a dual-band on-body repeater antenna: Design and transmission performance," *IEEE transactions on antennas and propagation,* vol. 62, no. 6, pp. 2899-2908, 2014.

[140] V. Pathak, S. Thornwall, M. Krier, S. Rowson, G. Poilasne, and L. Desclos, "Mobile handset system performance comparison of a linearly polarized GPS internal antenna with a circularly polarized antenna," in *IEEE Antennas and Propagation Society International Symposium. Digest. Held in conjunction with: USNC/CNC/URSI North American Radio Sci. Meeting (Cat. No. 03CH37450)*, 2003, vol. 3: IEEE, pp. 666-669.

[141] N. Kumprasert, "Theoretical study of dual-resonant frequency and circular polarization of elliptical microstrip antennas," in *IEEE Antennas and Propagation Society International Symposium. Transmitting Waves of Progress to the Next Millennium. 2000 Digest. Held in conjunction with: USNC/URSI National Radio Science Meeting (C*, 2000, vol. 2: IEEE, pp. 1015-1020.

[142] J. G. Kretzschmar, "Wave propagation in hollow conducting elliptical waveguides," *IEEE Transactions on microwave theory and techniques,* vol. 18, no. 9, pp. 547-554, 1970.

[143] K. K. Mistry *et al.*, "A design of elliptical edge-fed circularly polarized patch antenna for GPS and Iridium applications," in *2018 2nd URSI Atlantic Radio Science Meeting (AT-RASC)*, 2018: IEEE, pp. 1-4.

[144] B. Liu, H. Aliakbarian, Z. Ma, G. A. Vandenbosch, G. Gielen, and P. Excell, "An efficient method for antenna design optimization based on evolutionary computation and machine learning techniques," *IEEE transactions on antennas and propagation,* vol. 62, no. 1, pp. 7-18, 2013.

[145] B. Liu, M. O. Akinsolu, N. Ali, and R. Abd-Alhameed, "Efficient global optimisation of microwave antennas based on a parallel surrogate model-assisted evolutionary algorithm," *IET Microwaves, Antennas & Propagation,* vol. 13, no. 2, pp. 149-155, 2018.

[146] M. O. Akinsolu, B. Liu, V. Grout, P. I. Lazaridis, M. E. Mognaschi, and P. Di Barba, "A parallel surrogate model assisted evolutionary algorithm for electromagnetic design optimization," *IEEE Transactions on Emerging Topics in Computational Intelligence,* vol. 3, no. 2, pp. 93-105, 2019.

[147] B. Liu, A. Irvine, M. O. Akinsolu, O. Arabi, V. Grout, and N. Ali, "GUI design exploration software for microwave antennas," *Journal of Computational Design and Engineering,* vol. 4, no. 4, pp. 274-281, 2017.

[148] V. Grout, M. O. Akinsolu, B. Liu, P. I. Lazaridis, K. K. Mistry, and Z. D. Zaharis, "Software Solutions for Antenna Design Exploration: A Comparison of Packages, Tools, Techniques, and Algorithms for Various Design Challenges," *IEEE Antennas and Propagation Magazine,* vol. 61, no. 3, pp. 48-59, 2019.

[149] B. Liu, Q. Zhang, and G. G. Gielen, "A Gaussian process surrogate model assisted evolutionary algorithm for medium scale expensive optimization problems," *IEEE Transactions on Evolutionary Computation,* vol. 18, no. 2, pp. 180-192, 2013.

[150] K. P. Esselle and A. Verma, "Wideband circularly polarized stacked microstrip antennas," *IEEE Antennas and wireless Propagation letters,* vol. 6, pp. 21-24, 2007.

[151] C. Haslett, *Essentials of radio wave propagation*. Cambridge University Press, 2008.

[152] "Federal Communications Commission Office of Engineering and Technology Laboratory Division, "GUIDELINES FOR DETERMINING THE EFFECTIVE RADIATED POWER (ERP)," 7 August 2015. [Online]. Available: https://apps.fcc.gov/kdb/GetAttachment.html?id=fzlsGm%2Fe68Ymx58IAmzNbw%3D%3D&desc=412172%20D01%20Determining%20ERP%20and%20EIRP%20v01r01&tracking_number=47469.."

[153] "LOS vs NLOS Difference between LOS and NLOS Wireless Channels," RF Wireless World, 2017. [Online]. Available: http://www.rfwireless-world.com/Terminology/LOS-vs-NLOS-wireless-channel.html.."

[154] *K. Bullington, "Radio propagation at frequencies above 30 Mc/s", Proceedings of the IRE, 35, pp. 1122-1186, 1947.*

[155] J. Deygout, "Multiple knife-edge diffraction of microwaves," *IEEE Transactions on Antennas and Propagation,* vol. 14, no. 4, pp. 480-489, 1966.

[156] J. Epstein and D. W. Peterson, "An experimental study of wave propagation at 850 Mc," *Proceedings of the IRE,* vol. 41, no. 5, pp. 595-611, 1953.

[157] C. Lee and S. Park, "Diffraction Loss Prediction of Multiple Edges Using Bullington Method with Neural Network in Mountainous Areas," *International Journal of Antennas and Propagation,* vol. 2018, 2018.

[158] O. Fratu *et al.*, "Comparative study of Radio Mobile and ICS Telecom propagation prediction models for DVB-T," in *2015 IEEE International Symposium on Broadband Multimedia Systems and Broadcasting*, 2015: IEEE, pp. 1-6.

[159] *ITM - ITS", Its.bldrdoc.gov, 2019. [Online]. Available: https://www.its.bldrdoc.gov/resources/radio-propagation-software/itm/itm.aspx.*

[160] "Hata and Davidson, "A Report on Technology Independent Methodology for the Modeling, Simulation and Empirical Verification of Wireless Communications System Performance in Noise and Interference Limited Systems Operating on Frequencies between 30 and 1500 MHz," TIA TR8 Working Group, IEEE Vehicular Technology Society Propagation Committee, 1997.."

[161] *B. Butterworth, "Emley Moor (Kirklees, England) Full Freeview transmitter", UK Free TV, 2019. [Online]. Available: https://ukfree.tv/transmitters/tv/Emley_Moor.*

[162] K. K. Mistry, P. I. Lazaridis, Z. D. Zaharis, M. Akinsolu, B. Liu, and T. Loh, "Accurate antenna gain estimation using the two-antenna method," *IET Conference Proceedings,* pp. 29 (4 pp.)-29 (4 pp.). [Online]. Available: https://digital-library.theiet.org/content/conferences/10.1049/cp.2019.0717